Development of a new *ab initio* approach for NMR chemical shifts in periodic systems

Von der Fakultät für Physik der Universität Stuttgart zur Erlangung der Würde eines Doktors der Naturwissenschaften (Dr. rer. nat.) genehmigte Abhandlung

Vorgelegt von

Daniel Sebastiani

aus Wiesbaden

Hauptberichter:	Prof. Dr. M. Parrinello
Mitberichter:	Prof. Dr. A. Muramatsu
Prüfungsvorsitzender:	Prof. Dr. M. Dressel
Tag der mündlichen Prüfung:	12. Februar 2001

Max-Planck-Institut für Festkörperforschung Stuttgart
Institut für Theoretische Physik der Universität Stuttgart
2001

Abstract

In this thesis work, a new method for computing NMR chemical shifts and magnetic susceptibilities in extended systems through an *ab-initio* density functional perturbation theory approach is presented. The method is applicable to crystalline and amorphous insulators under periodic boundary conditions, as well as to isolated molecules.

The formalism exploits the exponentially decaying nature of localized Wannier orbitals, allowing a simple representation of the angular momentum operator under periodic boundary conditions. The method is implemented in the context of a density functional theory pseudopotential approach with a basis set of plane waves.

The results are in good agreement with experiment and with calculations that use other theoretical methods.

Contents

1 Zusammenfassung 8

2 Introduction 19

3 Density functional theory 29

3.1 General 29

3.2 Born Oppenheimer approximation 30

3.3 Many-body electronic wave function 31

3.4 Hohenberg Kohn theorems 35

3.5 Kohn Sham equations 39

3.6 Local Density Approximation 42

3.7 Gradient Corrections 43

3.8 Pseudopotential approximation 44

3.9 Plane wave representation 46

3.10 Density functional perturbation theory 49

4 Construction of localized orbitals 53

4.1 General 53

4.2 Definition of localized orbitals 54

4.3 Derivation of the functional 55

4.4 Localization procedure 62

4.5 Orbital rotations 64

5 Chemical shifts and susceptibilities 66

5.1 General 66

5.2 Hamiltonian formalism 68
5.3 Magnetic DFPT 70
5.4 Electronic current density 72
5.5 Derived quantities: induced field, susceptibility and shielding . 74

6 The gauge origin problem 76

6.1 General 76
6.2 Continuous set of gauge transformations 77
6.3 Individual origin translations 78

7 The position operator problem 82

7.1 General 82
7.2 Virtual cells 83
7.3 Discussion 84

8 Pseudopotential correction 87

9 Application to isolated molecules 90

9.1 Convergence of the chemical shift 90
9.2 Comparison with experiment and other theoretical methods . 92
9.3 Magnetic susceptibilities 95
9.4 Electronic current densities 97

10 Periodic systems 100

10.1 Current distribution of ice Ih 100
10.2 Simple polymers 101
10.3 Diamond under pressure 102

11 Pepstatin A / HIV-1 protease complex 104
11.1 Introduction . . . 104
11.2 Methods . . . 107
    11.2.1 Structural models . . . 107
    11.2.2 Quantum-mechanical calculations . . . 109
    11.2.3 Calculated Properties . . . 111
11.3 Results . . . 113
11.4 Discussion . . . 115

12 Liquid water 118
12.1 Water under normal and supercritical conditions . . . 118
    12.1.1 Molecular dynamics . . . 120
    12.1.2 Magnetic susceptibilities . . . 121
12.2 Liquid water under ambient conditions . . . 124
12.3 Water under supercritical conditions . . . 125
    12.3.1 Anomalous hydrogen bond configurations . . . 129
    12.3.2 Validity of empirical functions for the shift . . . 131
12.4 Discussion . . . 135

13 Conclusion 137

A Discrete Fourier transformations 140

B A particular Fourier transformation 145

C Macroscopic susceptibility 148
C.1 General . . . 148

C.2 Special case: spherical geometry 151

List of abbreviations

BLYP: Becke Lee Yang Parr

BO: Born-Oppenheimer

CPMD: Car Parrinello molecular dynamics

CSGT: continuous set of gauge transformations

DFT: density functional theory

DFPT: density functional perturbation theory

GC: gradient correction

HK: Hohenberg-Kohn

IGLO: individual gauges for localized orbitals

KS: Kohn-Sham

LDA: local density approximation

MPL: Mauri Pfrommer Louie

NMR: nuclear magnetic resonance

ppm: parts per million

PW: plane wave

Ry: Rydberg

TMS: tetramethylsilane

VC: virtual cell

1 Zusammenfassung

In den letzten Jahren haben parameterfreie Rechnungen zur Bestimmung der Elektronenstruktur (*ab-initio*) in der Festkörperphysik und -chemie zunehmend an Bedeutung gewonnen. Die Untersuchung struktureller und dynamischer Größen von isolierten Molekülen in der Gasphase sowie von kondensierter Materie ist mittlerweile mit standardisierten Computerprogrammen möglich, die aus diesem Forschungszweig entstanden sind. Mit diesen Werkzeugen ist eine detaillierte Beschreibung der elektronischen Eigenschaften der untersuchten Systeme auf mikroskopischer Skala möglich.

Die Entwicklung von Berechnungsmethoden innerhalb dieser *ab-initio* Theorien ist daher von besonderem wissenschaftlichen Interesse. Sowohl in der experimentellen als auch in der theoretischen Physik und Chemie können computergestützte Berechnungen das Verständnis vieler Prozesse verbessern, die auf mikroskopischer Basis ablaufen und dennoch das makroskopische Verhalten der untersuchten Systeme bestimmen. In letzter Zeit hat besonders die Analyse großer ungeordneter Systeme an Aufmerksamkeit gewonnen. Die quantenmechanische Berechnung der zeitlichen Entwicklung solcher in der Regel amorphen Festkörper oder Flüssigkeiten bei endlicher Temperatur gelangt immer mehr in den Bereich des Möglichen. Natürlich läßt sich die Genauigkeit, die bei Voraussagen für kleine Moleküle inzwischen üblich ist, nicht auf größere Systeme übertragen. Die mit hochgenauen Computersimulationen verbundenen Resourcenkosten übersteigen ab einer gewissen Komplexität der Systeme den Bereich des Angemessenen, insbesondere wenn es um die Bestimmung der zeitlichen Entwicklung geht. In solchen Fällen ist es erforderlich, durch die Anwendung von bestimmten kontrollierten Näherungen einen Kompromiß zwischen Genauigkeit und Effizienz zu finden.

In diesem Geist hat sich in den letzten Jahren die von Hohenberg und Kohn entwickelte Dichtefunktionaltheorie mehr und mehr durchgesetzt [1]. Insbesondere findet hierbei die Formulierung von Kohn und Sham [2] Anwendung. Es handelt sich dabei um eine *ab-initio* Elektronenstrukturtheorie, die alle physikalisch meßbaren Größen anhand der Elektronendichteverteilung beschreiben kann. Die explizite Kenntnis der Vielteilchen-Wellenfunktion wird hierbei nicht benötigt, was den rechentechnischen Aufwand enorm reduziert. Die Dichtefunktionaltheorie ist im Grunde exakt, jedoch können die zu lösenden Gleichungen nicht vollständig analytisch formuliert werden. Die genaue Form der kinetischen Energie und der Austausch- und Korrelationsenergien als Funktional der Elektronendichte ist nicht bekannt. An dieser Stelle ist es erforderlich, näherungsweise Ausdrücke für diese Funktionale einzuführen, um die Berechnungen auch tatsächlich ausführen zu können.

Die Kohn–Sham–Darstellung erlaubt überdies, die Dichte der Elektronen aus einem System unabhängiger, nicht-wechselwirkender Teilchen zu bestimmen. Dabei befinden sich diese unabhängigen Teilchen in einem Potential, welches durch ihre eigene Dichteverteilung sowie die Atomkerne erzeugt wird. Die Beschreibung erfolgt deshalb durch ein System unabhängiger Gleichungen für die Elektronen, welches mittels iterativer Verfahren selbstkonsistent gelöst werden muß. In diesen Gleichungen findet sich das oben erwähnte Austausch-Korrelations-Potential wieder, für das geeignete Ausdrücke gefunden werden müssen. Es gibt mehrere Ansätze für dieses Problem, welches aber noch immer ein aktives Forschungsgebiet ist. Mit den inzwischen verfügbaren Varianten ist aber bereits eine sehr genaue Berechnung elektronischer Eigenschaften des Grundzustandes möglich.

Oft ist die Kenntnis der zeitlichen Entwicklung eines Systems von großem Interesse. Ein besonders effizientes Verfahren, die Bewegungsgleichungen der Atome mit der Berechnung der Elektronenstruktur im Rahmen der Dichtefunktionaltheorie zu verbinden, ist von Car und Parrinello entwickelt worden [3]. Mit Hilfe dieser Technik können auch dynamische Vorgänge auf quantenmechanischer Basis dargestellt und analysiert werden [4]. Zwar sind die zugänglichen Zeitskalen aufgrund des Rechenaufwandes sehr klein, sie liegen in der Größenordnung von Pikosekunden. Die Möglichkeit, viele wichtige physikalische Prozesse wie beispielsweise Transportvorgänge, aber auch ganze chemische Reaktionen, die auf gerade dieser Zeitskala stattfinden, in ihrem Ablauf zu studieren, hat dieser Kombination zum Durchbruch verholfen.

Die Analyse experimenteller Meßdaten aus beispielsweise Röntgenbeugung, Neutronen- und Ramanstreuung sowie die chemische Verschiebung, die später noch genauer erklärt werden soll, können tiefe Einblicke in die Physik und Chemie vieler Systeme liefern. Experimentelle Spektren sind jedoch ab einer gewissen Komplexität schwierig zu interpretieren. Der Vergleich mit simulierten Spektren kann hierbei eine sehr nützliche Verbindung zwischen Theorie und Praxis darstellen, um die mikroskopischen Ursachen der beobachteten Phänomene zu erklären.

In dieser Arbeit soll daher eine neue Methode vorgestellt werden, mit deren Hilfe die Berechnung der magnetischen Suszeptibilitäten sowie der chemischen Verschiebung in der Kernspinresonanz (nuclear magnetic resonance, NMR) in Systemen unter periodischen Randbedingungen möglich ist.

Die Messung der chemischen Verschiebung ist eines der aussagekräftigsten Analyseverfahren in der strukturellen Chemie. Mit ihrer Hilfe kann die Elektronenstruktur in der Umgebung eines Atomkerns mit sehr großer Genauigkeit ermittelt werden. Koordinationszahlen, Bindungslängen und sogar Bindungswinkel sind aus geeigneten Resonanzspektren ablesbar. Es gibt hierzu eine Reihe von empirischen Regeln, die oftmals sehr umfangreiche Informationen über diese Größen liefern. Sobald aber die Geometrie des Systems zu komplex wird, sind diese Regeln nicht mehr anwendbar.

Chemische Verschiebungen beschreiben die Wechselwirkung der Elektronen eines Systems mit einem starken externen homogenen Magnetfeld. Hierbei verändert das äußere Feld die Wellenfunktion dieser Elektronen derart, daß elektronische Ringströme induziert werden. Diese Ströme, die natürlich stark von der elektronischen Struktur abhängen, erzeugen ein Zusatzfeld, welches sich dem externen überlagert und das Gesamtmagnetfeld somit inhomogen macht. Insbesondere sind die Feldwerte an den Positionen der Atomkerne alle leicht gegeneinander verschoben, sofern die Kerne sich nicht an strukturell äquivalenten Orten befinden. Ein nichtverschwindender Kernspin im magnetischen Feld besitzt Energiezustände, deren Abstand proportional zur Stärke des Feldes ist. Damit bestimmt der Feldwert auch die Resonanzfrequenz, die durch Absorptionsspektroskope bestimmbar ist. Die gegenseitige Verschiebung der Resonanzfrequenzen wird chemischen Verschiebung genannt. Mit ihr kann man zusammenfassend also die elektronische Struktur in der Umgebung eines Atomkerns direkt auf einen Meßwert abbilden, der darüberhinaus mit sehr hoher Genauigkeit bestimmt werden kann.

Aufgrund dieser großen Präzision und der konzeptuellen Einfachheit des Versuchsaufbaus ist die Kernspinresonanz im Laufe der Jahre zu einer Standard-Analysemethode in der gesamten Chemie geworden. Im Laufe der Zeit sind die Meßverfahren laufend verfeinert worden, und neue Analysemethoden wurden entwickelt. Bei der einfachsten denkbaren Messung wird die Frequenz eines eingestrahlten Wechselfeldes im Radiofrequenzbereich variiert (continuous-wave-Messung), bis Absorption auftritt. Dieses Verfahren stellt das grundlegende Experiment der Kernspinresonanzmessung dar, wird aber heute kaum mehr verwendet. An seine Stelle ist die Fourierspektroskopie getreten, mit der ein ganzer Frequenzbereich auf einmal gemessen wird.

Auf der theoretischen Seite steht dieser Evolution die Entwicklung immer genauerer quantenchemischer Verfahren zur Bestimmung der chemischen Verschiebung einzelner Atomkerne in genau definierten Umgebungen gegenüber. Diese Verfahren sind in der Lage, die Resonanzlinien eines Atoms mit beinahe experimenteller Genauigkeit vorauszusagen. Dabei ist allerdings die insgesamt beschreibbare Systemgröße auf weniger als hundert isolierte und statisch angeordnete Atome beschränkt.

Sehr viele physikalische und chemische Prozesse laufen jedoch in Lösung oder in amorphen und kristallinen Phasen ab. Biologisch relevante Vorgänge beruhen zum Beispiel nicht zuletzt auch auf der Präsenz von Wasser als Lösungsmittel, und industrielle Prozesse werden in der Regel auch nicht in der Gasphase durchgeführt. Die Kernspinresonanz wird in der Praxis jedoch auch auf solche Systeme mit großem Erfolg angewendet. Eine Berechnung als isolierte Moleküle würde in diesen Fällen eine schwer zu rechtfertigende Näherung darstellen. Weiterhin wird die dynamische Entwicklung eines isolierten Systems durch Oberflächeneffekte dominiert, da die hiermit verbundenen Energien in der Regel deutlich größer sind als die im Innern auftretenden. In kondensierten Phasen ist die Oberflächenenergie jedoch nicht vorhanden, was zu einem vollständig anderen Verhalten führen kann.

Eine mit Erfolg praktizierte Methode zur Vermeidung dieser Probleme bei Molekulardynamiksimulationen ist die Verwendung periodischer Randbedingungen für kondensierte Systeme. Dabei nimmt man eine bestimmte Periodizität des Systems an, so daß die vollständige Information über das Gesamtsystem bereits in einem entsprechend geeignet dimensionierten, aber beliebig angeordneten Ausschnitt, der sogenannten Einheitszelle, enthalten ist. In der Computersimulation werden alle physikalischen Größen unter der Annahme berechnet, daß sich diese Einheitszelle in alle Raumrichtungen periodisch wiederholt, so daß das System insgesamt unendlich weit ausgedehnt ist. Die hierbei künstlich erzeugte Periodizität hat keinen nachhaltigen Einfluß auf das Verhalten des Gesamtsystems, sofern die typischen Korrelations-Längenskalen kleiner als die angenommene Periodizitätslänge ist. Diese Eigenschaft kann überdies durch Vergrößerung der Einheitszelle überprüft werden.

Die meisten der bereits angesprochenen physikalisch meßbaren Größen können erfolgreich unter der Annahme periodischer Randbedingungen berechnet werden. Im Gegensatz hierzu gestaltet sich die Berechnung der Elektronenreaktion auf ein externes homogenes magnetisches Feld jedoch schwieriger. Grundsätzlich besteht dabei das fundamentale Problem, daß der quantenmechanische Ortsoperator, der bei der Beschreibung des Magnetfeldes explizit auftritt, nicht wohldefiniert ist. Es gibt keine einfache Möglichkeit, ihn im Einklang mit der Periodizität des Systems zu bringen, sein Wert ist in jeder Replika der Einheitszelle anders.

Erst vor kurzer Zeit wurde von Mauri et al. eine erste Methode vorgestellt, die die Berechnung von NMR chemischen Verschiebungen und magnetischen Suszeptibilitäten auch in Systemen unter periodischen Randbedingungen erlaubt [5]. In diesem Verfahren wird das Problem des Ortsoperators umgangen, indem zunächst angenommen wird, daß das externe Magnetfeld nicht homogen, sondern in Feldrichtung sinusförmig moduliert ist. Dies ermöglicht eine Beschreibung des Feldes mit einem periodisch definierten Vektorpotential einer bestimmten Wellenlänge. Die experimentelle Situation eines konstanten Feldes wird über den Grenzwert unendlicher Modulationswellenlänge erreicht.

Hierdurch konnte gezeigt werden, daß das zuvor geschilderte Problem nicht ausweglos ist. Die Methode hat jedoch gewisse praktische Nachteile. Zunächst ist natürlich die Wahl der Wellenlänge der Modulation nicht einfach. Grundsätzlich müßte für jedes untersuchte System ein Konvergenztest durchgeführt werden, um sicherzustellen, daß der oben genannte Grenzwert unendlicher Modulationswellenlänge auch erreicht wird. Weiterhin ist die minimal erforderlicher Wellenlänge typischerweise größer als die Dimension einer Einheitszelle, so daß eine repräsentative Darstellung der Blochvektoren innerhalb der Brillouin-Zone für die Berechnung der Wellenfunktion erforderlich wird. Die Beschränkung auf den Gamma-Punkt ($\mathbf{k} = 0$) ist in dieser Methode nicht ausreichend. Alle $\mathbf{k}$-Vektoren außer $\mathbf{k} = 0$ implizieren jedoch komplexe Wellenfunktionen, wohingegen am Gamma-Punkt eine relle Darstellung ausreicht. Des weiteren muß die Wellenfunktion für jeden **k**-Vektor einzeln betrachtet werden. All dies erhöht letztlich den Rechenaufwand zur Bestimmung der magnetischen Reaktion beträchtlich im Vergleich zur Berechnung des elektronischen Grundzustandes.

In der vorliegenden Dissertation ist deshalb eine weitere alternative Methode entwickelt worden, in der die Probleme, die durch die verwendeten periodischen Randbedingungen entstehen, auf eine andere Art und Weise angegangen und gelöst werden.

Anstatt das externe Magnetfeld zu modulieren, wird der Ortsoperator in einer periodischen Sägezahn-Form neu definiert. Um die aus der teilweise unphysikalischen Form des neuen Operators resultierenden Effekte zu minimieren, ist die Darstellung der elektronischen Wellenfunktionen in Form von maximal lokalisierten Wannier-Orbitalen erforderlich, die in der Quantenchemie bereits seit längerem verwendet werden. Durch diese Darstellung kann der Effekt des magnetischen Feldes auch innerhalb periodischer Randbedingungen direkt beschrieben werden, ohne das Feld künstlich modulieren zu müssen. Unter Zuhilfenahme einer bestimmten weiteren Näherung, die im Hauptteil der Arbeit ausführlich besprochen wird, kann die Rechnung mit diesem Ansatz gegenüber der Modulationsmethode deutlich effizienter durchgeführt werden.

Diese neue Methode ist implementiert in einem Computerprogramm, das auf der bereits vorgestellten parameterfreien *ab-initio* Berechnung der Elektronenstruktur mit Hilfe der Dichtefunktionaltheorie basiert. Die elektronische Reaktion in Form der oben diskutierten Ringströme wird dabei im Rahmen der variationellen Dichtefunktional-Störungstheorie realisiert, die die Störungsenergie zweiter Ordnung mittels des Verfahrens der konjugierten

Gradienten minimiert. Aus den hierdurch erhaltenen elektronischen Ströme lassen sich die Werte des induzierten inhomogenen Magnetfeldes an den Aufenthaltsorten der Kernspins errechnen. Diese Werte wiederum sind gleichzeitig die gesuchten chemischen Verschiebungen.

Zunächst werden im Hauptteil dieser Arbeit die chemischen Verschiebungen für eine Reihe von repräsentativen kleinen organischen Molekülen vorgestellt, die hauptsächlich zum Test und Vergleich der Methode mit bereits existierenden Verfahren gedacht sind. Weiterhin wird die Berechnung zweier einfacher unendlicher Polymerketten und des Diamantkristalls vorgestellt, die insbesondere als Testfälle für tatsächlich unendlich periodische Systeme gedacht sind. Dabei wird gezeigt, welche Genauigkeit die beschriebene Implementierung erreichen kann und wo ihre Grenzen liegen. Auch wenn die hohe Präzision von modernen quantenchemischen Rechnungen nicht erreicht wird, so ist mit der hier vorgestellten Methode durchaus eine sinnvolle Vorhersage der Resonanzlinien möglich. Dabei sind Trends typischerweise deutlich besser voraussagbar als absolute Werte.

Im weiteren wird die Methode auf mehrere große Systeme vorgestellt, deren Analyse Gegenstand aktueller Forschung ist und die bislang nur unzureichend verstanden sind. Insbesondere ist dies die Bestimmung des Protonierungszustandes des aktiven Zentrums der HIV-1-Protease. In einem funktionsfähigen AIDS-Virus arbeitet diese Protease als Schere für Polypeptid-Segmente und ist in dieser Funktion für den Metabolismus des Virus von essentieller Bedeutung. Vor einigen Jahren wurde festgestellt, daß die Anwesenheit eines Pepstatin-Moleküls die Funktionsfähigkeit der Protease beeinträchtigt, so daß fortan nur noch unfertige HIV-Viren hergestellt werden, die nicht mehr infektiös sind.

Um aus dieser Erkenntnis eventuell vermehrungshemmende Medikamente herstellen zu können, ist die Kenntnis der Funktion dieses Pepstatin-Inhibitors an der Schneidstelle der Protease von fundamentaler Bedeutung. Aufgrund des gemessenen ^{13}C-NMR-Spektrums wurde vor kurzem eine bestimmte geometrische Anordnung für den Komplex vorgeschlagen, die sich jedoch in der Computersimulation als instabil erweist. Sie entwickelt sich zu einer Konfiguration, deren berechnete NMR-Linien nicht die experimentell gefundene Charakteristik aufweisen. Stattdessen wird eine alternative Geometrie vorgestellt, die zeitlich stabil ist und deren simulierte chemische Verschiebung gut zum tatsächlichen Spektrum paßt. An diesem Beispiel wird gezeigt, wie fruchtbar die Verbindung von numerischer Theorie und experimentellen Meßverfahren durch die neu entwickelte Berechnungsmethode sein kann.

Schließlich wird noch ein weiteres System vorgestellt werden, daß durch die Berechnung von chemischen Verschiebungen analysiert werden kann. Unter Standardbedingungen liegt Wasser in der flüssigen Phase vor, und stellt eines der wichtigsten – wenn nicht *das* wichtigste – polare Lösungsmittel in Biologie und Chemie dar. Unter hohem Druck und hoher Temperatur, jenseits des kritischen Punktes, zeigt Wasser jedoch gänzlich neue Eigenschaften. Insbesondere ist es in der Lage, organische Abfälle zu oxidieren. Diese und andere Eigenschaften haben diese überkritische Phase zum Gegenstand aktueller Forschung gemacht. Das besondere an Wasser ist sein ausgeprägtes Netzwerk aus Wasserstoffbrückenbindungen. Diese Brücken beeinflussen die chemische Verschiebung ganz wesentlich, weshalb sich hier die Untersuchung mit der oben vorgestellten Methode anbietet. Im Ergebnis kann gezeigt werden, daß die Molekulardynamiksimulationen in Verbindung mit der Berechnung der chemischen Verschiebungen die experimentellen Spektren sehr gut reproduzieren können und so ein tiefgreifendes Verständnis der Vorgänge in überkritischem Wasser ermöglichen.

Zusammenfassend läßt sich sagen, daß mit Hilfe der vorliegenden Arbeit eine effiziente Berechnung der magnetischen Suszeptibilität sowie der NMR chemischen Verschiebungen von nichtmetallischen Systemen unter periodischen Randbedingungen möglich ist. Die experimentellen Spektren werden mit guter Genauigkeit reproduziert, was wesentlich zu deren Interpretation beitragen kann.

2 Introduction

In the past, the determination and prediction of the properties of matter by means of parameter-free calculations of the electronic structure (*ab initio*) has turned out to be a key tool of condensed matter science. The investigation of structural and dynamical properties in physics and chemistry can now be done with the help of various computer program packages which have emerged from this domain. Isolated molecules in the gas phase as well as extended solids can be described very accurately on a microscopic scale.

For this reason, the development of methods in the framework of *ab initio* calculations is of great scientific interest. This interest comes both from the theoretical and from the experimental side, since scientists from either direction can improve their understanding of the processes that determine the macroscopic behavior of matter. In particular, a lot of emphasis has been attributed in the past to the development of methods that are suited to model the dynamical evolution of large disordered systems at finite temperature, such as liquids and amorphous solids. Unfortunately, the high numerical precision that can be used for the analysis of small systems is unaffordable and often impossible to achieve when it comes to the calculation of more complex structures. In particular, the evaluation of statistical averages can represent a prohibitive computational cost. Often, in order to treat such systems, a compromise must be found between accuracy and efficiency of the calculation. This can be done by means of approximate theories, which can nevertheless be shown to produce reliable results.

In this context, density functional theory (DFT) as developed by Hohenberg and Kohn [1] in the formulation of Kohn and Sham [2] has become the state-of-the-art approach for extended systems. The key point of the Hohenberg–Kohn theorem is that the electronic ground state of any system can be represented by its electronic density alone. This provides a way to calculate physical observables of a variety of systems without having to construct the whole electronic many-body wavefunction, which is computationally a very expensive task. However, while this theory is in principle exact, it is not possible to write down analytically the form of the equations to be solved. The kinetic energy and the exchange and correlation functional cannot be expressed directly as a functional of the density. Here, several approximations must be made in order to obtain a practical scheme.

The Kohn–Sham formulation provides a way to map the system of interacting particles to an ensemble of electrons which only interact through their total density. The approach yields a system of equations describing non-interacting particles within a potential created by the electronic density. This system of equations must be solved self-consistently in order to obtain the electronic density in the ground state. Again, in these equations, the exchange and correlation term cannot be stated explicitly; it has to be approximated by appropriate expressions. In the last decades, there have been several attempts to find an optimal functional in the framework of the generalized gradient approximation, and this point is presently still an active field of research. But already with the functionals developed up to now, many ground state properties can be calculated to a very good accuracy with the Kohn–Sham formulation of density functional theory.

The study of dynamically evolving systems which sample a large phase space requires the combination of the electronic structure calculation with a scheme that provides the equations of motion of the nuclei in the field created by all the other nuclei and the electrons. A particularly efficient approach to combine the nuclear motion with the solution of the Kohn–Sham equations has been developed by Car and Parrinello [3]. This method has proven to be very successful for the investigation of many processes that happen on the timescale of a few picoseconds, such as many transport phenomena and also some chemical reactions. The possibility of simulating such processes has been a breakthrough in computational physics and chemistry.

Examples of physically interesting quantities like X-ray diffraction, neutron scattering, Raman scattering and chemical shifts can provide a deep insight into the physics and the chemistry of the considered systems. However, the experimental results can be difficult to interpret if the systems are very complex. In these cases, a comparison with computed values can help in assigning experimental features and explaining their microscopic origin. Hence, computational physics and chemistry can serve as a powerful bridge between experiment and theory.

In this thesis, a new method shall be presented which allows the calculation of nuclear magnetic resonance (NMR) chemical shifts and magnetic susceptibilities in periodic systems. Nuclear magnetic resonance is one of the most powerful experimental methods in structural chemistry. The quantities extracted from NMR spectra, in particular chemical shifts, are widely used to characterize the chemical environment of individual atoms. Coordination numbers, bond types and even bonding distances and angles can be obtained by analyzing the resonance lines of the nuclear spins. Many empirical rules exist to relate chemical shifts to these properties, and they often provide very useful information. However, when the geometric configuration becomes too complicated, these rules are not applicable any more, and the only way to unambiguously interpret experimental spectra are *ab initio* calculations.

The fundamental mechanism of nuclear magnetic resonance is the interaction of the electrons with an external strong magnetic field. The field perturbs the electronic wavefunction in such a way that ring currents are induced in the system. These currents produce an additional magnetic field, which is superimposed to the external one. The induced field is much weaker, but in contrast to the external one, it is spatially inhomogeneous. It depends very sensitively on the electronic structure of the system. Therefore, the values of the total magnetic field at the positions of non-equivalent nuclei are different.

A nucleus which has a non-zero spin has several energetically different states in a magnetic field, depending on the spin quantum number I_z. The energy difference between those levels is proportional to the strength of the field at the position of the nucleus and can be measured by absorption spectroscopy of radio frequency pulses. Thus, by means of the induced currents and the particular field they create, the electronic structure determines the nuclear absorption frequency. This quantity is experimentally accessible with a very high precision.

Due to this precision and the amount of information that can be extracted from more sophisticated experimental setups, nuclear magnetic resonance has become a very important standardized analysis tool in chemistry. In the course of time, the experimental apparatus has been improved enormously and new analysis tools have been developed. The simplest possible measurement, the continuous-wave technique, consists of varying the radio frequency until resonance occurs. This method is nowadays replaced by Fourier spectroscopy, which probes a large range of resonance frequencies at once. Further, there are techniques such as Magic-Angle Spinning which can partly suppress direct dipolar interactions between nuclear spins, which give rise to an undesired broadening of the NMR resonance lines. These techniques are well-established and routinely used in structural chemistry.

On the theoretical side, various methods have been developed to predict the NMR resonance lines of molecules by quantum chemical calculations with a very high accuracy. Nowadays, there are several methods implemented in various computer packages which are able to determine chemical shifts of most nuclei in a well-defined environment of typically one hundred atoms at maximum. In these programs, it is assumed that the system is in the gas phase.

Many other physical processes and chemical reactions, however, take place in condensed matter, such as solutions, polymers, and amorphous and crystalline phases. For instance, the properties of biologically relevant systems and many industrially important processes crucially depend on the presence of water as a solvent. Hence, it would be a non-realistic approximation to calculate those systems statically and in vacuum, neglecting that they are normally in a very complex environment. In an isolated cluster of atoms, the energetics and hence the dynamical evolution is dominated by surface effects, which are absent in condensed matter. This can yield to a completely different behavior.

In many of these cases, the alternative description of the system by means of periodic boundary conditions turns out to be more reliable. To this purpose, the whole system is thought to have a certain periodicity in space. It can then be described by the information contained in one elementary unit cell only, supposing this cell has the appropriate dimensions. The unit cell contains the minimum information necessary to reconstruct the whole system and can be taken at an arbitrary position. In the computer simulation, all electronic and atomic interactions and properties are then calculated under the assumption that the unit cell is infinitely repeated in each direction of space. In nature, such a periodicity never occurs. However, if the typical correlation length of the particles is smaller than the size of the unit cell, this artificial periodicity has only little impact on the physical behavior of the system. In addition, this can easily be verified by increasing the cell size and comparing whether the properties of the system change.

Many experimentally accessible quantities of condensed matter can be calculated by adopting periodic boundary conditions. The calculation of orbital magnetic properties like magnetic susceptibilities and NMR chemical shifts, however, turns out to be more difficult. The fundamental problem is related to the position operator which appears explicitly in the quantum formulation of the interaction of the magnetic field with the electrons. This operator is not well-defined in an infinitely repeated periodic system, since it is different in every image of the cell. During the last years, a solution has been found for the problem of representing the expectation value of the position operator in periodic systems in terms of the Berry phase [6]. Unfortunately, this theory cannot help to define the position *operator* properly, but only its expectation value.

However, it has been shown recently by Mauri and Louie [5] that it is actually possible to calculate electronic magnetic response in periodic systems. In their approach, the problem of the application of the explicit position operator is circumvented by assuming that the magnetic field is not homogeneous, as in reality, but modulated with a small but finite wavevector. This transforms the explicit position operator into a periodic one with the wavelength of this modulation, which can thus be treated properly. To return to the experimental situation of a spatially constant field, the limit of infinite modulation wavelength is evaluated.

This method has several drawbacks. The choice of the modulation vector, although being crucial for the success of the calculation, is not unique. In principle, a convergence test would have to be done for each calculation in order to ensure that the limit of infinite wavelength is actually reached. Further, this modulation wavelength is typically different from the unit cell size. Thus, to describe the electronic orbitals properly, an accurate sampling of the Brillouin zone is required. The use of the Γ-point ($\mathbf{k} = 0$) only is not sufficient any more in this case. This sampling induces first an additional computational overhead due to the additional k-points considered, and secondly, a calculation at $\mathbf{k} \neq 0$ implies that the electronic wavefunctions cannot be chosen as purely real any more. This again doubles the number of operations.

In this thesis, an alternative method is developed and implemented in a DFT-pseudopotential based plane-wave code, and finally applied to a variety of systems.

The problems that arise from the position operator are solved by a different method: Instead of modulating the magnetic field, the position operator is redefined in a periodic way. This induces a non-physical shape of the new operator, and requires it to be applied to spatially confined electronic wavefunctions. The latter can be achieved by a well-established localization procedure. By means of this representation of the electronic structure, the effect of an external magnetic field on the electronic wavefunctions within periodic boundary conditions can be calculated directly, without the assumption of a modulated field. By adopting an additional particular approximation, the calculation becomes significantly more efficient than the previous method.

The new approach is realized in the framework of a variational density functional perturbation scheme, implemented in a state-of-the-art DFT code. The magnetic response is obtained by a computationally optimized minimization procedure which is based on the variational principle for the second order energy functional. The actual minimization uses the method of conjugate gradients to speed up its convergence and returns the wavefunction correction in the presence of the magnetic field. After evaluation of the induced electronic currents, their additional magnetic field is determined as a periodic response to the external perturbative field, yielding directly the chemical shift values for all nuclei in the system.

First test calculations on small organic molecules in the gas phase are presented to validate both the approach and the implementation, and a simple infinite polymer chain serves to test the extension to a periodic system. Various tests and convergence series are performed in order to investigate the behavior of the code and to determine the accuracy in different regimes. It is shown that the new method delivers reliable results, although the precision of quantum chemical calculations is evidently not reached. However, trends and tendencies are reproduced with a good precision that enables the unique distinction of individual atoms in many systems.

Further, the method is applied to a variety of systems of practical interest. In particular, the protonation state of the cleavage site of the HIV-1 protease in the presence of a pepstatin molecule, is determined by analyzing its NMR chemical shift during an *ab initio* molecular dynamics simulation. This part of the protease of the human immunodeficiency virus is responsible for cutting polypeptide segments. It was discovered a few years ago that the inhibition of this site by binding it to pepstatin leads to the production of immature, non-infectious viral particles. For this reason, the analysis of this complex, and in particular its protonation state, is important for the design of anti-AIDS drugs. From the experimental NMR spectrum of the complex, a particular configuration was proposed. Upon investigation of this suggestion and also several alternative geometries in an aequous environment, it is shown that the structure proposed experimentally is not stable and evolves towards another one whose nuclear resonance lines disagree with experiment. Instead, an alternative configuration turns out to be energetically stable and to reproduce the experimental carbon NMR shifts.

Finally, the calculation of the time-averaged hydrogen chemical shift in liquid water under normal and supercritical conditions is presented. A detailed analysis of the change in the distributions of the individual instantaneous resonance lines provides a deep insight into the nature of the hydrogen bond network of water under these conditions. In comparison to experiment, it can also be used to show the validity of the simulated trajectories of the water systems and can thus help to improve the computational setup of the simulation.

In conclusion, the results provided by the new approach agree well with existing calculations and with experiment. Hence, the method presented in this work can help to describe those systems with a good accuracy and a low computational effort.

3 Density functional theory

3.1 General

In the following sections, the general theory for the quantum mechanical description of matter that is used in this work will be presented.

When it comes to the actual calculation of the properties of matter through a numerical description of the atoms and electrons, a theoretical framework is needed to represent them in a suitable way. In this work, the density functional theory (DFT) approach in combination with gradient corrected exchange correlation energy functionals is chosen [1, 2, 7, 8]. A pseudopotential plane wave representation of the electronic structure is used in the frozen core approximation. This allows the efficient calculation of large systems and, in combination with molecular dynamics, good statistical sampling. It constitutes the fundamental concept underlying all the calculations done lateron, thus justifying that it be described in detail in this section.

The starting point is the basic equation of quantum theory, the Schrödinger equation, which is then transformed to simplified formulations that can be treated by computer programs. Then, several additional approximations are introduced, which need to be used in order to lower the consumption of computational resources. Finally, the details of the implementation that is used for this work are explained.

3.2 Born Oppenheimer approximation

The Schrödinger equation for a system containing n electrons and N nuclei has the form of an eigenvalue problem:

$$\mathcal{H}\Psi(\mathbf{r}_1,..,\mathbf{r}_n,\mathbf{R}_1,..\mathbf{R}_N) = E\Psi(\mathbf{r}_1,..,\mathbf{r}_n,\mathbf{R}_1,..\mathbf{R}_N), \tag{1}$$

with the eigenvalue E of the many body Hamiltonian operator $\mathcal{H}$, given in atomic units by:

$$\begin{aligned}\mathcal{H} &= \sum_i -\frac{1}{2}\nabla_i^2 + \sum_I -\frac{1}{2M_I}\nabla_I^2 + \frac{1}{2}\sum_{i\neq j}\frac{1}{|\mathbf{r}_i-\mathbf{r}_j|} + \\ &\quad \frac{1}{2}\sum_{I\neq J}\frac{Q_I Q_J}{|\mathbf{R}_I-\mathbf{R}_J|} - \sum_{iI}\frac{Q_I}{|\mathbf{r}_i-\mathbf{R}_I|}.\end{aligned} \tag{2}$$

Note that in this Hamiltonian, $\mathbf{r}_i$ and $\mathbf{R}_I$ designate the position operators acting on the indicated electronic particles i and the nucleis I, respectively. M_I and Q_I are the masses and charges of the nuclei in atomic units. Electronic charge and mass as well as $\hbar$ are all equal to one in this system of units.

The Born Oppenheimer (BO) approximation [8, 9] is based on the fact that the mass of the ions is much larger than the mass of the electrons. This implies that the typical electronic velocities are much larger than the ionic ones, and that by consequence, the dynamical evolution can be decoupled. Energetically, the decoupling corresponds to a separation of the spectra in such a way that the electrons are practically always in their instantaneous ground state. The total wavefunction is therefore written as the product of the nuclear and electronic parts:

$$\Psi(\mathbf{r}_1,\ldots,\mathbf{r}_n,\mathbf{R}_1,\ldots,\mathbf{R}_N) = \Psi^{\mathrm{el}}_{\mathbf{R}_1,\ldots,\mathbf{R}_N}(\mathbf{r}_1,\ldots,\mathbf{r}_n)\Psi^{\mathrm{i}}(\mathbf{R}_1,\ldots,\mathbf{R}_N) \tag{3}$$

where the electronic wavefunction $\Psi^{\mathrm{el}}_{\mathbf{R}_1,\ldots,\mathbf{R}_N}(\mathbf{r}_1,\ldots,\mathbf{r}_n)$ parametrically depends on the ionic position variables. In most cases, this approximation turns out to be justified.

Formally, this adiabatic behaviour leads to separating the Schrödinger Equation (1) into two decoupled equations: the time-independent Schrödinger equation of the electrons in the constant field of the fixed nuclei, and the time-dependent Newton-like equation of movement for the nuclei. A further approximation is to treat the nuclei like classical particles, so that in the end, the nuclear position operators can all be turned into position variables. The quantum effects are then limited to the electronic wavefunctions, which obey a simpler Schrödinger equation:

$$\mathcal{H}^{\mathrm{el}}\Psi^{\mathrm{el}}_{\mathbf{R}_1,\ldots,\mathbf{R}_N}(\mathbf{r}_1,\ldots,\mathbf{r}_n) = E^{\mathrm{el}}_{\mathbf{R}_1,\ldots,\mathbf{R}_N}\Psi^{\mathrm{el}}_{\mathbf{R}_1,\ldots,\mathbf{R}_N}(\mathbf{r}_1,\ldots,\mathbf{r}_n) \tag{4}$$

with

$$\mathcal{H}^{\mathrm{el}} = \sum_i -\frac{1}{2}\nabla_i^2 + \frac{1}{2}\sum_{i\neq j}\frac{1}{|\mathbf{r}_i - \mathbf{r}_j|} - \sum_{iI}\frac{Q_I}{|\mathbf{r}_i - \mathbf{R}_I|}. \tag{5}$$

This also allows to replace the interaction between nuclei and electrons, the last term in Eq. (5), by a generalized external potential $v_{\mathrm{ext}}(\mathbf{r})$:

$$\mathcal{H}^{\mathrm{el}} = \sum_i -\frac{1}{2}\nabla_i^2 + \frac{1}{2}\sum_{i\neq j}\frac{1}{|\mathbf{r}_i - \mathbf{r}_j|} + \sum_i v_{\mathrm{ext}}(\mathbf{r}_i). \tag{6}$$

3.3 Many-body electronic wave function

The exact quantum mechanical treatment of systems consisting of nuclei and electrons is not possible at present, even within the BO approximation, and independently of the system size. A simple analysis of the complexity of the problem shows that its computational requirements are prohibitive. Also in the foreseeable future, such calculations will very probably be impossible.

One of the simplest systems that one can assume to be a representative example for a practical calculation is a single isolated atom, for instance the neon atom. As a first simplification, only the electronic wavefunction shall be described as a system of ten particles. The electronic wavefunction has the form

$$\Psi(\mathbf{r}_1, \mathbf{r}_2, \ldots, \mathbf{r}_{10}) \tag{7}$$

where $\mathbf{r}_i$ are the position variables of the electrons. For simplicity, this wavefunction shall be described on a real space grid of only ten points per axis, and the values of Ψ on this mesh are assumed to be representable by numbers requiring ten bytes of storage capacity. The various simplifications that can be made thanks to the symmetry of this particular system shall not be taken into account, as these symmetries can easily be broken.

The storage requirements of the wavefunction for this isolated system are then

$$10\frac{\text{bytes}}{\text{point}} \times \left(10\frac{\text{points}}{\text{axis}}\right)^{3\text{axis}\times 10\text{particles}} = 10^{31}\text{ bytes.} \tag{8}$$

This number of bytes needs to be stored in order to represent the wavefunction of the ten electrons. Assuming heuristically that a DVD disc has a theoretical storage capacity of 10 Gigabytes = 10^{10} bytes, one needs a total of 10^{21} DVD discs for the storage. With a weight of ten grams per DVD, the total weight of those discs is 10^{16} tons. A heavy truck can carry less than 100 tons of weight, so that more than 10^{14} trucks are needed to carry the DVDs to the computer that is responsible for the calculation. If these trucks are ten meters long, the distance of 10^{15}m or 10^{12}km is equivalent to ten thousand times the distance between the sun and the planet on which this work has been done.

This little example makes evident that an exact solution of the quantum many body problem is not feasible. Therefore, many concepts have been developed to overcome the complexity of the problem and to introduce physically reasonable simplifications.

Fortunately, it turns out that the use of several approximations still reproduces the experimental results with a good accuracy. Only these approximations make numerical calculations affordable. In this chapter, one of the currently most popular theories shall be described in detail. It basically consists of taking the electronic density instead of the wavefunction as the fundamental variable, thus reducing the degrees of freedom drastically.

The BO approximation provides a way to separate the ionic degrees of freedom from the electronic ones. The additional simplifications and approximations are necessary to describe the electrons numerically therefore concern the Schrödinger equation (1) only.

Several branches of approaches exist for the simplification of the Hamiltonian in Eq. (1).

Quantum chemistry methods are based on the fact that any antisymmetric many-electron wavefunction can be written as a sum of Slater determinants of atomic basis functions. The simplest method is just to take one determinant, built from the occupied states of the atom. This is called the Hartree-Fock wavefunction.

When not only considering occupied, but also unoccupied or virtual atomic orbitals, one can increase the accuracy of the method. The size of the set of atomic orbitals used in the determinants characterizes the level of precision of these methods: configuration interaction [10], multi-configuration Hartree-Fock [11], multi-reference configuration interaction [12] and the coupled cluster methods [13, 14, 15] belong to this category and are nowadays routinely used to calculate molecular properties. Their accuracy is very high, and especially the coupled cluster approach can actually compete with experiment.

In the configuration interaction method, the wavefunction is a linear combination of Slater determinants constructed from occupied and virtual atomic basis functions, and the linear coefficients are varied to find the minimum of the total energy. In the limit of a complete atomic basis, the configuration interaction approaches yield the correct solution of the Schrödinger equation. In practice, the basis set is truncated after a few excited states. In the multi configuration configuration interaction method, not only the linear coefficients of the determinants, but also the orbital coefficients of the underlying atomic basis orbitals within each determinant are varied to find the minimum energy. This procedure basically speeds up the convergence with respect to the simple configuration interaction scheme. Another approach is the so-called Møller-Plesset perturbation theory (MP2), where the wavefunction contributions from excited states are taken into account through a perturbation theory calculation, starting with the standard Hartree-Fock determinants.

The disadvantage common to all these approaches is that they have a relatively high computational cost and are therefore restricted to small systems.

The definition of small changes in time, but the scaling of these methods with the system size is such that at a reasonable expense, only systems with less than roughly hundred atoms can be treated.

Density functional theory (DFT) is conceptually different from the previous approaches. In this method, the large-dimensional many body problem of interacting electrons is transformed into a system of equations of independent electrons. This method is described in detail in the following sections. It shall be noted here that in the following, DFT will be used as a synonym for ground state DFT. It has turned out that DFT is able to treat excited states as well [8], even though its results need to be used with more care. However, in this work, only the electronic ground state shall be considered.

3.4 Hohenberg Kohn theorems

Density functional theory is essentially based on two theorems by Hohenberg and Kohn [1]. The first one states:

> The all electron many body ground state wavefunction $\Psi(\mathbf{r}_1, \ldots, \mathbf{r}_n)$ of a system of n interacting electrons is a unique functional of the electronic density $n(\mathbf{r})$.
>
> $$\begin{aligned} \Psi(\mathbf{r}_1, \ldots, \mathbf{r}_n) &= \Psi[n(\mathbf{r})](\mathbf{r}_1, \ldots, \mathbf{r}_n) & (9) \\ n(\mathbf{r}) &= |\Psi(\mathbf{r}, \ldots, \mathbf{r})|^2 & (10) \end{aligned}$$

The immediate consequence of this theorem is that all physically measurable quantities based on the electronic structure are in fact unique functionals of the electronic ground state density alone. Note that in general, there is no closed expression for these functionals.

The proof of this theorem is based on the variational Ritz principle: The wavefunction which minimizes the energy functional, i.e. the expectation value of the Hamiltonian, is the ground state solution of the Schrödinger equation.

In Eq. (5), the electronic Hamiltonian is completely determined by the Coulomb potential of the nuclei, which can be generalized to a universal external potential $v(\mathbf{r})$. The all electron wavefunction being well defined through the variational principle from this fixed Hamiltonian, it follows that this wavefunction is a functional of this external potential. Thus, the Hohenberg Kohn theorem as stated above is equivalent to saying that the ground state electronic density determines the external potential. It shall be noted here that this external potential has nothing to do with the Coulomb potential the electronic density creates by itself, this interaction is taken into account by the second term in Eq. (5).

Assume there were two external potentials v and v' differing by more than a constant and leading to the same ground state density n. This density would be obtained through the solutions Ψ and Ψ' determined from the variational principle of the corresponding Hamiltonians $\mathcal{H}$ and $\mathcal{H}'$, respectively. Then, the following inequalities hold:

$$E_0 = \langle\Psi|\mathcal{H}|\Psi\rangle < \langle\Psi'|\mathcal{H}|\Psi'\rangle \tag{11}$$

$$E_0' = \langle\Psi'|\mathcal{H}'|\Psi'\rangle < \langle\Psi|\mathcal{H}'|\Psi\rangle \tag{12}$$

Adding Eq. (11) to Eq. (12) yields

$$\begin{aligned} E_0 + E_0' &< \langle\Psi'|\mathcal{H}|\Psi'\rangle + \langle\Psi|\mathcal{H}'|\Psi\rangle \\ &= \langle\Psi'|\mathcal{H}'|\Psi'\rangle + \langle\Psi'|\mathcal{H} - \mathcal{H}'|\Psi'\rangle \\ &\quad + \langle\Psi|\mathcal{H}|\Psi\rangle + \langle\Psi|\mathcal{H}' - \mathcal{H}|\Psi\rangle \\ 0 &< \langle\Psi'|\mathcal{H} - \mathcal{H}'|\Psi'\rangle + \langle\Psi|\mathcal{H}' - \mathcal{H}|\Psi\rangle. \qquad (13) \end{aligned}$$

But since the difference of the two Hamiltonians in Eq. (13) is equal to the difference of their external potentials, this becomes:

$$0 \ < \ \langle\Psi'|v - v'|\Psi'\rangle + \langle\Psi|v' - v|\Psi\rangle. \qquad (14)$$

This external potential, however, is a local operator, so that it can be expressed as a simple integral:

$$0 \ < \ \int d^3r \ [v(\mathbf{r}) - v'(\mathbf{r})] \ |\Psi'|^2(\mathbf{r}) + [v'(\mathbf{r}) - v(\mathbf{r})] \ |\Psi|^2(\mathbf{r}). \qquad (15)$$

But since the two solutions Ψ and Ψ' were supposed to give the same electronic density, $|\Psi'|^2(\mathbf{r}) = |\Psi|^2(\mathbf{r})$ and the right hand side of Eq. (15) vanishes and the inequality results in a contradiction

$$0 \ < \ 0. \qquad (16)$$

Therefore, there cannot be two external potentials that yield the same electronic density. Or, in other words, a given electronic density can be uniquely assigned to one external potential.

In this theorem, it is important to note that it can not be applied to any arbitrary density. Only densities that result from the solution Ψ of the true Schrödinger equation by Eq. 10) can be assigned to the originating external potential. If a density can be obtained this way, it is said to be v-representable.

The second Hohenberg Kohn theorem is essentially a minimum principle for the density. In contrast to the ordinary variational principle, which is formulated only with respect to the wavefunctions in combination with the energy functional, it states:

> For all v-representable densities n, the one that minimizes the energy functional with a given external potential is the ground state density, i.e. the density which corresponds to the solution of the Schrödinger equation.

The proof is a direct consequence of the first theorem and the ordinary variational principle: Given the external potential, the solution of the Schrödinger equation is obtained from the minimization of the energy functional with respect to the electronic wavefunction. All v-representable densities that differ from the ground state one can be assigned an originating wavefunction that differs from the variational one. Thus, the energy functional is not minimum for all of them.

The important drawback of this theorem is that it is only valid for v-representable densities. It is still a problem up to now that not every trial density has this property, so that by simple minimization of the energy functional, a non physical (not v-representable) density could be found.

Fortunately, it turns out that only a weaker condition needs to be imposed on the density [8], assuring practical usefulness of the Hohenberg Kohn theorems. A detailed discussion of this theoretical aspect, however, is out of the scope of this work.

3.5 Kohn Sham equations

The Hohenberg Kohn theorems show that it is possible in principle to calculate all quantities of physical interest from the electronic density alone. The remaining problem, how to find this density in practice, is more involved than it seems at first glance. In terms of wavefunctions, the total electronic energy is given by the expectation value of the Hamiltonian, Eq. (5):

$$E^{\mathrm{el}} = \mathcal{E}_{\mathrm{tot}}[\Psi] \;=\; \left\langle \Psi \left| \sum_i -\frac{1}{2}\nabla_i^2 + \frac{1}{2}\sum_{i\neq j}\frac{1}{|\mathbf{r}_i - \mathbf{r}_j|} + \sum_i v_{\mathrm{ext}}(\mathbf{r}_i) \right| \Psi \right\rangle \tag{17}$$

Here and in the following, calligraphic letters shall indicate a functional, whereas arabic ones designate a scalar quantity. There are no closed expressions to calculate the first two parts of the total energy directly from the electronic density only. In order to turn DFT into a practical tool for real calculations, Kohn and Sham [2] proposed an indirect approach to this functional. They introduce a fictitious parallel system of independent electrons that do not interact.

The idea is to define a new functional subtracting from Eq. (17) several terms calculated from the wave function of a non interacting gas of electrons with the same density as would have the exact solution of interacting particles. Let $|\varphi_i\rangle$ be the single particle wavefunctions of the independent electron gas. Its kinetic energy and density are:

$$\mathcal{T}[\varphi_i] \;=\; -\frac{1}{2}\sum_i \langle\varphi_i|\nabla^2|\varphi_i\rangle \tag{18}$$

$$n(\mathbf{r}) \;=\; |\varphi_i(\mathbf{r})|^2. \tag{19}$$

This density is by construction equal to the one created by the interacting electrons. If this density was a classical charge distribution, its interaction energy would be:

$$\mathcal{E}_{\mathrm{H}}[n] = \frac{1}{2}\int d^3r \int d^3r' \, \frac{n(\mathbf{r})n(\mathbf{r}')}{|\mathbf{r}-\mathbf{r}'|}. \tag{20}$$

$\mathcal{E}_H[n]$ is called he Hartree energy of the system. Finally, the interaction with the external potential remains:

$$\mathcal{E}_{\mathrm{ext}}[n] \quad = \quad \int d^3r \; v_{\mathrm{ext}}(\mathbf{r})n(\mathbf{r}) \tag{21}$$

Thus, the Kohn Sham energy functional of the fictitious non interacting system is:

$$\mathcal{E}_{\mathrm{KS}}[n] \quad = \quad \mathcal{T}[\varphi_{i[n(\mathbf{r})]}] + \mathcal{E}_{\mathrm{H}}[n] + \mathcal{E}_{\mathrm{ext}}[n]. \tag{22}$$

When substituting $\mathcal{T}$, $\mathcal{E}_{\mathrm{H}}$ and $\mathcal{E}_{\mathrm{ext}}$ in the energy functional of the interacting system, an error is introduced, even when assuming identical electronic densities. It contains all the many body effects, and it cannot be treated in an exact way. This difference between the correct functional and the one which can be computed, $\mathcal{E}_{\mathrm{KS}}$, is known as the exchange-correlation functional $\mathcal{E}_{\mathrm{xc}}$ of the system. Formally, it is given by the difference between Eq. (17) and Eq. (22):

$$\mathcal{E}_{\mathrm{xc}}[n] \quad = \quad \mathcal{E}_{\mathrm{tot}}[n] - \mathcal{E}_{\mathrm{KS}}[n]. \tag{23}$$

If this functional was known, one would be able to compute the the ground state density at fixed external potential by minimizing the total energy $\mathcal{E}_{\mathrm{KS}} + \mathcal{E}_{\mathrm{xc}}$. Since this is not the case, approximations have to be adopted for $\mathcal{E}_{\mathrm{xc}}$. They are discussed in the next section.

The minimization of the functional must be done requiring the electronic wavefunctions be orthonormal to each other:

$$\langle \varphi_i | \varphi_j \rangle \quad = \quad \delta_{\,ij} \;\; \forall i, j. \tag{24}$$

This is achieved by a Lagrange multiplier method [16] in combination with the stationarity condition for the energy functional:

$$\frac{\delta}{\delta\ \varphi_i(\mathbf{r})}\left(\mathcal{E}_{\mathrm{KS}} + \mathcal{E}_{\mathrm{xc}}\right) \quad = \quad 0. \tag{25}$$

This technique yields the Kohn Sham equations, which read:

$$\left[-\frac{1}{2}\nabla^2 + v_{\mathrm{H}}(\mathbf{r}) + v_{\mathrm{xc}}(\mathbf{r}) + v_{\mathrm{ext}}(\mathbf{r})\right]\varphi_i(\mathbf{r}) \quad = \quad \epsilon_i\, \varphi_i(\mathbf{r}). \tag{26}$$

Here, ϵ_i are the eigenvalues of the KS Hamiltonian and the potentials are the derivatives of the corresponding energy functionals with respect to the density:

$$v_{\mathrm{H}}(\mathbf{r}) \quad = \quad \frac{\delta}{\delta\ n(\mathbf{r})}\mathcal{E}_{\mathrm{H}}[n] \quad = \quad \int d^3r' \frac{n(\mathbf{r}')}{|\mathbf{r}-\mathbf{r}'|} \tag{27}$$

$$v_{\mathrm{xc}}(\mathbf{r}) \quad = \quad \frac{\delta}{\delta\ n(\mathbf{r})}\mathcal{E}_{\mathrm{xc}}[n] \tag{28}$$

$$v_{\mathrm{ext}}(\mathbf{r}) \quad = \quad \frac{\delta}{\delta\ n(\mathbf{r})}\mathcal{E}_{\mathrm{ext}}[n] \quad = \quad \sum_I \frac{Q_I}{|\mathbf{r}-\mathbf{R}_I|} \tag{29}$$

Since these potentials still depend on the density, Eq. (26) has to be solved self-consistently. For a density computed from a set of trial wavefunctions, the potentials are calculated, and inserted in (26). Then, a better set of trial wavefunctions is obtained and the procedure is repeated until no changes in the orbitals and the density occur any more.

At first sight, this single particle formulation due to Kohn and Sham has some similarity with a mean-field approach: the independent electrons move in the electrostatic field created by themselves and by the nuclei. However, all the many body effects are taken into account through the exchange-correlation functional, even if there is no straightforward way to write down this functional. Hence, the notion of a mean-field theory in terms of neglecting correlation and exchange effects is not correct.

3.6 Local Density Approximation

As already mentioned, DFT is formally an exact theory, but the difficulties related to the many body nature of the Schrödinger equation have only been reformulated in the exchange-correlation energy functional. To proceed to a practical calculation, an approximation has to be found for this expression. Even if nowadays, there is a tendency towards more elaborated theories, the most common one is the local density approximation (LDA) which yields good results in a large number of systems and which is still used in ab initio calculations [17, 7].

In this approximation, the exchange-correlation energy functional is chosen to have the same formal expression as has the one of a uniform electron gas with the same density:

$$\mathcal{E}_{\mathrm{xc}}^{\mathrm{LDA}} = \int d^3r\, \varepsilon_{\mathrm{xc}}(n(\mathbf{r}))\, n(\mathbf{r}), \tag{30}$$

where the function $\varepsilon_{\mathrm{xc}}(n(\mathbf{r}))$ depends locally on the density at the position $\mathbf{r}$. This function has been calculated through a Monte Carlo simulation [18], providing the total energy of the ground state of a homogeneous interacting electron gas. This data, which was obtained for several densities, has been parametrized [19], yielding a function usuable in Eq. (30).

Considering the way this approximation has been obtained, it is obvious that for a uniform system, it is exact. Further, it is expected to be still valid for a slowly varying electronic density. In other cases, its behaviour is not well controlled. It is used anyhow, mainly because of its ability to reproduce experimental ground state properties of many systems. Although there is no direct proof why it works correctly, it turns out that LDA can successfully deal with atoms, molecules, clusters, surfaces and interfaces. Even for dynamical processes like the phonon dispersion, it has been shown to yield good results [20, 21]. However, in the course of time, many systems have been found that are incorrectly described by LDA. The most popular examples of this class are dielectric constants and related quantities, as well as weak bonds, in particular hydrogen bonds. In the field of metals, the ground state structure of crystalline iron is predicted to be paramagnetic fcc instead of ferromagnetic bcc [22].

3.7 Gradient Corrections

Various approximations have been introduced in the course of the years to improve the local density approximation, but none of them has yet been generally accepted as being "the best". In this chapter, a class of gradient corrected (GC) functionals shall be presented that can in many situations significantly increase the accuracy of DFT calculations. These functionals assume that the exchange correlation energy does not only depend on the density, but also on its spatial derivative:

$$\mathcal{E}_{\mathrm{xc}}[n, \nabla n] \quad = \quad \int d^3r \, \varepsilon_{\mathrm{xc}}[n(\mathbf{r}), \nabla n(\mathbf{r})] \, n(\mathbf{r}) \tag{31}$$

Whether gradient corrections are an improvement over LDA or not is still under debate. In the past the years several GC functional were introduced and their properties were studied. In particular the description of the hydrogen bond, which plays a very important role in the systems investigated in this work, is well achieved using the exchange functional of Becke [23] and the correlation functional of Lee, Yang, and Parr [24] (BLYP), as discussed in ref. [25]. Their form of the exchange correlation function is:

$$\begin{aligned}
\varepsilon_{\mathrm{xc}} &= \varepsilon_{\mathrm{xc}}[n(\mathbf{r}), \nabla n(\mathbf{r})] \\
&= -\left(C_X + \beta \frac{x[n]^2}{1 + 6\beta \sinh^{-1} x[n]} \right) n^{1/3} \\
&\quad -a \, \frac{1 + b\, n^{-5/3} \left[C_F\, n^{5/3} - 2\tfrac{1}{9} t_W[n] + \tfrac{1}{18} \nabla^2 n \right] \mathrm{e}^{-c\, n^{-1/3}}}{1 + d\, n^{-1/3}} && (32) \\
x[n] &= \frac{|\nabla n|}{n^{4/3}} && (33) \\
t_W[n] &= \frac{1}{8} \frac{|\nabla n|^2}{n} - \frac{1}{8} \nabla^2 n && (34)
\end{aligned}$$

where for simplicity, an implicit dependence $n \equiv n(\mathbf{r})$ is assumed. The parameters $C_X, C_F, \beta, a, b, c, d$ are chosen in such a way that to fit the known exchange-correlation energy of selected atoms in their ground state.

3.8 Pseudopotential approximation

The Kohn Sham equations, Eq. (17), can be solved expanding the KS orbtials in a complete set of known basis functions. Among the various existing possibilities, only the plane wave (PW) basis set shall be discussed in further detail. When describing a periodic system, they have invaluable numerical advantages, besides their conceptual simplicity. PWs allow a simple integration of the Poisson equation for the calculation of the Hartree potential, Eq. (20), and for the calculation of the kinetic energy expression, Eq. (18).

Due to the large oscillations of the core orbitals in the neighborhood of the atoms, plane waves cannot be used directly in the Kohn Sham formalism, Eq. (26). These oscillations would require an enormous basis set size to be described with acceptable resolution. However, the total energies associated with the core orbitals are several orders of magnitude larger than those of the valence band wavefunctions. Further, chemical reactions involve exclusively the valence electrons which are relatively far away from the nuclei. In contrast to this, the core electrons remain almost unaffected by the chemical bonding situation. They can be approximated to be "frozen" in their core configurations. This approximation considerably simplifies the task of solving the Kohn Sham equations, by eliminating all the degrees of freedom related to the core orbitals.

This process of mapping the core electrons out of Eq. (26) is done by the introduction of pseudopotentials. In the Hamiltonian, the nuclear potential is replaced by a new one, whose lowest energies coincide with the energies of the valence electrons in an all-electron calculation. In addition, this pseudopotential is required to reproduce the shape of the valence wavefunctions in regions sufficiently far from the nucleus. Close to the nucleus, the strong oscillations of the valence orbitals due to orthogonality requirements in the all-electron case are smoothed out.

In a typical pseudopotential, there is an attractive Coulomb term, whose charge is given by the atomic valence, as well as a short-ranged term, which is supposed to reproduce the effects of core-valence orthogonality, core-valence Coulomb interaction, exchange and correlation between core and valence. In a practical pseudopotential, these requirements are only partially satisfied. Nevertheless, it turns out that pseudopotentials allow the description of the valence properties up to a very good accuracy with a reasonable number of plane waves.

Common pseudopotentials are mostly norm-conserving. This means that in addition to reproducing the all-electron valence wavefunctions outside a certain core radius, the charge of the pseudo-wavefunction inside this core region is required to be identical to the corresponding charge in an all-electron calculation. This can be achieved through non-local pseudopotentials of the form:

$$V_I(\mathbf{r}) \;=\; V_I^{\mathrm{loc}}(\mathbf{r}) + \sum_{l=0}^{l_{\max}} V_{I,l}^{\mathrm{nl}}(r)\,\mathcal{P}_l \tag{35}$$

where $\mathcal{P}_l$ is a projector on the angular momentum l:

$$\mathcal{P}_l \;=\; \sum_{m=-l}^{m=+l} |l,m\rangle\langle l,m| \tag{36}$$

with the spherical harmonics $|l,m\rangle$, the eigenfunctions of the angular momentum operator $(\mathbf{L}^2, L_3)$. The functions $V_I^{\mathrm{loc}}(\mathbf{r})$ and $V_{I,l}^{\mathrm{nl}}(r)$ are the local and nonlocal radial parts of the pseudopotential, respectively, and their concrete forms vary. These functions are optimized numerically in such a way that the criteria mentioned above are best satisfied. Several expressions have been proposed for $V_I^{\mathrm{loc}}(\mathbf{r})$ and $V_{I,l}^{\mathrm{nl}}(r)$ [26, 27, 28, 29, 30].

In general, it turns out that by means of pseudopotentials, the number of plane waves necessary to obtain physically meaningful valence orbitals is drastically reduced.

3.9 Plane wave representation

The electronic wavefunction can be represented in terms of basis functions. There are basically three possibilities for this:

- Localized basis sets have a direct physical meaning, derived from the atomic orbital picture. Often, radial Gaussians combined with spherical harmonics are used to this purpose. They are commonly used in quantum chemistry program packages, since they can be used in all-electron schemes to increase the overall accuracy.

- Plane waves are more suited for calculations of periodic solids, as they naturally have the desired periodicity. They have a striking conceptual simplicity, and the kinetic energy and Coulomb interaction expressions between them are straightforward to implement. In addition, plane waves are not attached to the ions, so that moving the latter during a simulation does not give rise to any Pulay forces [31]. To obtain a physical picture of the electronic state, they have to be transferred to direct space or R-space. This can be done very efficiently by using the Fast Fourier Transformations technique [32].

- Mixed schemes try to combine the advantages of localized basis functions in the regions close to the nuclei with the computationally very efficient description by plane waves in the interstitial space. Unfortunately, this combination induces an important complication of the formalism.

In the ab initio code underlying this work, plane waves are used as basis set. One of their drawbacks is that large oscillations in R-space cannot be represented easily. Nevertheless, when adopting the pseudopotential approximation as described above, the description is sufficiently accurate and provides an efficient method to analyze extended systems, in particular under periodic boundary conditions.

The electronic wavefunction in a periodic system can be written according to Bloch's theorem [9]:

$$\psi_{n,\mathbf{k}}(\mathbf{r}) \quad = \quad \varphi_{n,\mathbf{k}}(\mathbf{r})\ \exp[i\mathbf{k}\cdot\mathbf{r}], \tag{37}$$

with a wavevector $\mathbf{k}$, a band index n and a function $\varphi_{n,\mathbf{k}}(\mathbf{r})$ which is periodic in space, with the periodicity of the primitive cell:

$$\varphi_{n,\mathbf{k}}(\mathbf{r}+\mathbf{R}) \quad = \quad \varphi_{n,\mathbf{k}}(\mathbf{r}) \tag{38}$$

for any lattice vector $\mathbf{R}$. In the plane wave representation, this periodic function can therefore be expanded as:

$$\varphi_{n,\mathbf{k}}(\mathbf{r}) \quad = \quad \frac{1}{\sqrt{\Omega}} \sum_{\mathbf{G}} c_{n,\mathbf{k},\mathbf{G}}\ \exp[i\mathbf{G}\cdot\mathbf{r}], \tag{39}$$

where Ω is the volume of the primitive cell and $\mathbf{G}$ are the reciprocal space vectors. These vectors are characterized through

$$\frac{1}{2\pi}\ |\mathbf{G}\cdot\mathbf{R}| \quad \in \quad \mathbb{N} \tag{40}$$

with $\mathbb{N}$ representing the set of integer numbers and $\mathbf{R}$ being any lattice vector. Thus, Eq. (38) is automatically satisfied. In fact, Eq. (39) is a discrete complex Fourier series development of the wavefunction $\varphi_{n,\mathbf{k}}$. The coefficients can be obtained by means of the inverse transformation:

$$c_{n,\mathbf{k},\mathbf{G}} \quad = \quad \frac{1}{\sqrt{\Omega}} \int_{\Omega} d^3r\ \varphi_{n,\mathbf{k}}(\mathbf{r})\ \exp[-i\mathbf{G}\cdot\mathbf{r}]. \tag{41}$$

In practice, the wavefunction $\varphi_{n,\mathbf{k}}(\mathbf{r})$ is not known for all points $\mathbf{r}$ in space, but rather on a finite mesh. Thus, the integral in Eq. (41) must be transformed into a discrete sum. This transformation is discussed in detail in appendix A.

In the reciprocal space representation, the kinetic energy of an orbital can be simply written as

$$\begin{aligned}\mathcal{T}_n &= -\frac{1}{2}\left\langle\varphi_{n,\mathbf{k}}\right|\nabla^2\left|\varphi_{n,\mathbf{k}}\right\rangle &(42)\\ &= \frac{1}{2\Omega}\sum_{\mathbf{G}}\left|\mathbf{k}+\mathbf{G}\right|^2\left|c_{n,\mathbf{k}}\right|^2. &(43)\end{aligned}$$

The accuracy of a calculation is determined by the number of plane waves in the series (39). In practice, this is commonly controlled through a maximum value for the contribution to the kinetic energy expression, Eq. (43), called cut-off energy E_c. Only those vectors **G** are taken into account which satisfy

$$\frac{1}{2}\left|\mathbf{k}+\mathbf{G}\right|^2 \leq E_c. \tag{44}$$

For the calculation of large and disordered nonmetallic systems, it is often sufficient to consider only one particular value for the wavevector, the Gamma point $\mathbf{k}$=0. This approximation shall be assumed in the following parts of this work. Then, the orbitals are only labeled by their band index, n.

3.10 Density functional perturbation theory

The study of the ground state and its properties can provide a lot of information about the physics of the system. However, many experimentally accessible quantities are related to second derivatives of the system's total ground state energy. As a simple example, vibrational modes in a crystal are a product of the atomic movement in the harmonic potential of the crystal. This potential is nothing but the second derivative of the total energy with respect to the ionic positions.

The calculation of such quantities is actually possible in the framework of density functional perturbation theory (DFPT), presented in this chapter. In standard perturbation theory, a small perturbation operator $\lambda\mathcal{H}^{(1)}$ is added to the Hamiltonian $\mathcal{H}$ of a system and its action evaluated. In this work, a slightly different approach will be presented, using the variational principle at second order in the framework of DFT [33].

The starting point is the Kohn-Sham density functional, Eq. (22). It can be rewritten in terms of the density matrix defined by:

$$\rho\left(\mathbf{r},\mathbf{r}'\right)=\sum_{i,j}=\overline{\varphi}_i(\mathbf{r})S_{ij}^{-1}\varphi_j(\mathbf{r}') \tag{45}$$

where S_{ij}^{-1} is the inverse of the overlap matrix $S_{ij}=\langle\varphi_i|\varphi_j\rangle$. The functional then reads:

$$\mathcal{E}_{\text{KS}}[\rho\left(\mathbf{r},\mathbf{r}'\right)] = \frac{1}{2}\int d\mathbf{r}\int d\mathbf{r}'\delta\ (\mathbf{r}-\mathbf{r}')\nabla_{\mathbf{r}}^2\rho\left(\mathbf{r},\mathbf{r}'\right) \tag{46}$$

$$+\frac{1}{2}\int d\mathbf{r}\frac{|\rho\left(\mathbf{r},\mathbf{r}'\right)|^2}{|\mathbf{r}-\mathbf{r}'|}+\mathcal{E}_{\text{xc}}[n]+\mathcal{E}^{\text{ext}}[n], \tag{47}$$

where the density n is simply

$$n(\mathbf{r}) = \rho\left(\mathbf{r},\mathbf{r}\right). \tag{48}$$

To take into account the external perturbation, a perturbation functional of arbitrary form is added to $\mathcal{E}_{\text{KS}}$:

$$\mathcal{E}_{\text{tot}}\left[\{|\varphi_i\rangle\}\ \right] = \mathcal{E}_{\text{KS}}\left[\{|\varphi_i\rangle\}\ \right]+\lambda\mathcal{E}_{\text{p}}\left[\{|\varphi_i\rangle\}\ \right]. \tag{49}$$

Here, λ is a small perturbative parameter and represents the strength of the interaction with the static, but otherwise arbitrarily complex external field $\mathcal{E}_{\text{p}}$.

The total functional Eq. (49) will have a minimum which is expanded perturbatively in powers of λ:

$$E = E^{(0)} + \lambda E^{(1)} + \lambda^2 E^{(2)} + \ldots \tag{50}$$

Similarly, the KS orbitals that minimize $\mathcal{E}_{\text{tot}}$ can be expanded in λ:

$$\varphi_i = \varphi_i^{(0)} + \lambda\varphi_i^{(1)} + \lambda^2\varphi_i^{(2)} + ... \tag{51}$$

To first order, the charge density reads:

$$n(\mathbf{r}) = n^{(0)}(\mathbf{r}) + \lambda n^{(1)}(\mathbf{r}) + \ldots \tag{52}$$

where

$$n^{(1)}(\mathbf{r}) = \sum_{i=1}^{N} \overline{\varphi}_i^{(0)}(\mathbf{r})\varphi_i^{(1)}(\mathbf{r}) + \overline{\varphi}_i^{(1)}(\mathbf{r})\varphi_i^{(0)}(\mathbf{r}). \tag{53}$$

The second-order energy of the system which is variational in the first order perturbation wavefunctions $\varphi^{(1)}$ can now be obtained by expanding Eq. (49) up to the second power in λ. The calculation yields [33]:

$$\begin{aligned} E^{(2)} = & \sum_k \left[\langle\varphi_k^{(1)}| \frac{\partial\,\mathcal{E}_{\text{p}}\left[|\varphi^{(0)}\rangle\right]}{\partial\,\langle\varphi_k|} + \frac{\partial\,\mathcal{E}_{\text{p}}\left[|\varphi^{(0)}\rangle\right]}{\partial\,|\varphi_k\rangle} |\varphi_k^{(1)}\rangle \right] \\ & + \sum_{kl} \langle\varphi_k^{(1)}|\mathcal{H}^{(0)}\,\delta_{\,kl} - \lambda_{kl}|\varphi_l^{(1)}\rangle \\ & + \frac{1}{2}\int \mathrm{d}^3r\, \mathrm{d}^3r'\, \frac{\delta^{\,2}\mathcal{E}_{\text{Hxc}}[n^{(0)}]}{\delta\, n(\mathbf{r})\delta\, n(\mathbf{r}')} n^{(1)}(\mathbf{r})n^{(1)}(\mathbf{r}'). \end{aligned} \tag{54}$$

The functional $\mathcal{E}_{\text{Hxc}}$ represents the sum of the Hartree and exchange-correlation energy functionals. The Lagrange multipliers λ_{kl} are the matrix elements of the KS-Hamiltonian $\mathcal{H}^{(0)}$:

$$\mathcal{H}^{(0)} = \mathcal{H}_{\text{KS}} \tag{55}$$

$$\lambda_{kl} = \langle\varphi_k^{(0)}|\mathcal{H}^{(0)}|\varphi_l^{(0)}\rangle, \tag{56}$$

The orthonormality of the total wavefunctions, expanded to first order in the perturbation, yields

$$\langle \varphi_k^{(0)} | \varphi_k^{(1)} \rangle + \langle \varphi_k^{(1)} | \varphi_k^{(0)} \rangle \quad = \quad 0 \quad \forall\, k. \tag{57}$$

This is achieved by imposing a general orthogonality condition on the first order perturbation wavefunctions:

$$\langle \varphi_k^{(0)} | \varphi_l^{(1)} \rangle \quad = \quad 0 \qquad \forall\, k, l. \tag{58}$$

This also automatically implies the conservation of the total charge of the system, by enforcing the integrated perturbation charge $q^{(1)}$ to vanish:

$$q^{(1)} \quad = \quad \int \mathrm{d}^3 r \;\, n^{(1)}(\mathbf{r}) \quad = \quad 0. \tag{59}$$

In many cases, the perturbation functional $\mathcal{E}_\mathrm{p}$ can be written as the expectation value of a perturbation Hamiltonian $\mathcal{H}^{(1)}$:

$$\mathcal{E}_\mathrm{p}[\{|\varphi_i\rangle\}] \quad = \quad \sum_k \langle \varphi_k |\, \mathcal{H}^{(1)} \,| \varphi_k \rangle. \tag{60}$$

However, the formulation through an arbitrary functional also allows orbital specific perturbations, i.e. a perturbation Hamiltonian that depends on k:

$$\mathcal{E}_\mathrm{p}[\{|\varphi_i\rangle\}] \quad = \quad \sum_k \langle \varphi_k |\, \mathcal{H}_k^{(1)} \,| \varphi_k \rangle. \tag{61}$$

In conclusion, the second order energy, Eq. (54), is variational in the first order perturbation wavefunctions, satisfying the stationarity condition:

$$\frac{\delta \;\, E^{(2)}}{\delta \;\, \varphi^{(1)}} \quad = \quad 0 \tag{62}$$

under the orthogonality constraint of Eq. (58).

4 Construction of localized orbitals

4.1 General

The approach presented in this work is based on the localized nature of the orbitals used in the calculation. Their exponential decay is vital for the procedure described in the next chapters. In this chapter, the procedure which is used to obtain localized orbitals shall be described in detail. These localized orbitals are also called Wannier functions [34], and the procedure to obtain them from canonical wavefunctions is closely related to the one presented by Berghold et al. [35].

The Kohn-Sham wavefunctions returned by a standard energy minimization (see section 3.1) are Bloch states that extend over the whole crystal and do never vanish. Thus, an additional treatment is neccessary to transform them in order to obtain orbitals with the desired spatial localization properties. In a periodic system, there is a fundamental problem when characterizing the degree to which a wavefunction is localized. The localization is usually quantified through a spread functional, commonly the second moment of the wavefunction:

$$\Delta_k^{(2)} \;=\; \langle\varphi_k\,|\mathbf{r}^2|\varphi_k\,\rangle - \langle\varphi_k\,|\mathbf{r}|\varphi_k\,\rangle^2. \tag{63}$$

Basically, the localization procedure corresponds to a minimization of this spread functional by applying a unitary rotation to the manifold of occupied states. Such a rotation leaves the electronic density invariant, so that the new ensemble of states still represents the electronic ground state.

In a periodic system, these expectation values of the position operator inside a Bloch state are not well defined a priori. However, it has been shown [36, 37, 38, 39] that the spread as such described by Eq. (63) can be quantified in a physically reasonable way, even in a periodic system.

4.2 Definition of localized orbitals

Wannier functions (WF) are defined in terms of a unitary transformation performed on the occupied Bloch orbitals (BO) [34]. One major problem in a practical calculation is their non-uniqueness. This is a result of the indeterminacy of the BOs, which are, in the case of a single band, only determined up to a phase factor, in the multi-band case, up to an arbitrary unitary transformation among all occupied orbitals at every point in the Brillouin zone. As proposed recently by Marzari and Vanderbilt [36], one can resolve this non-uniqueness by requiring that the total spread of the localized function be minimal. This criterion is in close analogy with the Boys-Foster method [40] for finite systems, here one uses the spread defined through the conventional position operator. The new technique has been successfully applied to crystal systems and to small molecules within a general **k**-point scheme [36]. An extension to disordered systems within the **Γ**-point approximation was recently performed [37]. This is of particular interest when one would like a localized orbital picture within the framework of Car-Parrinello molecular dynamics (CPMD).

Here, the subject of investigation is the problem focusing on the **Γ**-point approximation only. For this case, Silvestrelli [41] has derived a formula for the spread in three dimensions for a molecular dynamics cell of arbitrary shape. The formula is based on the formulation of Marzari and Vanderbilt. Recently Resta has proposed a formula for the spread in one dimension which reduces to that of Marzari and Vanderbilt in the limit of large cell size [39]. Resta's formulation can be generalized to three dimensions and arbitrary molecular dynamics cells.

Upon minimization of the spread functional, the appropriate unitary transformation to the localized orbitals can be calculated. With explicit knowledge of the spread functional, one can derive the complete expressions required to implement the iterative minimization procedure beyond a steepest descent scheme. The steepest descent method, used in [36, 41], performs reasonably well for simple molecular systems, but it is known to have convergence problems when more complicated systems are analyzed. This can only be remedied by calculating the required gradient of the spread functional without any simplification, thus allowing the iterative calculation of maximally-localized orbitals with very efficient optimization schemes.

4.3 Derivation of the functional

First, the work of Resta [38] shall be reviewed. In his treatment, the fundamental object for studying localization of an electronic state within Born–von Karman boundary conditions is the dimensionless complex number z:

$$z = \int_L dx \;\exp(i2\pi x/L)\, |\psi(x)|^2 \; . \tag{64}$$

Here, L is the linear dimension, and $\psi(x)$ denotes the wavefunction. By considering the definition of the spread of the wavefunction to be $\Delta^{(2)} = \langle x^2 \rangle - \langle x \rangle^2$, where $\langle \cdots \rangle$ denotes an expectation value, Resta has shown that up to order $\mathcal{O}(1/L^2)$, the functional for the spread in one-dimension can be taken as:

$$\Delta^{(2)} = \frac{1}{(2\pi)^2} \ln |z|^2. \tag{65}$$

One goal of this section is to generalize Eq. (64) to three dimensions and thus to obtain the appropriate generalization of Eq. (65). To this effect, the following dimensionless complex number is used within Born–von Karman boundary conditions:

$$z_I = \int_V d^3r \ \exp(i\mathbf{G}_I \cdot \ \mathbf{r}) \ |\psi(\mathbf{r})|^2. \tag{66}$$

Here, I represents a general reciprocal lattice vector, $\mathbf{G}_I = l_I\mathbf{b}_1 + m_I\mathbf{b}_2 + n_I\mathbf{b}_3$, where $\mathbf{b}_\alpha$ are the primitive reciprocal lattice vectors, the integers l, m, and n are the Miller indices, V is the volume of the supercell, and $\psi(\mathbf{r})$ denotes the wavefunction.

First, an appropriate function must be found that gives the three dimensional spread in the case of an arbitrary simulation cell in function of these numbers z_I.

It shall be assumed that in a molecular dynamics simulation the cell parameters (primitive lattice vectors) to describe systems of general symmetry are given by $\mathbf{a}_1$, $\mathbf{a}_2$ and $\mathbf{a}_3$. It is convenient to form a matrix of these cell parameters:

$$\overleftrightarrow{\mathbf{h}} \ = \ (\mathbf{a}_1, \mathbf{a}_2, \mathbf{a}_3) \tag{67}$$

where the volume V of the simulation cell is given by the determinant of $\overleftrightarrow{\mathbf{h}}$. It is also very useful to define scaled coordinates,

$$\mathbf{s} \ = \ \overleftrightarrow{\mathbf{h}}^{-1} \cdot \ \mathbf{r} \tag{68}$$

that lie in the unit cube.

In molecular dynamics simulations, this simplifies the work with periodic boundary conditions for systems with general symmetry, by means of first transforming to the unit cube, assuming standard cubic periodic boundary conditions, and transforming back to the general cell through the action of $\overleftrightarrow{\mathbf{h}}$ [42].

One can also compute the reciprocal space vectors for systems of general symmetry with knowledge of the matrix of cell parameters. The I-th reciprocal lattice vector is given by:

$$\mathbf{G}_I = 2\pi \left(\overleftrightarrow{\mathbf{h}}^{-1} \right)^{\mathrm{T}} \cdot \ \hat{\mathbf{g}}_I. \tag{69}$$

Here, the superscript T denotes transposition, and $\hat{\mathbf{g}}_I = (l_I, m_I, n_I)$ is the I-th Miller index. This expression is substituted into Eq. (66), and with the definition of $\mathbf{r}$, one obtains:

$$z_I = \det \overleftrightarrow{\mathbf{h}} \int_0^1 d^3s \ \exp\left(i2\pi \hat{\mathbf{g}}_I^{\mathrm{T}} \cdot \ \mathbf{s} \right) \ |\psi(\overleftrightarrow{\mathbf{h}} \ \cdot \ \mathbf{s})|^2. \tag{70}$$

The exponential in Eq. (70) is independent of any coordinate system. Following Resta [38], one can write the electron density in terms of a superposition of localized density $n_{\mathrm{loc}}(\mathbf{r})$ and its periodic images:

$$\left| \psi(\overleftrightarrow{\mathbf{h}} \ \cdot \ \mathbf{s}) \right|^{\,2} \ = \ \sum_{\hat{\mathbf{m}}=-\infty}^{\infty} n_{\mathrm{loc}} \left(\overleftrightarrow{\mathbf{h}} \cdot (\mathbf{s} - \mathbf{s}_0 - \hat{\mathbf{m}}) \right). \tag{71}$$

Here, $\hat{\mathbf{m}}$ is a vector of integers and $\overleftrightarrow{\mathbf{h}} \ \cdot \ \mathbf{s}_0$ is the center of the distribution such that

$$\int_{-\infty}^{\infty} d^3s \ \overleftrightarrow{\mathbf{h}} \cdot (\mathbf{s} - \mathbf{s}_0) \ n_{\mathrm{loc}} \left(\overleftrightarrow{\mathbf{h}} \cdot (\mathbf{s} - \mathbf{s}_0) \right) = 0. \tag{72}$$

Using the Poisson summation formula [43], Eq. (70) can be rewritten as:

$$z_I = \exp\left(i2\pi \hat{\mathbf{g}}_I^{\mathrm{T}} \cdot\ \mathbf{s}_0\right)\ \hat{n}_{\mathrm{loc}}\left(-2\pi \hat{\mathbf{g}}_I^{\mathrm{T}} \cdot\ \overleftrightarrow{\mathbf{h}}^{-1}\right), \tag{73}$$

where $\hat{n}_{\mathrm{loc}}$ denotes the Fourier transform of n_{loc}. Furthermore, since n_{loc} is considered to be localized, its Fourier transform is smooth over reciprocal distances and it can be assured that it is well represented about $\hat{g}_I = 0$. Expanding $\hat{n}_{\mathrm{loc}}(-2\pi \hat{\mathbf{g}}_I^{\mathrm{T}} \cdot\ \overleftrightarrow{\mathbf{h}}^{-1})$ to second order, one obtains:

$$\begin{aligned}
&\hat{n}_{\mathrm{loc}}\left(-2\pi \hat{\mathbf{g}}_I^{\mathrm{T}} \cdot\ \overleftrightarrow{\mathbf{h}}^{-1}\right) \\
&= 1 + \sum_{\alpha} \hat{g}_{\alpha,I}\ \left.\frac{\partial\, \hat{n}_{\mathrm{loc}}}{\partial\, \hat{g}_{\alpha,I}}\right|_{\hat{g}_I=0} \\
&+ \frac{1}{2}\sum_{\alpha,\beta} \hat{g}_{\alpha,I}\hat{g}_{\beta,I}\ \left.\frac{\partial^{\,2} \hat{n}_{\mathrm{loc}}}{\partial\, \hat{g}_{\alpha,I}\partial\, \hat{g}_{\beta,I}}\right|_{\hat{g}_I=0} + \ldots .
\end{aligned} \tag{74}$$

The second term in Eq. (74) is zero because of $\left\langle \overleftrightarrow{\mathbf{h}} \cdot \mathbf{s}\right\rangle = 0$. Thus:

$$\begin{aligned}
\hat{n}_{\mathrm{loc}}\left(-2\pi \hat{\mathbf{g}}_I^{\mathrm{T}} \cdot\ \overleftrightarrow{\mathbf{h}}^{-1}\right) &= \\
1 - \frac{(2\pi)^2}{2} V \sum_{\alpha,\beta} \hat{g}_{\alpha,I}\hat{g}_{\beta,I} \int_{-\infty}^{\infty} d^3s\ s_\alpha s_\beta\ n_{\mathrm{loc}}\left(\overleftrightarrow{\mathbf{h}}\ \cdot\ \mathbf{s}\right).
\end{aligned} \tag{75}$$

Combining Eq. (75) and Eq. (73), it follows that:

$$1 - |z_I| = V\,\frac{(2\pi)^2}{2} \sum_{\alpha,\beta} \hat{g}_{\alpha,I}\hat{g}_{\beta,I} \int_{-\infty}^{\infty} d^3s\ s_\alpha s_\beta\ n_{\mathrm{loc}}\left(\overleftrightarrow{\mathbf{h}}\ \cdot\ \mathbf{s}\right). \tag{76}$$

Keeping in mind that

$$\int_{-\infty}^{\infty} d^3s\ \overleftrightarrow{\mathbf{h}}\ \cdot\ \mathbf{s}\, n_{\mathrm{loc}}\left(\overleftrightarrow{\mathbf{h}}\ \cdot\ \mathbf{s}\right) \ = \ 0, \tag{77}$$

one can define the spread of the electronic distribution for the case of a general box through:

$$
\begin{aligned}
\langle r^2\rangle - \langle r\rangle^2 &= \left\langle \left(\overleftrightarrow{\mathbf{h}} \cdot \mathbf{s}\right)^2 \right\rangle \\
&= \sum_{\alpha,\beta} g_{\alpha\beta}\, V \int_{-\infty}^{\infty} d^3s\; s_\alpha s_\beta\; n_{\mathrm{loc}}\left(\overleftrightarrow{\mathbf{h}} \cdot \mathbf{s}\right). \qquad (78)
\end{aligned}
$$

Here, $g_{\alpha\beta} = \sum_\mu \overleftrightarrow{\mathrm{h}}^{\mathrm{T}}_{\alpha\mu} \overleftrightarrow{\mathrm{h}}_{\mu\beta}$ can be thought of as a metric tensor to describe the corresponding distances in the unit cube. Eq. (78) shows exactly how the length scales are built into the spread through the metric tensor. From direct comparison of Eq. (76) and Eq. (78) it follows that for supercells of general symmetry, linear combinations of $\hat{g}_{\alpha,I}\hat{g}_{\beta,I}$ need to be chosen that reproduce the metric tensor, $g_{\alpha\beta}$. However, as stated earlier, $\hat{g}_{\alpha,I}$ are dimensionless numbers. Thus, an appropriate generalization takes the form of a sum rule,

$$
g_{\alpha\beta} \;=\; \sum_I \omega_I\; \hat{g}_{\alpha,I}\; \hat{g}_{\beta,I}. \qquad (79)
$$

Here, ω_I are the "weights" with appropriate dimensions that have to be determined [35].

Thus, it is also clear that $g_{\alpha\beta}$ will have at most six independent entries (for triclinic symmetry), and thus that a maximum of six weights are needed. It is interesting to note that by multiplying Eq. (79) on the left and right hand sides by $\overleftrightarrow{\mathbf{h}}^{-1}$ and using the definition of $\mathbf{G}_I$, one will recover the rule used by Silvestrelli [41] and by Marzari and Vanderbilt [36].

Finally, the generalization to more than one state, $|\varphi\rangle \rightarrow |\varphi_n\rangle$ yields for the desired spread expression $\Delta^{(2)}$ in a supercell of general symmetry:

$$\begin{aligned}\Delta^{(2)} &= \frac{2}{(2\pi)^2} \sum_{n}^{\mathrm{N_{states}}} \sum_{I} \omega_I \left(1 - |z_{I,n}|\right) \\ &\quad + \mathcal{O}\left(2\pi \hat{\mathbf{g}}_I^{\mathrm{T}} \cdot \overleftrightarrow{\mathbf{h}}^{-1}\right)^2 \qquad (80)\\ z_{I,n} &= \int_V d^3r \; \exp(i\mathbf{G}_I \cdot \mathbf{r}) \, |\varphi_n(\mathbf{r})|^2, \qquad (81)\end{aligned}$$

where Eq. (79) determines the $\mathbf{G}_I$.

At this point, it is useful to make contact with other spread formulae that are present in the current literature. Following Resta's derivation [39], one finds the following formula:

$$\Delta^{(2)} = -\frac{1}{(2\pi)^2} \sum_{n}^{\mathrm{N_{states}}} \sum_{I} \omega_I \log |z_{I,n}|^2 \;, \qquad (82)$$

with $z_{I,n}$ defined as above. Eq. (82) is obtained by inserting Eq. (75) into Eq. (73), taking the logarithm of the absolute value and expanding to consistent order.

Silvestrelli [41] on the other hand uses:

$$\Delta^{(2)} = \frac{1}{(2\pi)^2} \sum_{n}^{\mathrm{N_{states}}} \sum_{I} \omega_I \left(1 - |z_{I,n}|^2\right), \qquad (83)$$

with a similar defininition for $z_{I,n}$. Obviously Eq. (83) is obtained from Eq. (82) by an expansion of the logarithm.

At first glance, it seems confusing that there are different definitions for the spread. Admittedly, one has to keep in mind that all formulae are only valid up to the order given in Eq. (80). Thus, although different, they are consistent and there is no fundamental reason to choose one definition of the spread over another. In [35], the spreads of various model systems using all different definitions are compared to each other. It turns out that for the calculation of magnetic response properties, the choice of the spread functional is of minor importance.

One can also derive a general expression for the expectation value of the periodic position operator for computing the center of the localized function. Recall, that for a cubic simulation supercell, the expectation value of the position operator is given as:

$$\begin{aligned} r_{\alpha,n} &= -\frac{L}{2\pi}\Im\ \log z_{\alpha,n} \\ z_{\alpha,n} &= \int_V d^3r\ \exp(i\mathbf{g}_\alpha\cdot\ \mathbf{r})\ \ |\varphi_n(\mathbf{r})|^2, \end{aligned} \tag{84}$$

where $\hat{\mathbf{g}}_1 = (1,0,0)$, $\hat{\mathbf{g}}_2 = (0,1,0)$, and $\hat{\mathbf{g}}_3 = (0,0,1)$, and $\Im$ denotes the imaginary part. Again, the salient feature of Eq. (84) is that the expectation value of the exponential is invariant with respect to the choice of the cell. Thus, a general equation for the expectation value of the position operator in supercells of arbitrary symmetry is:

$$r_{\alpha,n} = -\frac{1}{2\pi}\sum_\beta \overleftrightarrow{\mathrm{h}}_{\alpha\beta}\ \Im\ \log z_{\alpha,n}. \tag{85}$$

It is important to note that Eq. (85) gives a suitable definition only for the *expectation value* of the position operator, and not for the operator itself. Regardless of the choice of the actual spread functional, the definition is always based on the translation operator and its matrix elements, $z_{\alpha,n}$. The fundamental aspect that underlies this concept is the intrinsic translational invariance of a system described through periodic boundary conditions.

In contrast to this, rotational invariance is impossible to achieve within the periodic description. As will be shown lateron (section 5), the formalism which describes the effect of a magnetic field is based on the application of the generator of the rotation operator, which is the angular momentum **L**, in periodic boundary conditions. So far, there is no theory that allows a proper re-definition of the expectation value and related quantities in periodically repeated systems. Therefore, the approach of this chapter cannot be generalized directly to incorporate magnetic response. It is only useful to transform the extended Bloch states, resulting from a total energy minimization, to localized orbitals which are spatially confined. While in principle, the energy is invariant under this kind of operations, the idea presented in the following sections is based on this peculiar property.

4.4 Localization procedure

Having established the definition of the spread formulae in the context of the wavefunctions, one can proceed to a description of their computation.

The mathematical problem which defines the localization procedure is to find the unitary transformation, U on the orbitals,

$$|\tilde{\varphi}_n\rangle = \sum_i U_{in} |\varphi_i\rangle, \tag{86}$$

that minimizes the spread functional, $\Delta^{(2)}$. To present a general formulation, it is convenient to work with a generalized form,

$$\begin{aligned} \Delta^{(2)} &= -\sum_n \sum_I f\left(|z_{I,n}|^2\right) && (87) \\ z_{I,n} &= \langle \varphi_n | \mathcal{O}^I | \varphi_n \rangle, && (88) \end{aligned}$$

where f and $\mathcal{O}^I$ denote an appropriate function and operator.

Neglecting the weights and constants in favour of simplicity, the different spread functionals of the last section are obtained, defined through Eq. (80), (82) and (83) by setting:

$$\begin{aligned} \mathcal{O}^I &= \exp(i\mathbf{G}_I \cdot\ \mathbf{r}) && (89)\\ f_1\left(|z_{I,n}|^2\right) &= \sqrt{|z_{I,n}|^2} = |z_{I,n}| && (90)\\ f_2\left(|z_{I,n}|^2\right) &= \log\left(|z_{I,n}|^2\right) && (91)\\ f_3\left(|z_{I,n}|^2\right) &= |z_{I,n}|^2. && (92) \end{aligned}$$

The values of index, I will range at most from one to six.

The actual calculation of maximally localized WFs or maximally localized MOs within the localization procedure is relatively simple. The starting point is always the output of a conventional electronic structure calculation, (BOs in the periodic, MOs in the finite case), and a given choice for the spread functional. Then, the unitary transformation U has to be calculated, producing the orbitals that minimize Eq. (87). As stated earlier, there are two choices for the spread functional for finite systems and three choices for periodic systems.

A maximally localized function is characterized through the stationary condition of the spread functional:

$$\frac{\partial\, \Delta^{(2)}}{\partial\, U_{ij}} = 0, \qquad (93)$$

where U is taken to be real within the $\boldsymbol{\Gamma}$-point approximation. There are two principal alternatives for parametrizing the unitary transformation, U, first as a direct product of elementary plane rotations, and second as the exponential of an antisymmetric matrix. The first parametrization scheme, discussed in the next subsection, amounts to the well known Jacobi optimization procedure for finding eigenvalues of general matrices. The second parametrization choice of U, is based on the exponential alternative as investigated in [35].

4.5 Orbital rotations

The traditional method in quantum chemistry for computing localized MOs is the method of two-by-two orbital rotations first introduced by Edmiston and Ruedenberg [44]. The basic idea of the method is to tackle the problem of finding U by performing a sequence of consecutive two-by-two rotations among all pairs of orbitals. The elementary step consists of a plane rotation where two orbitals i and j are rotated through an angle, ϕ . To proceed an optimal angle must be selected to ensure that the spread functional, as defined in Eq. (87), is iteratively minimized. The transformed expectation values are denoted with $\tilde{z}_{I,i/j}$ and are obtained through the standard two dimensional rotation with an angle ϕ :

$$\begin{aligned} \tilde{z}_{I,i} &= \cos(\phi\ ) z_{I,i} + \sin(\phi\ ) z_{I,j} \\ \tilde{z}_{I,j} &= -\sin(\phi\ ) z_{I,i} + \cos(\phi\ ) z_{I,j}. \end{aligned} \tag{94}$$

Thus, by combining Eq. (94) with Eq. (87), it is straightforward to calculate the change in the functional value, $\delta\ \Delta^{(2)}$ as a function of ϕ . The most natural way to obtain the optimal angle which maximizes the change in the functional value is to compute the stationary point of $\Delta^{(2)}$ with respect to ϕ , thus solving

$$\frac{\partial\, \delta\ \Delta^{(2)}_{ij}}{\partial\, \phi} = 0. \tag{95}$$

The explicit calculation yields:

$$\tan(4\phi) = -\frac{a}{b} \tag{96}$$

with

$$\begin{aligned} a &= \Re\left[M_{ij}\left(\bar{M}_{ii} - \bar{M}_{jj}\right)\right] && (97) \\ b &= |M_{ij}|^2 - \frac{1}{4}|M_{ii} - M_{jj}|^2 && (98) \\ M_{ij} &= \sum_I z_{I,ij} && (99) \end{aligned}$$

where $\Re$ denotes the real part. The solutions of Eq. (96) corresponding to maxima and minima are given by:

$$\phi + n\pi/4, \qquad n \in \mathbb{Z}, \tag{100}$$

For the desired minimum, the condition

$$\begin{aligned} \frac{\partial^2 \delta\Delta^{(2)}}{\partial \phi^2} &= 16\, b \cos(4\phi) - 16\, a \sin(4\phi) && (101) \\ &< 0 && (102) \end{aligned}$$

has to be fulfilled.

Unfortunately, one severe restriction applies to the derivation presented above. Eq. (96) is only valid for the choice f_3 of the function, Eq. (92), corresponding to the Silvestrelli-Marzari-Vanderbilt, the Boys and the Pipek-Mezey functional. In the other cases, $f_1(x) = \sqrt{x}$ and $f_2(x) = \log(x)$, Eqs. (90) and (91), no analogous formula is derivable. The reason is that the explicit solution of Eq. (95) with respect to ϕ seems not analytically tractable. Nevertheless, one can still implement the method of orbital rotations in the above cases by a numerical maximization of $\delta\Delta^{(2)}$ as a function of ϕ using derivative information. A detailed description of the implementation of this scheme is contained in [35].

5 Chemical shifts and susceptibilities

5.1 General

When a magnetic field is applied to a medium, it interacts with the electrons contained in this medium and modifies their ground state. The electrons react by creating a current distribution which itself induces an additional magnetic field. In contrast to the external one, the latter is not constant in space, so that the sum of both fields is inhomogeneous as well. Its spatial distribution depends very sensitively on the electronic structure in the system. In particular, its values at the positions of non-equivalent nuclei are different. As already mentioned in the introduction, section 2, the strength of the total magnetic field at an atomic position determines the resonance frequency of the nuclear spin. By means of the resonance spectrum of a system, the electronic structure of a system can thus be analyzed in great detail.

The simplest experimental arrangement to measure such a spectrum consists of irradiating with a varying radio frequency until resonance occurs. This setup is called sweeping or continuous-wave-technique. It is nowadays only used in tutorials, but it nevertheless represents the fundamental resonance experiment. State-of-the-art apparatus measure with the Fourier spectroscopy technique, where the sample is submitted to a pulse of large frequency bandwidth. This pulse turns the nuclear spins into a plane orthogonal to the homogeneous external field, inducing a subsequent precession movement. Since the angular velocity of this precession depends on the strength of the local magnetic field, which is inhomogeneous, the individual spins have different precession frequencies. This effect makes the net spin relax, still being confined in the plane orthogonal to the external field. This relaxation can be measured, and through an inverse Fourier transform, the normal absorption spectrum can be obtained.

Further, the spins also relax back to their original orientation, which is parallel to the external field. This second relaxation is induced by thermal transitions as well as by dipolar coupling between the spins. It represents a second quantity that is experimentally accessible.

In normal experiments, dipolar coupling represents a perturbation of the actual measurement, since the dipolar field may have a strength comparable to the electronically induced one. In the usual case of a non-regular arrangement of the atoms, the dipolar field has a random pattern and leads thus to a broadening of the resonance lines. The information contained in the spectrum can be significantly reduced by this effect. In the liquid and gas phases, the fast particle movement averages out these perturbing dipolar interactions, since the timescale of the brownian movement is smaller than the time window of the experiment. However, in solids, these interactions are a serious problem, because the atoms are quasistatic during the NMR measurement. To compensate this problem, a special technique exists. When the sample is spinned about its own axis under a particular angle of 54.2° relative to the external magnetic field, the average internuclear vector between spins will form that same angle with the external field, making the dipole-dipol interactions vanish. The higher the rotation frequency is, the thinner the dipolar broadening becomes. The upper limit of this frequency is determined by the mechanical properties of the sample and the sample holder, which usually allow a spinning up to a few 10 kHz. This method of rotating the sample is called *Magic Angle Spinning*, after the "magic" angle of 54.2°.

Both relaxation times provide a lot of information about the structure of the investigated system. However, because of the long timescale of the involved relaxation processes, they can not be calculated directly by *ab-initio* approaches. Only their interaction parameters can be determined. In particular, the calculation of the chemical shift, which represents the strength of the field induced by the electronic currents, will be the subject of this section.

5.2 Hamiltonian formalism

The standard procedure to obtain the orbital electronic current density $\mathbf{j}$ is perturbation theory. The starting point is the electron in its ground state without any external field, the so-called unperturbed system. Its Hamiltonian shall be denoted $\mathcal{H}^{(0)}$, it is given by

$$\mathcal{H}^{(0)} = \frac{1}{2m}\mathbf{p}^2 + \mathcal{V}(\mathbf{r}). \tag{103}$$

All quantities appearing in Eq. (103) are related to the electron: $\mathbf{p}$ is the momentum operator, m the electronic mass and $\mathcal{V}(\mathbf{r})$ the potential from the ions and the other electrons acting on the electron under consideration. The solution of Eq. (103) is the unperturbed electronic wavefunction. This ground state wavefunction shall be denoted as $\varphi^{(0)}$ and is constructed through a variational principle: It is that wavefunction which minimizes the total energy of the system, expressed as the expectation value of the Hamiltonian:

$$\mathcal{E}[\varphi] = \langle\varphi^{(0)}|\, \mathcal{H}\, |\varphi^{(0)}\rangle. \tag{104}$$

The minimization is done in the framework of density functional theory (DFT). A description of this theory can be found in section 3.1.

According to Maxwell's equation, a magnetic field $\mathbf{B}$ is divergence-free, $\nabla \cdot \mathbf{B} = 0$. Therefore, a given field which is applied to this system can be represented by a vector potential $\mathbf{A}$ satisfying

$$\mathbf{B} \;=\; \nabla \times \mathbf{A}(\mathbf{r}). \tag{105}$$

This vector potential is only an auxiliary quantity, it has no direct physical meaning. For a given magnetic field, there is no unique vector potential, any field which fulfills Eq. (105) can be used and will give the same physical results. In particular, any good field $\mathbf{A}$ can be transformed to a new one through

$$\mathbf{A} \;\mapsto\; \mathbf{A}' = \mathbf{A} + \nabla \Phi_{\mathrm{g}}(\mathbf{r}) \tag{106}$$

where $\Phi_{\mathrm{g}}(\mathbf{r})$ is an arbitrary scalar function. It is called the gauge of the magnetic field, and the fact that its choice is arbitrary and does not affect any physical results is called gauge invariance. In this respect, it is similar to the phase factor of an electronic wavefunction, which also represents a degree of freedom that does not influence any measurements. If the gauge is changed, the magnetic field remains the same, because it is given by the curl of $\mathbf{A}$, Eq. (105). However, the actual calculation can change a lot, because it depends numerically on the explicite value of the vector potential.

A typical choice for $\mathbf{A}$ in the case of a given homogeneous magnetic field $\mathbf{B}$ is

$$\mathbf{A}(\mathbf{r}) \;=\; -\frac{1}{2}\,\mathbf{r} \times \mathbf{B}. \tag{107}$$

It obviously satisfies Eq. (105). A special set of gauges for this vector field is defined by the functions

$$\Phi_{\mathrm{g}}(\mathbf{r}) \quad = \quad \frac{1}{2}\,\mathbf{r}\cdot\mathbf{R}_{\mathrm{g}}\times\mathbf{B} \tag{108}$$

with a particular position in space denoted by $\mathbf{R}_{\mathrm{g}}$. When the original vector field (107) is transformed according to Eq. (106), the new potential becomes

$$\mathbf{A}'(\mathbf{r}) \quad = \quad -\frac{1}{2}\,(\mathbf{r}-\mathbf{R}_{\mathrm{g}})\times\mathbf{B}. \tag{109}$$

This transformation only changes the origin of the coordinate system seen by the vector potential to $\mathbf{R}_{\mathrm{g}}$. For this reason, the position $\mathbf{R}_{\mathrm{g}}$ is called the gauge origin of the new vector potential (109). It is a cyclic variable, because it does not change the physics of the system, but it modifies the values of the actual operators. The importance of this gauge origin will be illustrated later on, it is the subject of section 6.

5.3 Magnetic DFPT

The incorporation of the magnetic field into the system's Hamiltonian is done by replacing the standard momentum operator by its generalized expression in the presence of a magnetic field [45]:

$$\mathbf{p} \quad \mapsto \quad \boldsymbol{\pi}=\mathbf{p}-e\mathbf{A}. \tag{110}$$

In combination with the Hamiltonian of Eq. (103), the total Hamiltonian of the system in the presence of the magnetic field can be written as

$$\mathcal{H} \quad = \quad \frac{1}{2m}(\mathbf{p}-e\mathbf{A})^2+\mathcal{V}(\mathbf{r}), \tag{111}$$

where m and e are the mass and charge of the electron, respectively. The separation in unperturbed and perturbation terms is straightforward, because $\mathbf{A}$ is linear in $\mathbf{B}$. There are contributions of first and second order in the perturbation:

$$\mathcal{H}^{(1)} = \frac{e}{2m}\left(\mathbf{p}\cdot\mathbf{A}(\mathbf{r}) + \mathbf{A}(\mathbf{r})\cdot\mathbf{p}\right) \tag{112}$$

$$\mathcal{H}^{(2)} = \frac{e^2}{2m}\,\mathbf{A}(\mathbf{r})\cdot\mathbf{A}(\mathbf{r}), \tag{113}$$

In the case of a magnetic field as the perturbation, the second order energy functional in the framework of density functional perturbation theory (DFPT) simplifies considerably because the first order density analytically vanishes everywhere. The reason is that the perturbation Hamiltonian and the first order wavefunctions are purely imaginary, and thus, the two terms in Eq. (53) cancel each other out. The matrix element of the magnetic perturbation Hamiltonian (112) in the position representation is given by:

$$\langle\mathbf{r}|\mathcal{H}^{(1)}|\mathbf{r}'\rangle = i\,\frac{\hbar e}{2m}\,\delta^{\,3}(\mathbf{r}-\mathbf{r}')\;\;(\mathbf{r}-\mathbf{R})\times\mathbf{B}\cdot\nabla. \tag{114}$$

It is purely imaginary, so that with real wavefunctions and a neccessarily real energy (54), the first order orbitals $\varphi_k^{(1)}$ must be purely imaginary, too:

$$\Re\,\varphi_k^{(1)} = 0. \tag{115}$$

Hence, the first order density (53) vanishes analytically for magnetic perturbations, and the energy functional (54) simplifies to:

$$\begin{aligned} E^{(2)} = {} & \sum_{kl}\langle\varphi_k^{(1)}|\mathcal{H}^{(0)}\,\delta_{kl} - \lambda_{kl}|\varphi_l^{(1)}\rangle \\ & + \sum_{k}\left[\langle\varphi_k^{(1)}|\mathcal{H}^{(1)}|\varphi_k^{(0)}\rangle + \langle\varphi_k^{(0)}|\mathcal{H}^{(1)}|\varphi_k^{(1)}\rangle\right] \quad . \end{aligned} \tag{116}$$

The stationarity condition on the energy, Eq. (62), can be written as an inhomogeneous system of coupled equations for the $\psi_k^{(1)}$:

$$\sum_l \left(\mathcal{H}^{(0)}\,\delta_{kl} - \lambda_{kl}\right)|\psi_l^{(1)}\rangle \quad = \quad -\mathcal{H}^{(1)}|\psi_k^{(0)}\rangle. \tag{117}$$

This equation could be formally inverted using Green's function (136). In the implementation, however, Eq. (117) is solved directly using a conjugate-gradient minimization algorithm [33]. Its computational cost is comparable to that of a total energy calculation. No wavefunctions of unoccupied states are required, in contrast to sum-over-states techniques.

5.4 Electronic current density

In general, the current can be obtained as the expectation value of the current operator,

$$\mathbf{j}_{\mathbf{r}'} \quad = \quad \frac{e}{2m}\left[\boldsymbol{\pi}|\mathbf{r}'\rangle\langle\mathbf{r}'| + |\mathbf{r}'\rangle\langle\mathbf{r}'|\boldsymbol{\pi}\right], \tag{118}$$

taken in the complete electronic state, i.e. using the total wavefunction:

$$\mathbf{j}(\mathbf{r}') \quad = \quad \frac{e}{2m}\,\langle\psi|\left[\boldsymbol{\pi}|\mathbf{r}'\rangle\langle\mathbf{r}'| + |\mathbf{r}'\rangle\langle\mathbf{r}'|\boldsymbol{\pi}\right]|\psi\rangle. \tag{119}$$

The generalized momentum operator $\boldsymbol{\pi}$ in Eqs. (118) and (119) is given by the derivative of the Hamiltonian with respect to the velocity, yielding

$$\boldsymbol{\pi} \quad = \quad \mathbf{p} - e\mathbf{A}. \tag{120}$$

Expanding the current in powers of the magnetic field, one finds that in the unperturbed state, the current density is zero:

$$\begin{aligned} \mathbf{j}^{(0)}(\mathbf{r}') &= \frac{e}{2m} \langle \varphi^{(0)} | \Big[\mathbf{p} | \mathbf{r}' \rangle \langle \mathbf{r}' | + | \mathbf{r}' \rangle \langle \mathbf{r}' | \mathbf{p} \Big] | \varphi^{(0)} \rangle & (121) \\ &= \frac{e}{2m} \Big[\left\{ i\hbar \nabla \overline{\varphi}^{(0)}(\mathbf{r}') \right\} \varphi^{(0)}(\mathbf{r}') \\ &\quad + \overline{\varphi}^{(0)}(\mathbf{r}') \left\{ -i\hbar \nabla \varphi^{(0)}(\mathbf{r}') \right\} \Big] & (122) \\ &= 0. & (123) \end{aligned}$$

This property essentially relies on the possiblity to choose the wavefunction $\varphi^{(0)}$ real (the bar $\overline{\varphi}$ indicates the complex conjugate of φ). Only then, the sum in Eq. (122) vanishes.

It will be shown lateron that the first order perturbation wavefunction is purely imaginary[1] when $\varphi^{(0)}$ is real. Thus, the previous argument does not hold any more and the current density which depends on $\varphi^{(1)}$, and which is therefore linear in the field, is nonzero. By expanding Eq. (119) to first order, one obtains:

$$\begin{aligned} \mathbf{j}(\mathbf{r}') &= \frac{e^2}{m} \mathbf{A}(\mathbf{r}') \, |\varphi^{(0)}|^2 \\ &\quad + i\hbar \, \frac{e}{2m} \Big[\nabla \overline{\varphi}^{(0)} \varphi^{(1)} - \overline{\varphi}^{(0)} \, \nabla \varphi^{(1)} \\ &\quad + \nabla \overline{\varphi}^{(1)} \varphi^{(0)} - \overline{\varphi}^{(1)} \, \nabla \varphi^{(0)} \Big]. & (124) \end{aligned}$$

For simplicity, the position arguments ($\mathbf{r}'$) have been omitted in Eq. (124), and the gradient operators are supposed to act only on the function which follows immediately. Under the assumption of a real $\varphi^{(0)}$ and an imaginary

---

[1] in particular, see Eq. (115). This is true only for a magnetic field perturbation, not in general.

$\psi^{(1)}$, the current further simplifies to:

$$\mathbf{j}(\mathbf{r}') \;=\; \frac{e^2}{m}\,\mathbf{A}(\mathbf{r}')\,|\psi^{(0)}|^2 + i\hbar\,\frac{e}{m}\Big[\psi^{(1)}\,\nabla\psi^{(0)} - \psi^{(0)}\,\nabla\psi^{(1)}\Big]. \tag{125}$$

5.5 Derived quantities: induced field, susceptibility and shielding

The chemical shielding tensor, whose calculation represents one of the main goals of this work, is defined as the proportionality factor between the induced and the externally applied magnetic field at the positions of the nuclei:

$$\sigma\,(\mathbf{R}) \;=\; \frac{\partial\,\mathbf{B}^{\mathrm{ind}}(\mathbf{R})}{\partial\,\mathbf{B}^{\mathrm{ext}}}. \tag{126}$$

The induced magnetic field is determined by the total electronic current $\mathbf{j}(\mathbf{r})$ through

$$\mathbf{B}^{\mathrm{ind}}(\mathbf{r}) \;=\; \frac{\mu_0}{4\pi}\int d^3r'\,\frac{\mathbf{r}'-\mathbf{r}}{|\mathbf{r}'-\mathbf{r}|^3}\times\mathbf{j}(\mathbf{r}'), \tag{127}$$

with the permeability of the vacuum μ_0. Since the system is treated under periodic boundary conditions, the current density will be periodic, and can be represented in reciprocal space. The induced magnetic field, $\mathbf{B}^{\mathrm{ind}}(\mathbf{r})$, can also be written in reciprocal space, and the integral in Eq. (127) turns into as simple equation, as described in detail in section B. It reads:

$$\mathbf{B}^{\mathrm{ind}}(\mathbf{G}\neq 0) \;=\; \mu_0\,i\,\frac{\mathbf{G}}{|\mathbf{G}|^2}\;\times\;\mathbf{j}(\mathbf{G}). \tag{128}$$

The general definitions of the Fourier transformation between direct and reciprocal space are presented is appendix A.

The $\mathbf{G}=0$ component of the field depends on the bulk magnetic susceptibility tensor, χ, and the shape of the sample. In general, it is expressed as:

$$\mathbf{B}_0^{\mathrm{ind}} = \kappa\,\chi\;\mathbf{B}^{\mathrm{ext}} \tag{129}$$

with the macroscopic bulk susceptibility χ and a prefactor which describes the dependence on the macroscopic geometry of the system. The bulk susceptibility χ can be expressed as a function of the orbital electronic current. The mathematical derivation is presented in appendix C. The result is:

$$\chi = \frac{\mu_0}{2\Omega}\,\frac{\partial}{\partial\,\mathbf{B}^{\mathrm{ext}}}\int_\Omega d^3r\;\mathbf{r}\times\mathbf{j}(\mathbf{r}), \tag{130}$$

where the integral is done over one unit cell of volume Ω. In the case of a spherical system, κ is given by $\kappa = 2/\,3$, cf. Eq. (207). The molar susceptibility is related to χ through $\chi^m = \Omega N_L \chi$.

6 The gauge origin problem

6.1 General

The *ab-initio* calculation of chemical shifts has become more and more popular, and over the years, many methods have been developed in the quantum chemistry community to perform such computations. One major problem that appears in these calculations is the choice of the gauge function, Eq. (108), or the the gauge origin $\mathbf{R}_{\mathrm{g}}$, respectively.

While being in principle a cyclic variable, this gauge can significantly affect the results in an actual calculation. To minimize this effect, several solutions have been proposed: in the GIAO method (Gauge Including Atomic Orbitals, [46]), one transforms the gauge of the basis set functions to the position of their nuclei, whereas in the IGLO method (Individual Gauges for Localized Orbitals, [47]), the gauges of the final wavefunctions are transformed to their centers of charge. The CSGT method (Continuous Set of Gauge Transformations, [48]) finally defines a gauge which depends on the position where the induced current is to be calculated. This approach is used in the method presented here, and it shall be described in detail in this section.

The current density (125), written in terms of the orbital contributions, can be separated into the dia– and paramagnetic terms:

$$
\begin{aligned}
\mathbf{j}(\mathbf{r}') &= \sum_k \mathbf{j}_k(\mathbf{r}') \quad = \quad \sum_k \mathbf{j}_k^{\mathrm{d}}(\mathbf{r}') + \mathbf{j}_k^{\mathrm{p}}(\mathbf{r}') \\
\mathbf{j}_k^{\mathrm{d}}(\mathbf{r}') &= \frac{e^2}{m}\, \mathbf{A}(\mathbf{r}')\, |\varphi_k^{(0)}(\mathbf{r}')|^2 \\
\mathbf{j}_k^{\mathrm{p}}(\mathbf{r}') &= \frac{e}{m}\, \langle \varphi_k^{(0)} | \Big[\mathbf{p} |\mathbf{r}'\rangle\langle\mathbf{r}'| + |\mathbf{r}'\rangle\langle\mathbf{r}'| \mathbf{p} \Big] | \varphi_k^{(1)} \rangle
\end{aligned} \tag{131}
$$

Both contributions individually depend on the gauge, whereas the total current $\mathbf{j}$ is gauge-independent. However, the two contributions are large numbers and have opposite signs. For the choice of the vector potential adopted here, Eq. (107), $\mathbf{A}(\mathbf{r})$ is linear in the gauge origin $\mathbf{R}_\mathrm{g}$. Therefore, the diamagnetic current $\mathbf{j}_k^\mathrm{d}$ grows linearly in $\mathbf{R}_\mathrm{g}$, and $\mathbf{j}_k^\mathrm{p}$ must compensate for this in order to fulfill the invariance of the total current.

Thus, for large distances $|\mathbf{r} - \mathbf{R}_\mathrm{g}|$, the current density $\mathbf{j}$ results from the cancellation of two large terms, making the actual calculation rather challenging. In a computer simulation using a finite basis set, the gauge invariance of $\mathbf{j}$ is no longer numerically verified.

6.2 Continuous set of gauge transformations

Several techniques have been developed to minimize this problem for small molecules [46, 47, 48]. The goal is to calculate magnetic properties in a periodic system. In this context, the probably most natural approach is the so-called "$\mathbf{R}_\mathrm{g} = \mathbf{r}$" – variant of the CSGT method [48]. For each point $\mathbf{r}'$ in space, the current density is calculated with the gauge origin $\mathbf{R}_\mathrm{g}$ being set equal to $\mathbf{r}'$. This method makes the diamagnetic part vanish analytically:

$$\mathbf{j}_k^\mathrm{d}(\mathbf{r}') \;=\; 0, \tag{132}$$

such that cancellations of large numbers no longer occur.

In practice, the current is computed as

$$\begin{aligned} \mathbf{j}_k(\mathbf{r}') \;=\; & \frac{e}{m} \langle \varphi_k^{(0)} | \Big(\mathbf{p} | \mathbf{r}' \rangle \langle \mathbf{r}' | + | \mathbf{r}' \rangle \langle \mathbf{r}' | \mathbf{p} \Big) \\ & \Big[| \varphi_k^{(\mathbf{r}\times\mathbf{p})} \rangle - \mathbf{r}' \times | \varphi_k^{(\mathbf{p})} \rangle \Big] \quad \cdot \mathbf{B}. \end{aligned} \tag{133}$$

Here, $|\varphi_k^{(\mathbf{r}\times\mathbf{p})}\rangle$ and $|\varphi_k^{(\mathbf{p})}\rangle$ are the first order perturbation wavefunctions for the special perturbation Hamiltonians:

$$|\varphi_k^{(\mathbf{r}\times\mathbf{p})}\rangle \quad \mapsto \quad \mathcal{H}^{(1)} = \mathbf{r}\times\mathbf{p} \tag{134}$$

$$|\varphi_k^{(\mathbf{p})}\rangle \quad \mapsto \quad \mathcal{H}^{(1)} = \mathbf{p}. \tag{135}$$

This formulation avoids actually calculating distinct wavefunctions $\varphi^{(1)}$ for each point $\mathbf{r}'$ in space.

6.3 Individual origin translations

It can be formally shown that within this gauge, the current is invariant under a translation of the origin in Eq. (133) for an individual orbital. This is done by using a special formulation which is no more used in the rest of this work, but which is well adapted for this particular purpose. Denoting the perturbation theory Green's function (see also section 3.10 for details):

$$\mathcal{G}_{lk} \;=\; -\left(\mathcal{H}^{(0)}\,\delta_{\;kl} - \langle\varphi_k^{(0)}|\mathcal{H}^{(0)}|\varphi_l^{(0)}\rangle\right)^{-1}, \tag{136}$$

the first order perturbation wavefunctions for an arbitrary perturbation Hamiltonian $\mathcal{O}$ can be expressed as:

$$|\varphi_k^{(\mathcal{O})}\rangle \;=\; \sum_l \mathcal{G}_{kl}\,\mathcal{O}\,|\varphi_l^{(0)}\rangle. \tag{137}$$

This Green's function formulation is not used in the actual calculation; instead, a variational energy minimization (see section 3.10) is performed. Eq. (137) serves only as a compact notation to obtain a closed expression for the current density.

In Eq. (137), $\mathcal{O}$ is either $\mathbf{p}$ or $\mathbf{r}\times\mathbf{p}$, so that the special first order wavefunctions of Eqs. (134) and (135) can be expressed as:

$$\begin{aligned} |\varphi_k^{(\mathbf{r}\times\mathbf{p})}\rangle &= \sum_l \mathcal{G}_{kl}\,\mathbf{r}\times\mathbf{p}\,|\varphi_l^{(0)}\rangle && (138)\\ |\varphi_k^{(\mathbf{p})}\rangle &= \sum_l \mathcal{G}_{kl}\,\mathbf{p}\,|\varphi_l^{(0)}\rangle. && (139)\end{aligned}$$

By expanding Eq. (137) in the basis of the unperturbed unoccupied orbitals, one obtains the well-known sum-over-states expression for the first order perturbation wavefunction for arbitrary perturbation operators. The current as a special case follows by combining Eqs. (133), (138) and (139):

$$\begin{aligned} \mathbf{j}_k(\mathbf{r}') &= \frac{e}{m}\sum_l \langle\varphi_k^{(0)}|\Big(\mathbf{p}|\mathbf{r}'\rangle\langle\mathbf{r}'| + |\mathbf{r}'\rangle\langle\mathbf{r}'|\mathbf{p}\Big)\\ &\qquad \Big[\mathcal{G}_{kl}\,\mathbf{r}\times\mathbf{p}\,|\varphi_l^{(0)}\rangle - \mathcal{G}_{kl}\,\mathbf{r}'\times\mathbf{p}\,|\varphi_l^{(0)}\rangle\Big]\quad\cdot\mathbf{B} \qquad (140)\end{aligned}$$

In this formulation, it becomes apparent that any simultaneous translation of the relative origin for the operator $\mathbf{r}$ and the gauge $\mathbf{R}_\mathrm{g} = \mathbf{r}'$ automatically cancel each other out. In particular, the current is invariant under arbitrary orbital-specific translations $\mathbf{d}_l$:

$$\begin{aligned} \mathbf{j}_k(\mathbf{r}') &= \frac{e}{m}\sum_l \langle\varphi_k^{(0)}|\Big(\mathbf{p}|\mathbf{r}'\rangle\langle\mathbf{r}'| + |\mathbf{r}'\rangle\langle\mathbf{r}'|\mathbf{p}\Big)\\ &\qquad \Big[\mathcal{G}_{kl}\,(\mathbf{r}-\mathbf{d}_l)\times\mathbf{p}\,|\varphi_l^{(0)}\rangle - \mathcal{G}_{kl}\,(\mathbf{r}'-\mathbf{d}_l)\times\mathbf{p}\,|\varphi_l^{(0)}\rangle\Big]\quad\cdot\mathbf{B}. \qquad (141)\end{aligned}$$

Note that in this equation, $\mathbf{p}$ and $\mathbf{r}$ as well as $\mathcal{G}_{kl}$ are operators, whereas $\mathbf{r}'$ and $\mathbf{d}_l$ are position variables.

This formulation, Eq. (141), looks somewhat similar to the well-known IGLO gauge transformation (individual gauges for localized orbitals, [47]), but it is not the same. The physical gauge in this work is always the $\mathbf{R}_\mathrm{g} = \mathbf{r}'$ version of the CSGT method.

However, this gauge still leaves the freedom to translate the coordinate system individually for each orbital, according to Eq. (141). This will turn out to be useful in the following.

A straightforward application of Eq. (141) would be too expensive. In fact, it would require one inversion of the Hamiltonian per real space mesh point $\mathbf{r}'$. Such an operation has approximately the cost of a total energy calculation, which leads to a prohibitive computational effort.

However, the the second term of $\mathbf{j}_k$ can be rewritten as

$$\begin{aligned}
&\frac{e}{m}\sum_l \langle\varphi_k^{(0)}|\Big(\mathbf{p}|\mathbf{r}'\rangle\langle\mathbf{r}'| + |\mathbf{r}'\rangle\langle\mathbf{r}'|\mathbf{p}\Big)\,\mathcal{G}_{kl}\,(\mathbf{r}'-\mathbf{d}_l)\times\ \mathbf{p}\,|\varphi_l^{(0)}\rangle\cdot\mathbf{B} \\
&\quad = \frac{e}{m}\sum_l \langle\varphi_k^{(0)}|\Big(\mathbf{p}|\mathbf{r}'\rangle\langle\mathbf{r}'| + |\mathbf{r}'\rangle\langle\mathbf{r}'|\mathbf{p}\Big)\,(\mathbf{r}'-\mathbf{d}_k)\times\ \mathcal{G}_{kl}\,\mathbf{p}\,|\varphi_l^{(0)}\rangle\cdot\mathbf{B} \\
&\qquad +\Delta\mathbf{j}_k(\mathbf{r}') \qquad (142)
\end{aligned}$$

where

$$\begin{aligned}
\Delta\mathbf{j}_k(\mathbf{r}') &= \frac{e}{m}\sum_l \langle\varphi_k^{(0)}|\Big(\mathbf{p}|\mathbf{r}'\rangle\langle\mathbf{r}'| + |\mathbf{r}'\rangle\langle\mathbf{r}'|\mathbf{p}\Big) \\
&\quad \mathcal{G}_{kl}\,(\mathbf{d}_k-\mathbf{d}_l)\times\ \mathbf{p}\,|\varphi_l^{(0)}\rangle\cdot\mathbf{B}. \qquad (143)
\end{aligned}$$

The evaluation the first term of Eq. (142) can be done at the computational cost of one total energy calculation, while $\Delta\mathbf{j}_k$ requires one such calculation per electronic state k.

At first sight, the sum $\Delta\mathbf{j} = \sum_k \Delta\mathbf{j}_k$ seems to be equal to zero, because the inner operator is antisymmetric in k, l. But since the momentum operators in Eq. (143) do not commute with the Green's function, $\Delta\mathbf{j}$ does not vanish unless all $\mathbf{d}_l$ are equal. However, it will be shown in the following that in most circumstances, $\Delta\mathbf{j}$ can be neglected.

However, some care is needed concerning the definition of $(\mathbf{d}_k - \mathbf{d}_l)$ in

Eq. (143). In a periodic system, this quantity is only defined modulo a lattice vector $\mathbf{R}_L$. The most natural way is to use a nearest image convention, where this lattice vector is chosen such that the distance $|\mathbf{d}_k - \mathbf{d}_l + \mathbf{R}_L|$ is minimum.

This also makes sense when looking at Eq. (143) as a matrix element of an operator $\mathcal{J}_{\mathbf{r}'}$, given by

$$\mathcal{J}_{\mathbf{r}'} \quad = \quad \Big(\mathbf{p}|\mathbf{r}'\rangle\langle\mathbf{r}'| + |\mathbf{r}'\rangle\langle\mathbf{r}'|\mathbf{p}\Big) \; \mathcal{G}_{kl} \; (\mathbf{d}_k - \mathbf{d}_l) \times \; \mathbf{p} \; \cdot \mathbf{B}. \tag{144}$$

This operator has a localized character in direct space, since the momentum operators $\mathbf{p}$ are quasilocal, and the Green's function, which is the inverse of the ground state Hamiltonian, connects only points in space that are close to each other. This can be seen be realizing that $\mathcal{G}_{kl}$ describes the reaction of the state k of the system to a perturbation of state l, and it is natural that if these two states are far away, one will not feel that the other has been perturbed.

Thus, the neglected current, Eq. (143), is the expectation value of a nearly local operator $\mathcal{J}_{\mathbf{r}'}$ between two localized states k and l, with the translation vector $(\mathbf{d}_k - \mathbf{d}_l)$ linking their centers of charge. Consequently, it is only non-zero for two orbitals that have a non-vanishing mutual overlap. Therefore, any definition for $(\mathbf{d}_k - \mathbf{d}_l)$ other than the minimum image convention would automatically lead to a zero expectation value, because the orbitals from more distant image cells will certainly not have the necessary overlap.

7 The position operator problem

7.1 General

The formalism described so far is straightforward to use in isolated systems, and many quantum chemical program packages exist in which magnetic response calculations are implemented.

However, none of these methods can be applied to extended systems. The reason for this restriction is that the Hamiltonian representing the magnetic field, Eq. (112), contains the position operator. In a system under periodic boundary conditions, this operator is ill-defined.

Recently, a new formalism has been presented which allows the calculation of chemical shifts and other magnetic properties in extended systems using periodic boundary conditions [49, 5]. This formulation is based on a magnetic field which is modulated in space. To return to the experimental situation of an homogeneous field, the limit of infinite modulation wavelength is evaluated numerically. In this work, an alternative method for extended systems in periodic boundary conditions is presented. It takes advantage of the exponential decay properties of localized Wannier orbitals [34, 50] and treat these localized orbitals as virtually isolated. This procedure is explained in detail in this section.

A first solution to this problem has been proposed and applied by Mauri et al. [49, 5, 51, 52, 53, 54] (MPL). They replace the homogeneous magnetic field $\mathbf{B}$ by a modulated one, $\mathbf{B}(\mathbf{r}) = \mathbf{B}_0 \cos \mathbf{q} \cdot \mathbf{r}$, with a finite wavevector $\mathbf{q}$. Consequently, also the perturbation Hamiltonian becomes $\mathbf{q}$-periodic and therefore well-defined for an extended system. The physically relevant case

$\mathbf{B}(\mathbf{r}) = \mathbf{B}_0$ is obtained by extrapolating numerically the results for $q \to 0$.

This is computationally relatively demanding since the same calculation has to be done several times, for several values of $\mathbf{q}$. In addition, this method always requires many k-points apart from Γ to be included, because $|\mathbf{q}|^{-1}$ typically far exceeds the unit cell dimensions. However, their work showed that it is feasible to compute NMR chemical shifts of periodic and amorphous systems with good accuracy using a pseudopotential plane-wave approach.

7.2 Virtual cells

Here, a conceptually different method shall be presented. Instead of transforming the homogeneous magnetic field to a periodic one, a new periodic position operator is defined. First, the wavefunctions are localized by means of a unitary rotation in the occupied subspace, as described in detail in section 4. This is a technique well-known in quantum chemistry, where it is used to determine the location and the nature of chemical bonds. The rotation is chosen such that the spatial extension of the wavefunctions is minimal, yielding maximally localized Wannier functions [34]. The extension is characterized by the second moment Δ_2 of the orbitals:

$$\Delta_2 \;=\; \sum_k \langle \varphi_k |\mathbf{r}^2| \varphi_k \rangle - \langle \varphi_k |\mathbf{r}| \varphi_k \rangle^2. \tag{145}$$

In a periodic system, special care is required to define the position operator properly. A solution to this problem in terms of a Berry phase approach [38] has been given by Vanderbilt et al. [36]. A practical scheme to calculate maximally localized Wannier orbitals has recently been presented by Berghold et al. [35]. The actual procedure used to transform the Bloch wavefunctions of a total energy minimization is described in detail in section 4.

It can be shown that in an insulator, the resulting localized wavefunctions decay exponentially [50]. If the unit cell is chosen such that the lattice parameter is larger than the decay length, the orbital is significantly different from zero only within a limited region of the cell, and it practically vanishes everywhere else.

The next step is to assign individual *virtual cells* to these Wannier orbitals. The virtual cells are chosen such that for the corresponding wavefunction, the cell walls are located in that region of space where the orbital density is close to zero over a certain range. Then, the position operator is defined normally running from $-L/\,2$ to $+L/\,2$ inside the virtual cell. At the walls, it makes a smooth transition back from $+L/\,2$ to $-L/\,2$, yielding a sawtooth shape (see fig. 1). This jump is not sharp in order to avoid components of very high frequency in the operator. As a consequence of this definition, the position operator now matches the periodic boundary conditions, since it is identical in every virtual cell and all its replica.

7.3 Discussion

Again, it must be stressed that the orbital's gauge is not transformed. In this case, one would have found additional terms in the perturbation Hamiltonian and the wavefunction orthonormality relations, as in the IGLO method. The crucial difference is that there are not individual orbital gauge origins; the gauge is always "$\mathbf{R} = \mathbf{r}'$". Instead, an individual reference system is defined for both $\mathbf{r}$ and $\mathbf{R}$ simultaneously, as described by the relative origins $\mathbf{d}_k$ in Eq. (141).

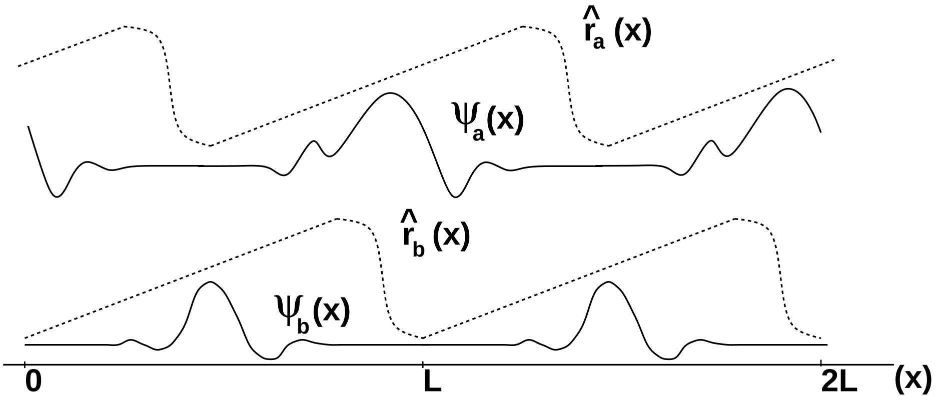

Figure 1: Two localized orbitals $\Psi_a(x)$, $\Psi_b(x)$ with specific position operators $r_a(x), r_b(x)$.

The problem that arises for this construction is that the new operator has a completely unphysical shape around the borders of the virtual cell, where it makes its jump (at $x = nL$). But by choosing the virtuall cells as described above, the unphysical transitions lie in those regions of space where the wavefunction vanishes. As a consequence, the problematic part of the operator is only applied where it has no effect anyway.

Hence, the saw-tooth shape of the position operator as indicated by fig. 1 is a reasonable approximation as long as the wavefunctions are sufficiently localized.

However, this represents a certain restriction for this method. We require that the decay length be significantly smaller than the lattice constant of the simulation box, as mentioned above. Only in such a case can the virtual cell be chosen with its borders in a region of vanishing density. It follows that for a system with truly delocalized orbitals, like a metal, this approach is not applicable. In such a system, the decay of the Wannier orbitals is only algebraic, and the necessary cell size would far exceed the computationally tractable volume and one would have to resort to the MPL approach, using a k-point sampling of the Brillouin zone.

8 Pseudopotential correction

The electrons of an atom can be classified by the energy eigenvalue of wavefunction in the Schrödinger equation or its simplified equivalents. Typically, the distinction made there is to separate those electrons of very low lying energy from those which have a higher energy value and to call them core and valence electrons, respectively.

The core electrons, having very negative energies, are tightly bound to the corresponding atom and feel almost exclusively the Coulomb interaction with other core electrons and the nucleus. Their wavefunction is practically invariant under changes in the chemical environment of the atom, i.e. they do not feel whether the atom is isolated in the vacuum or chemically bound within a molecule. In addition, they are spatially localized, i.e. their wavefunction is confined within the close surroundings of the nucleus, called the core region.

The other group of electrons, belonging to the valence band, have an energy which is much closer to the Fermi level. They are located relatively far away from the nucleus, and its Coulomb potential is strongly screened by the core electrons. The wavefunction of these valence wavefunctions is subject to strong changes upon modification of the chemical bonding situation of the atom. Thus, only the valence electrons make and break a chemical bond. In contrast to core electrons, their wavefunction is less localized and much smoother, except for the core region. There, in order to maintain the orthogonality to the other wavefunctions necessary to satisfy the Pauli exclusion principle, they oscillate strongly. However, these oscillations do not determine the chemical properties of the atom, they are only necessary for reasons of orthogonality.

In a plane-wave representation, the computational cost required to describe a wavefunction directly depends on the magnitude of these oscillations. The smoother the orbital is, the fewer plane waves are needed to construct the wavefunction up to a given accuracy. Therefore, one seeks to make approximations concerning the shape of the orbitals in order to reduce the number of Fourier coefficients. The solution is to use pseudopotentials as presented in section 3.8. A pseudopotential exploits the fact that the core electrons are not of big interest concerning the reactivity of an atom. Thus, the nucleus and its core orbitals are taken as frozen and replaced by a fake potential. The requirement such a fake potential has to verify is that it should reproduce the valence wavefunctions exactly as in the presence of core orbitals. Only in the core region, the shape of the valence orbitals is not so important; they are allowed to differ in order to reduce the necessary number of plane waves.

The calculations which have been done in the context of this work are based on a plane-wave pseudopotential implementation. Therefore, in the whole calculation, no core orbitals are taken into account, and the valence wavefunctions have an incorrect shape in the core region. In the analysis of chemical bonding, this frozen core approximation has been shown to work reliably, since only changes in the valence region are of interest.

The chemical shift, however, is extremely sensitive to the core region, because the interaction between nuclear spin and electronic current is proportional to $1/\,r^2$. Thus, it is not clear a priori whether a pseudopotential implementation can give meaningful results at all. This problem has already been investigated for a lot of molecules and atoms [55]. It turns out that often, the contribution of the core orbitals to the chemical shift is almost constant with respect to the chemical environment of the atom. In [55], an analysis of the orbital contributions is done for many atoms and molecules for the IGLO method.

It has been shown elsewhere [56], that the frozen-core approximation can successfully be used for calculations of orbital magnetic response properties. A simple additive constant is sufficient to reproduce the all-electron shieldings satisfactorily in many cases. This constant must take into account the direct contributions from the core orbitals as well as the error made due to the physically incorrect shape of the valence wavefunctions inside the core region. Since this shape depends on the type and the parameters of the pseudopotential used, the constant by which the approximation is corrected cannot be given by a unique number. In order to avoid the need of always specifying the pseudopotential parameters and the correction constant, a convention that is also used in experiments shall be adopted in this work:

> The cited shieldings are obtained from the difference between the calculated valence-electron shieldings and the calculated shieldings for a commonly used reference molecule.

This convention is also used in most other pseudopotential calculations.

However, now the reference molecule must always be specified. For hydrogen and carbon atoms, another convention for the choice of this reference molecule exists, which is also adopted here. Usually, tetramethylsilane $Si(CH_3)_4$ (TMS) is used because of its chemical stability.

9 Application to isolated molecules

9.1 Convergence of the chemical shift

The approach has been implemented in CPMD [57], a DFT pseudopotential suite of programs based on a plane-wave (PW) representation. These methods are described in detail in the first part of this work, sections 3.1 and 3.8. Using a supercell technique, the method has been applied to isolated molecules in order to validate the approach and the implementation.

For all molecules, the experimental geometries have been used [58]. As discussed in section 8, the carbon shifts need to be corrected for the core contribution through a semi-empirical additive constant. Pseudopotentials were taken from Goedecker et al. [29] with a BLYP gradient corrected functional [23, 24], and a unit cell of size (20 a.u.)^3.

As a first test, an investigation of the convergence properties of the results with the plane wave cutoff E_c have been performed. This cutoff determines the size of the basis set, which is mathematically complete at $E_c \mapsto \infty$. At standard values of 50-70 Ry, this limit is not reached, even within the frozen core approximation. However, the electronic structure is usually well reproduced by that point. The convergence of the chemical shifts with the wavefunction cutoff is shown in fig. 2 and 3 for a representative set of small organic molecules in the gas phase.

The extrapolation of the chemical shift of the isolated molecules to infinite cutoff ($E_c^{-1} \rightarrow 0$) shows that a good convergence is already reached at a typical value of 70-90 Ry. The convergence error is in the range of about 0.3 ppm for hydrogen and a few ppm for carbon.

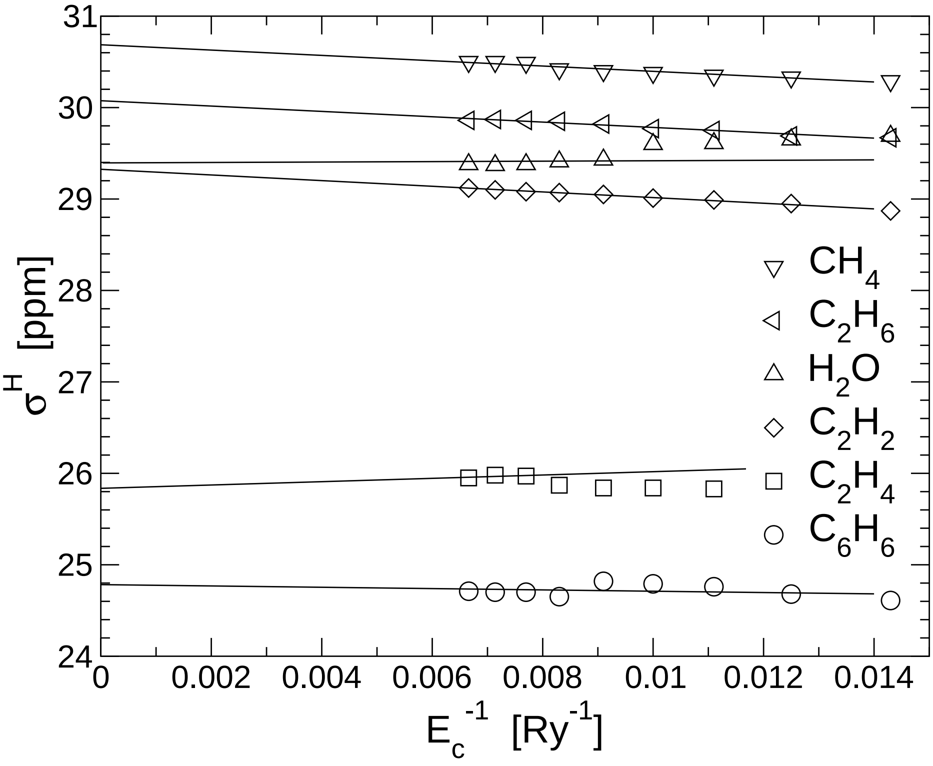

Figure 2: Convergence of ^{1}H shielding with cutoff.

Another approximation is the finite size of the unit cell in the calculation. To check the influence of the interaction between a molecule and its periodic replica, also the convergence with the cell volume has been studied with a PW cutoff fixed at E_c=70Ry (fig. 4). Obviously, the standard cell size of (20 a.u.)^3 mentioned above is enough to eliminate the influence of neighboring cells.

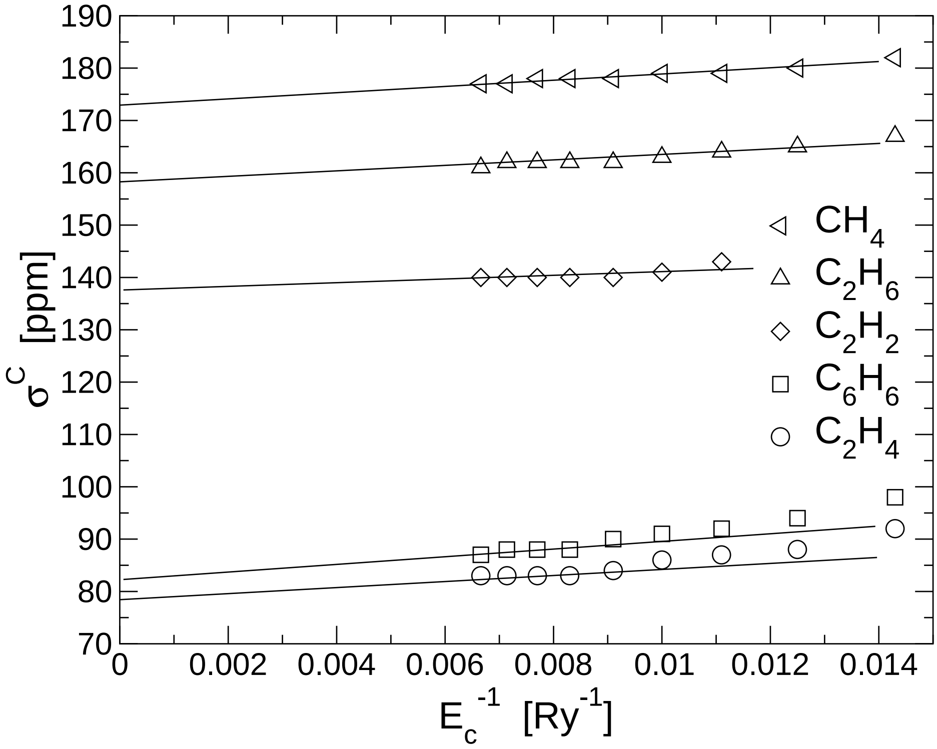

Figure 3: Convergence of ^{13}C shielding with cutoff.

9.2 Comparison with experiment and other theoretical methods

The extrapolated results for a representative set of small organic molecules with the values calculated with the Gaussian 94 package [59], with the MPL results [5] and with experiment are presented in fig. 5 and 6). In [51], only carbon shifts relative to TMS are given. They were converted to an absolute scale using the experimental value for TMS σ^C_{TMS}=188.1ppm. Experimental shieldings have been taken from [60]. The Gaussian calculation was done in DFT using the CSGT method [48], the BLYP exchange-correlation functional

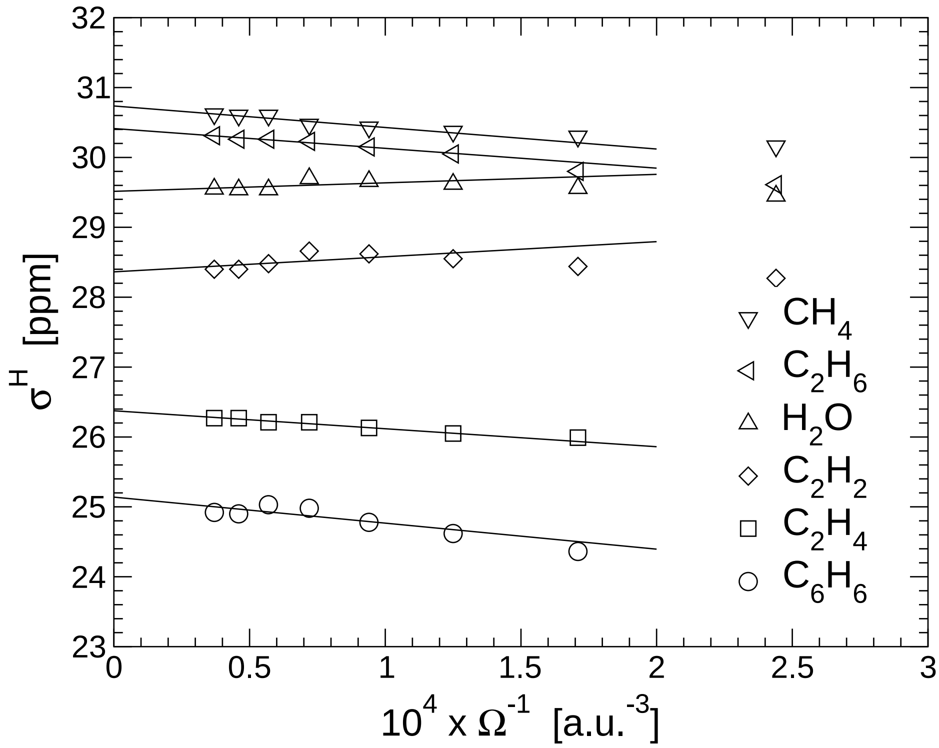

Figure 4: Convergence of ^{1}H shielding with cell volume.

[23, 24] and a 6-311G(3df,3pd) basis set.

In the case of an isolated system, we can perform the calculation imposing that the virtual cells are all equal ($\mathbf{d}_k = \mathbf{d}_l \;\; \forall k, l$), which makes $\Delta\mathbf{j}_k = 0$ in Eq. (143). In fig. 5 and 6, this exact calculation is compared with the approximation $\Delta\mathbf{j}_k = 0$ in the case of different virtual cells, where $\mathbf{d}_k \neq \mathbf{d}_l$. In both cases, the results are extrapolated to infinite cutoff, as described in the previous section.

For the ^{1}H shifts, the agreement of the values with both Gaussian and experiment is in general very good. The numbers essentially coincide with the experimental ones up to a maximum difference of about 0.6 ppm which is comparable to the error of Gaussian and that of the MPL approach. The difference between the full and the approximate calculation is negligible except in the presence of strongly overlapping delocalized orbitals, as in C_6H_6. Thus, for a system containing π-electrons, it is a good practice to choose the same virtual cells for all π-orbitals.

The differences compared to Gaussian are relatively small, except for C_6H_6 and C_2H_2. Considering the use of different basis sets and the different methodology of the calculation, overall agreement is satisfactory.

The differences with respect to the MPL method are mostly due to different computational approximations. Using the same cutoff (70Ry) and the same level of theory (LDA) as Mauri, the results agree up to 0.3 ppm.

Concerning the ^{13}C–atoms, the agreement with other theories and with experiment is still good but less satisfactory. Here, the limits of the approach become apparent, in particular of the frozen core approximation. The rigid additive correction for the pseudopotential is not able to reproduce the different hybridization states quantitatively. A change in the coordination induces an error of about 20ppm. The approximation of neglecting $\Delta\mathbf{j}$ in the current density accounts for an error of typically less than 15 ppm. However, the shifts still compare well to experiment, especially between similar chemical environments. There, the relative error is only a few ppm. Again, the method has an accuracy comparable to the other ones.

Concerning the ^{13}C–atoms, the agreement is still good but less satisfactory. Here, the limits of the approach become apparent, in particular of the frozen core approximation. The rigid additive correction for the pseudopotential is not able to reproduce the different hybridization states quantitatively.

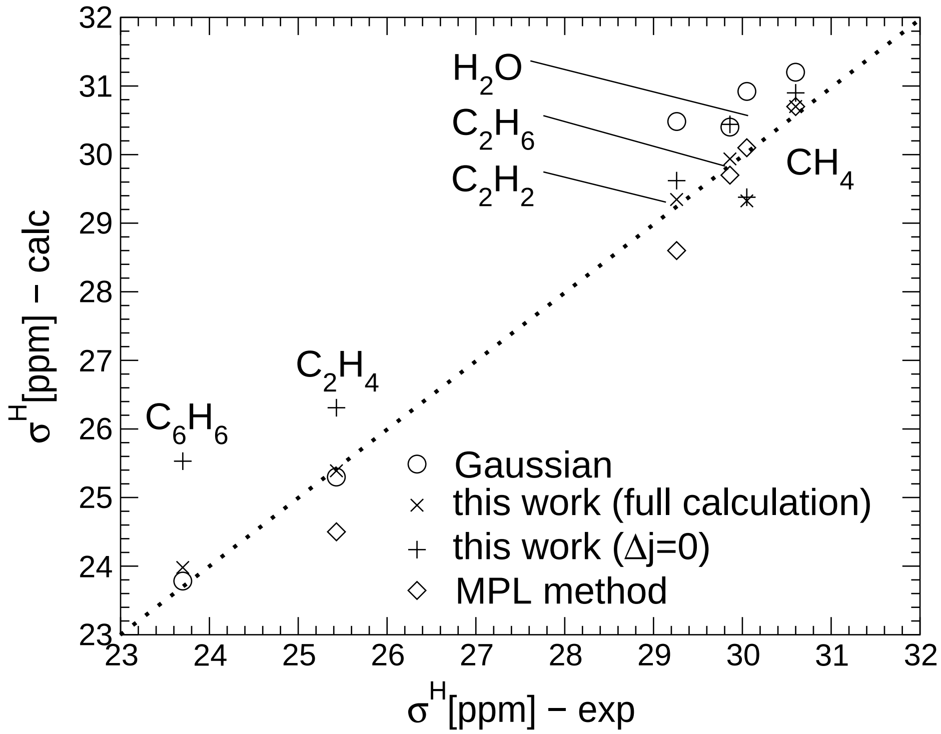

Figure 5: ^{1}H NMR chemical shifts

A change in the coordination induces an error of about 20ppm. However, the shifts still compare well to experiment, especially between similar chemical environments. There, the relative error is only a few ppm. Again, the method presented in this work has an accuracy comparable to the other ones.

9.3 Magnetic susceptibilities

The magnetic susceptibility, Eq. (130), is a by-product of the calculation and can be obtained almost for free. The isotropic molar susceptibilities of the test molecules are presented in fig. 7. They have also been extrapolated to infinite cutoff. Experimental values are taken from [61].

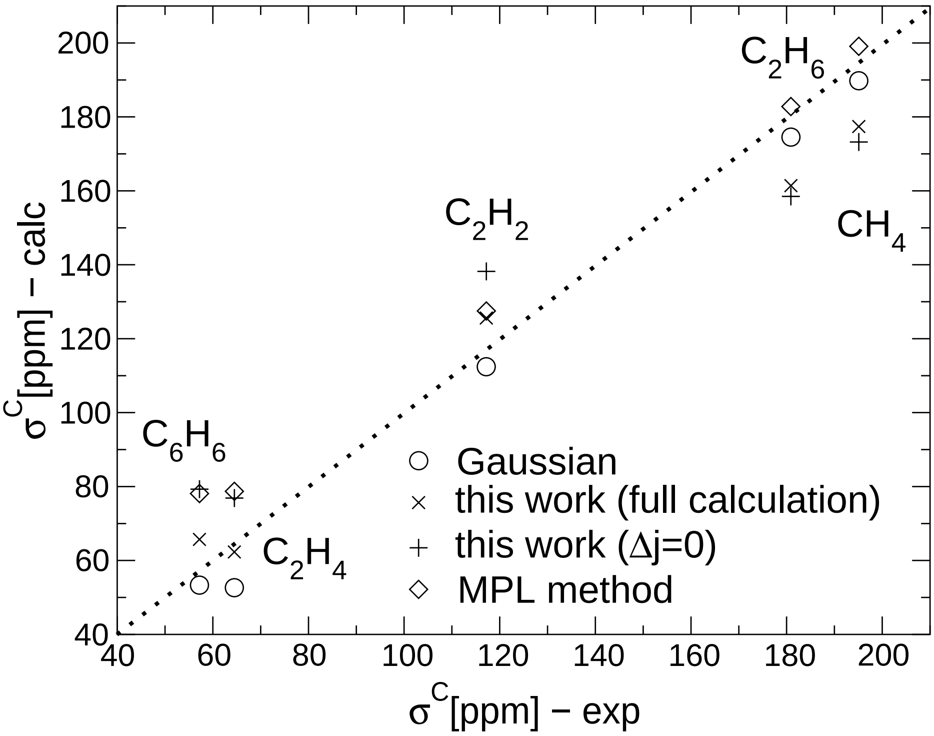

Figure 6: ^{13}C NMR chemical shifts

As in the case of the chemical shifts, there is a good agreement with existing theoretical methods and experiment.

The calculation of χ also suffers from the use of pseudopotentials. The contribution of the core electrons to the magnetic bulk susceptibility is not considered. This approximation is valid for light elements, but would fail for nuclei with spatially extended core electrons [49].

The comparison between the full and approximate calculations show that for the magnetic susceptibility, neglecting $\Delta\mathbf{j}$ has a maximum effect of 2cm^3/mol, which can safely be ignored. Again, the exception is benzene, where the contribution of Eq. (143) accounts for a deviation of 10cm^3/mol.

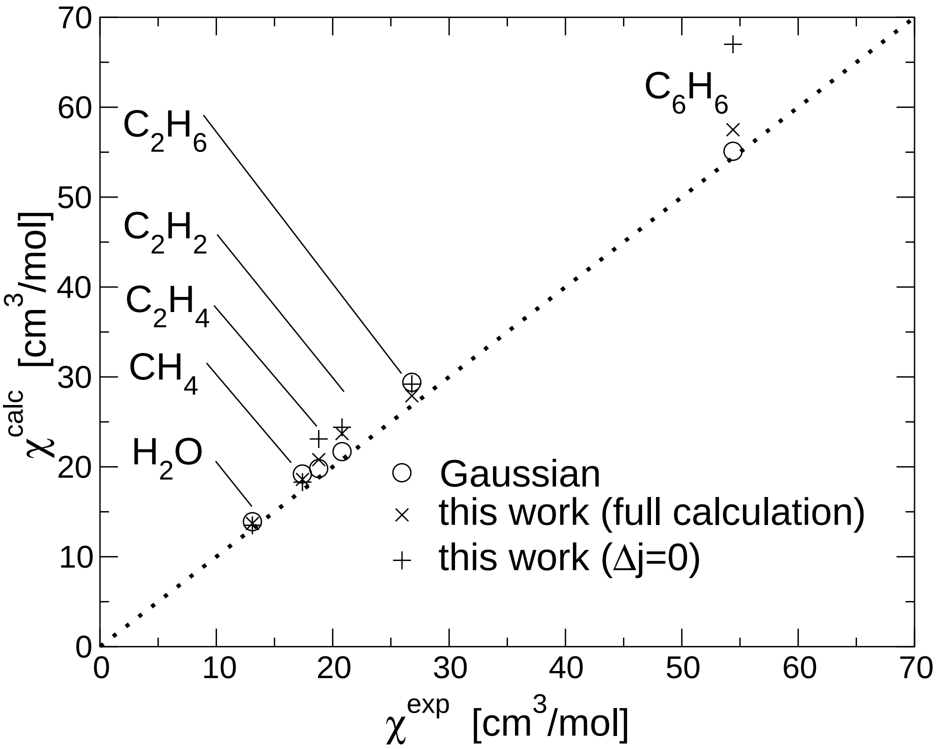

Figure 7: Magnetic susceptibilities in cm^3/mol.

9.4 Electronic current densities

The current which is induced by the electrons as a reaction to the external magnetic field, Eq. (125), provides an intuitive picture of the processes that happen in a molecule. In figures 8 and 9, the current density distribution $|\mathbf{j}(\mathbf{r})|$ of two organic molecules is plotted in a plane z =constant.

The first one, tetramethylsilane Si $(CH_3)_4$, is the standard reference molecule for H-, C-, and Si-chemical shifts. The current plot is done at 1Å below the place defined by three carbon atoms.

The second one, triphenylene, is a planar aromatic molecule, where the

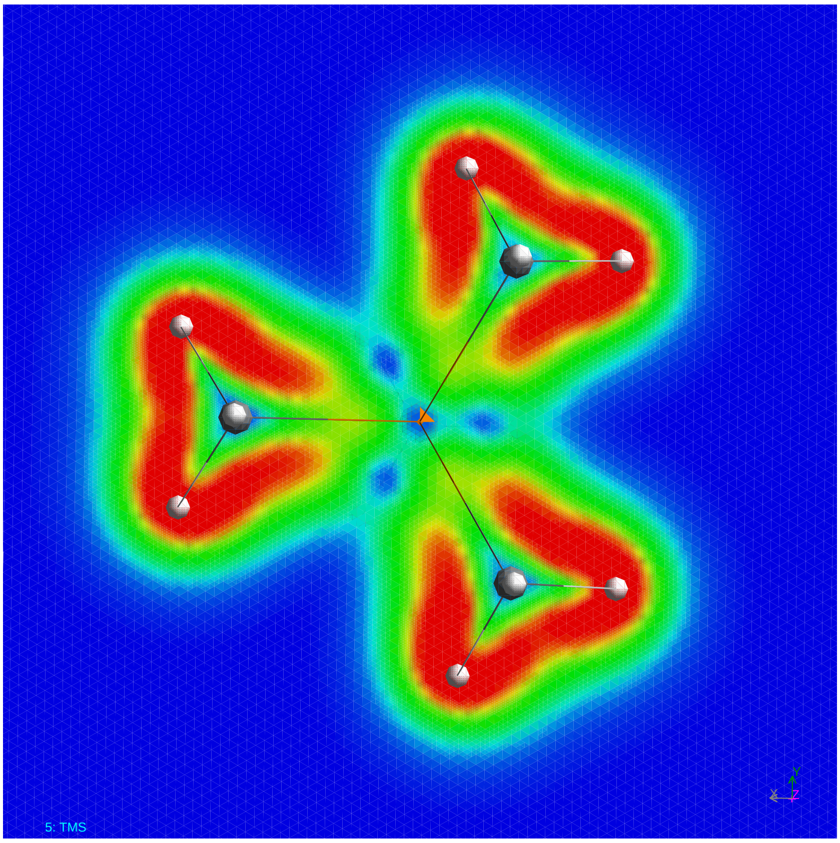

Figure 8: Electronic current density $|\mathbf{j}(\mathbf{r})|$ in tetramethylsilane, Si $(CH_3)_4$.

ring currents around the outer carbon rings due to the delocalized π-orbitals come out nicely. The plot is taken at z=0.5Å above the molecular plane, so that currents from σ -bonds are not visible any more. They can be seen when looking at the z=0 plane of the molecule.

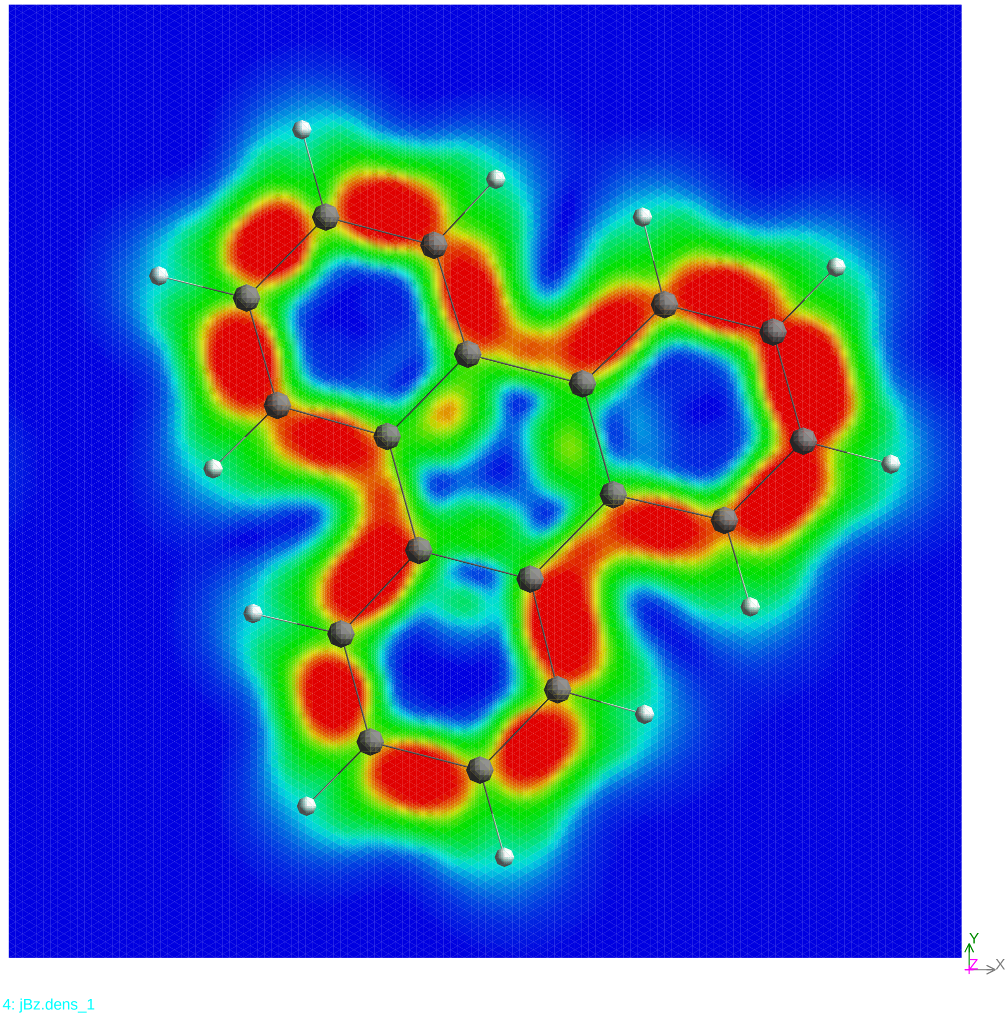

Figure 9: Electronic current density $|\mathbf{j}(\mathbf{r})|$ in triphenylene, $(C_6H_4)_3$.

10 Periodic systems

10.1 Current distribution of ice Ih

As an example for a truly periodic system, the current density distribution in ice Ih is shown in figure 10.

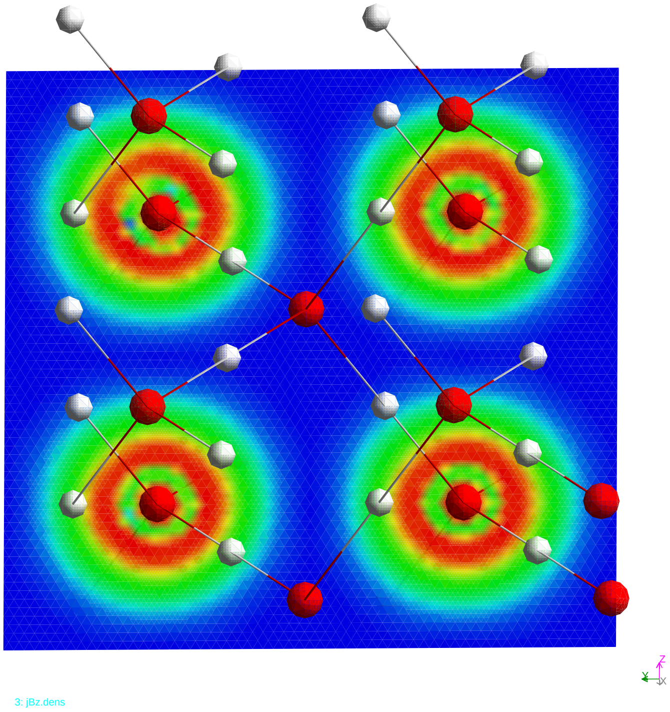

Figure 10: Electronic current density $|\mathbf{j}(\mathbf{r})|$ in ice Ih.

The plot is taken at a plane right below the positions of the oxygens. It can be seen that close to the oxygen atoms, the current density vanishes; this is due to the use of pseudopotentials which replace the core electrons. In an all-electron calculation, the currents close to the nuclei would not disappear.

10.2 Simple polymers

The most simple system that can be considered to be truly periodic is an infinite polymer chain. While being rather simple from the chemical point of view, it is very interesting for the study of the properties of the NMR calculation method. To this purpose, two polymer chains with different hybridizations, $(CH_2)_n$ and $(CH\text{–}CH\text{–}O)_n$, are investigated in this section. The computational setup is similar to that used for the isolated molecules: For $(CH_2)_n$, the unit cell of 19 a.u. size accomodates eight monomers at a cutoff of 50 Ry, and for $(CH\text{–}CH\text{–}O)_n$, it is 25 a.u. large and contains four monomers $(CH)_2O$ at a cutoff of 70 Ry. These cell dimensions are sufficient to assure that the localized Wannier wavefunctions do not extend over more than half of the cell width. Hence, the saw-tooth position operator can safely be applied.

In particular, the influence of the neglected current $\Delta\mathbf{j}$ on the ^{1}H shift in the case of a periodically repeated system shall be investigated. The number of particles in these systems is sufficiently small so that a direct calculation of $\Delta\mathbf{j}_k$ can be done for each orbital. Further, the unit cell is large enough to allow a proper definition of the displacement vectors $(\mathbf{d}_k - \mathbf{d}_l)$ in Eq. (143), according to the minimum image convention as described in section 6.3.

The dependence of the orbital corrections $\Delta\sigma_k^{\mathrm{H}}$ on the distance of the orbital's center of charge to the proton is shown in fig. 11. Only the nearest orbitals have a significant contribution, and there is a partial cancellation.

When summing over $\Delta\sigma_k^{\mathrm{H}}$, the total error is about -0.5ppm for $(CH_2)_n$ and -1.0ppm for $(CH\text{–}CH\text{–}O)_n$. This is about the same as for the isolated molecules (see fig. 5), and stays within the global accuracy of the calculation.

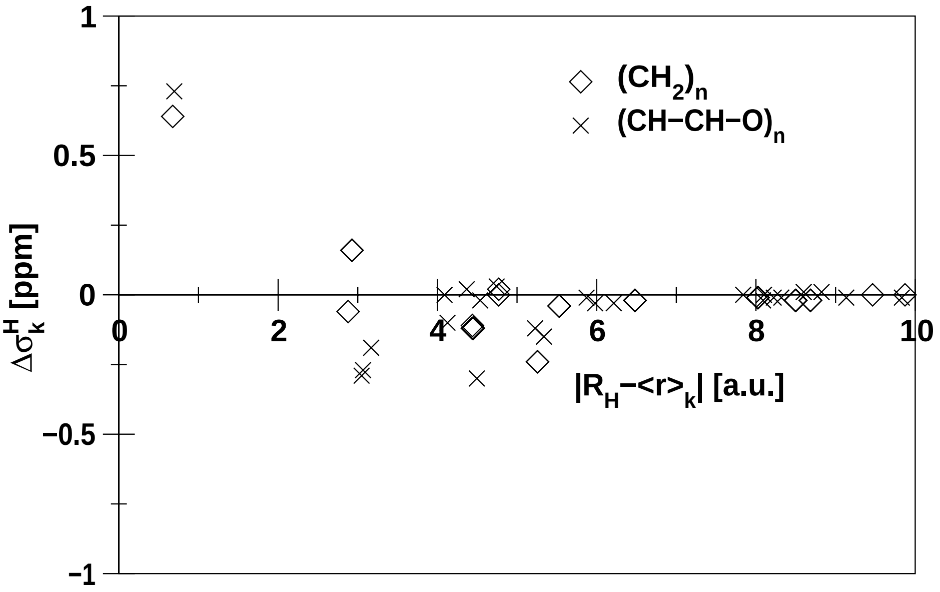

Figure 11: Contribution to the ^{1}H shift due to the (normally neglected) orbital currents $\Delta\mathbf{j}_k$ in infinite linear polymers as a function of the distance between the orbital's center of charge and the proton.

10.3 Diamond under pressure

In a previous study [51], Mauri et al. have calculated the carbon chemical shifts of diamond in function of pressure. Translating this pressure to molar volumes, they find that the carbon shielding is linear in the volume per atom, with a proportionality factor of 3.44 ppm/a.u.^{3}.

To check the reliability of the new method quantitatively in a true crystal, this calculation is repeated using a cubic supercell of 64 carbon atoms. The results are shown in fig. 12. The dependence of σ^C on the atomic volume yields 3.4 ppm/a.u.^{3}, which is very close to the value found by Mauri.

In the diamond system, the calculation of the neglected current yields

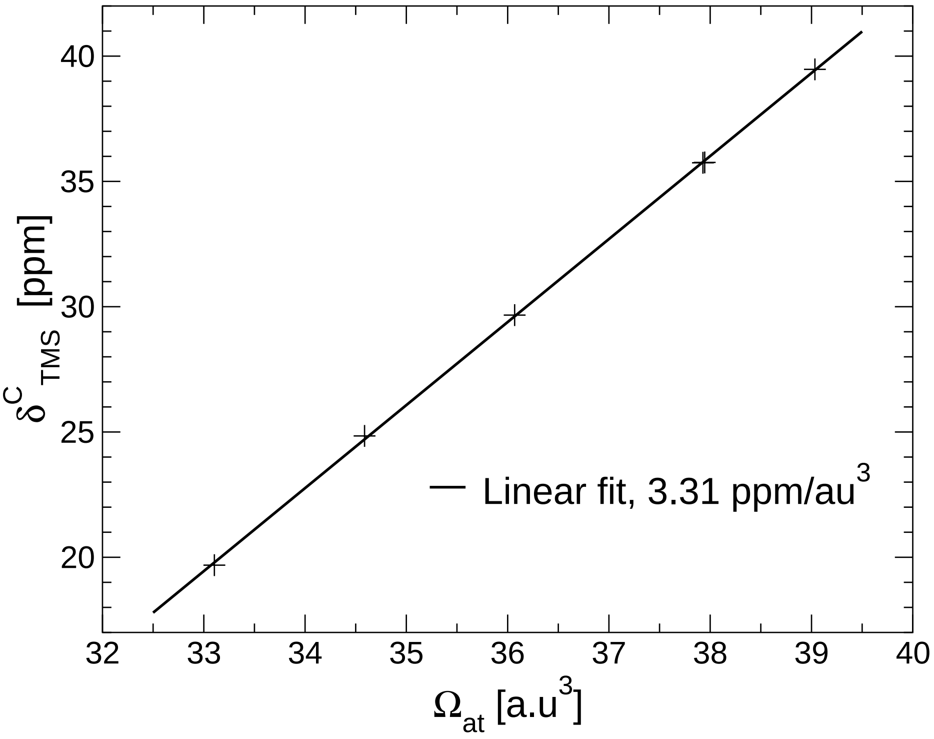

Figure 12: Dependence of $\delta^{\ C}_{\ TMS}$ on the volume per atom.

a total error of 28ppm for the carbon shielding, due to the proximity and the mutual overlap of the orbitals. The correction due to $\Delta\mathbf{j}$ is found to be almost constant with respect to the cell volume, its maximum variation is ±1.5ppm. This is another case in which relative shieldings are more accurate than absolute ones.

11 Pepstatin A / HIV-1 protease complex

11.1 Introduction

The protease from the human immunodeficiency virus (HIV-1 PR) is a homodimeric proteolytic enzyme essential for the virus metabolism [62, 63]. HIV-1 PR cleaves polypeptide segments at specific locations, which subsequently fold to form structural proteins and enzymes, among which the protease itself [63, 64, 65, 66]. Since the discovery that inhibition with pepstatin A - the defining inhibitor of aspartic proteinases - leads to production of immature, non-infectious viral particles [64, 67, 68, 69], HIV-1 PR has become a fundamental target for design of anti-AIDS therapeutics [70, 71, 72, 73, 74, 75, 76]. In developing new and powerful HIV-1 PR inhibitors, it soon became clear that enzyme/inhibitor interactions depend dramatically on the ionization states of the catalytically essential aspartyl dyad [70, 77, 78, 79, 80, 81]. Thus, defining the protonation state is critical for computer-aided design of novel drugs based on crystal structure determination. Furthermore, it is required for elucidating the enzymatic mechanism [82, 83, 84].

The method of choice for determining the exact charge state of the HIV-1 PR active site is ^{13}C NMR spectroscopy. Measures of chemical shifts on ^{13}C-enriched protease have provided information of the chemical microenvironment of the catalytic apparatus for the free enzyme [85] and for inhibitor/enzyme complexes [85, 86, 87, 88, 89, 90, 91, 92, 93]. However, signal assignment can be very difficult because of the complexity of the chemical/physical molecular interactions at the active site. NMR measurements ad different pH values show that, upon inhibitor binding, the catalytic aspartates do not titrate in the pH range 3-7 and that their ionization state is inhibitor-dependent [89, 91].

An exemplar case in this respect is the adduct with the transition-state analog pepstatin A. Figure 13 displays the 3D structure of the complex with the chemically similar acetyl pepstatin [85]. The complex exhibits two distinct signals at 172.4 and 178.8 ppm in the pH range of 2.5 to 6.5. The low-field peak, which undergoes an isotopic shift, was attributed to a protonated group; in contrast, the other signal (which is unaltered in D_2O) was assigned to an ionized aspartate. As stated by the authors themselves, the assignment is rather surprising as the chemical shifts of ionized and neutral Asp groups are reversed both in aqueous solution [94] and in the adduct with the chemically similar, transition-state analog KNI-27228. The proposed H-bond pattern A1 (Fig. 14), constructed by examining the X-ray structure of the complex with acetyl pepstatin [95], accounts for the inequivalence of the two carboxylates.

In this section, the *ab-initio* analysis of the stability, conformational flexibility and NMR properties of the Asp dyad in the pepstatin/HIV-1 PR complex as published recently by Piana et al. [96] will be presented. Calculations are carried out on structural models of the enzyme's cleavage site (Fig. 14). Anticipating the results, the postulated H-bond pattern A1 is not stable and evolves to a different rearrangement (A2 in Fig. 14) characterized by two almost equivalent ^{13}C chemical shifts. In contrast, the calculations point to stability and experimentally-observed chemical inequivalence of the Asp dyad in the doubly protonated state B (Fig. 14) which has been suggested for other protease-inhibitor complexes [78, 80, 91].

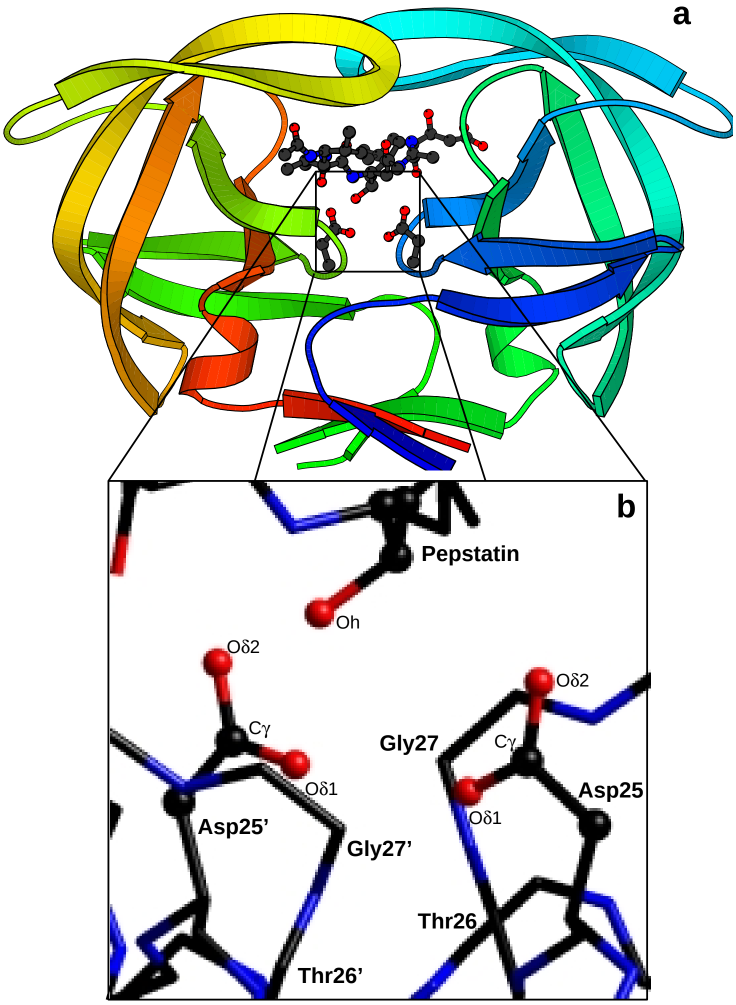
a
b
Pepstatin
Oh
Oδ2
Cγ
Oδ1
Asp25'
Gly27'
Thr26'
Gly27
Oδ2
Cγ
Oδ1
Asp25
Thr26

Figure 13: Acetyl pepstatin/HIV-1 PR complex [95]. (a) The entire adduct and (b) a close up on the cleavage site region (b). Note that the asymmetric inhibitor pepstatin A contains a central hydroxyl group (mimicking the diol catalytic intermediate) tightly bound to the catalytic Asp dyad that imposes a strong asymmetry in the two groups.

11.2 Methods

11.2.1 Structural models

The enzymatic system. The structure of pepstatin A/HIV-1 PR complex has not been solved yet. The structure of the complex with acetyl pepstatin is instead known at 2.0Å resolution [95] (5HVP entry in the PDB database [97]). Acetyl pepstatin is chemically and structurally very similar to pepstatin A, and its portion that binds to the active site is identical to that of pepstatin A. Initial structural models of pepstatin/HIV-1 PR are therefore built from this X-ray structure.

The model complexes include the side-chains of Asp 25/Asp 25' (modeled as acetic acid and acetate, respectively) and groups interacting with them: i) Thr 26(26')-Gly 27(27') peptide bonds (modeled as N-methyl formamide); ii) the alcoholic moiety of acetyl pepstatin (modeled as isopropanole). A model at a similar level of sophistication has been shown to describe accurately the conformational flexibility and the electronic properties of the catalytic dyad in the free enzyme [98].

Two protonation states are considered: in A (Fig. 14), one of the two Asp side chain is protonated (overall net charge -1); in B, both Asp are protonated. Configuration A represents the protonation pattern of HIV-1 PR/pepstatin A proposed on the basis of ^{13}C NMR measurements [85]. The alternative pattern B is chosen in analogy to other protease-inhibitor complexes binding to the catalytic Asp dyad with the same alcoholic functional group [78] to account for the observed abnormal isotope shift. The fully deprotonated state is not considered, as it has not been observed so far in

HIV-1 PR-transition state analog complexes binding at the aspartates with an hydroxyl group.

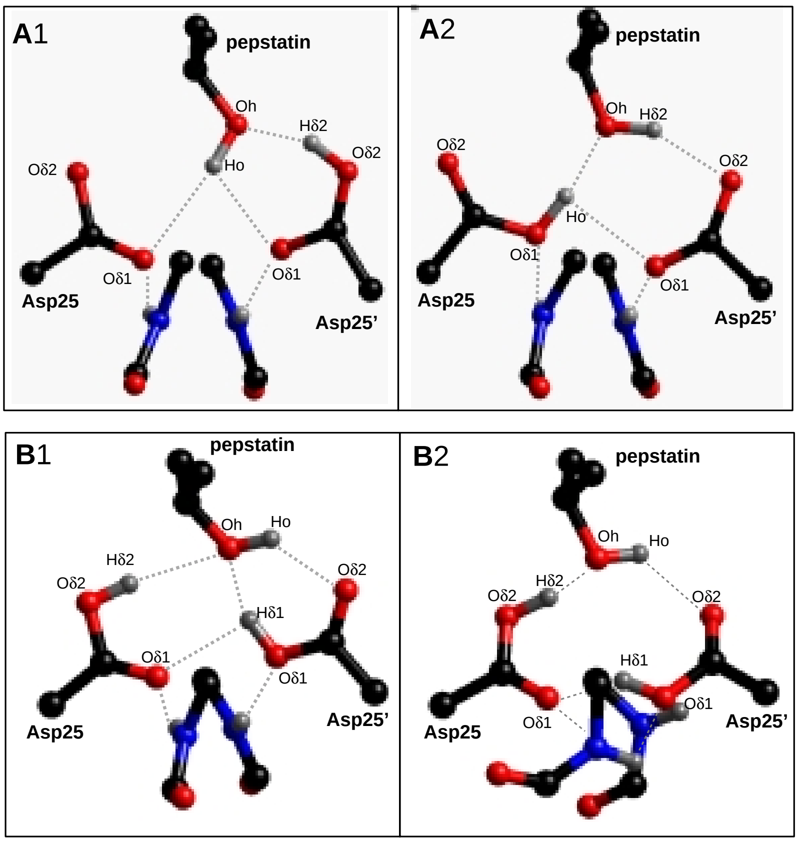
A1
pepstatin
Oh
Hδ2
Oδ2
Ho
Oδ2
Oδ1
Oδ1
Asp25
Asp25'
A2
pepstatin
Oh
Hδ2
Oδ2
Oδ2
Ho
Oδ1
Oδ1
Asp25
Asp25'
B1
pepstatin
Oh
Ho
Hδ2
Oδ2
Oδ2
Hδ1
Oδ1
Oδ1
Asp25
Asp25'
B2
pepstatin
Oh
Ho
Oδ2
Hδ2
Oδ2
Hδ1
Oδ1
Oδ1
Asp25
Asp25'

Figure 14: Quantum mechanical models representing possible H-bond patterns and protonation states of the Acetyl pepstatin-HIV-1 PR complex. A1: postulated pattern (monoprotonated form) based on NMR data [85]. A2: pattern obtained after 2.5 ps of ab initio MD simulation. B: Diprotonated form at the beginning (left) and after 5.0 ps (right) of ab initio MD simulation.

Formic Acid/water complexes. Formic acid (0) and its conjugated base (0-) are constructed assuming standard bond lengths and bond angles (Fig. 15; complexes are named according to the number of water models included). Water/formic acid complexes I-IV are built adding an increasing number of water molecules to 0. IIa (IIc) is the same as III except that WATA(WATB) is removed; IIb is the same as IV except that WATB and WATC are removed.

11.2.2 Quantum-mechanical calculations

The quantum problem is solved within the density functional theory framework, as described in section 3.1. Exchange and correlation functionals are those of Becke [23] and Lee, Yang, Parr [24], respectively. The Kohn-Sham orbitals are expanded in plane waves up to a cutoff energy of 70 Ry. Martin Troullier [28] pseudopotentials were used to describe the interactions between the ionic cores and the valence electrons. The systems were treated as isolated as in ref [99].

Geometry optimizations were carried out using the direct inversion in the iterative subspace method [100]. DFT-based molecular dynamics simulations were performed according to the Car Parrinello scheme [3] for complexes A and B. A time step of 0.1 fs and a fictitious electron mass of 400 au were used. Constant temperature was achieved by coupling the systems to Nosé thermostats of 500 cm^{-1} frequency. A simulation time of 2.3 ps and 5.2 ps of molecular dynamics is performed for model A and B, respectively. In a well-established procedure [98, 101], the positions of terminal atoms are kept fixed during the MD simulations in order to mimic the rigid protein frame

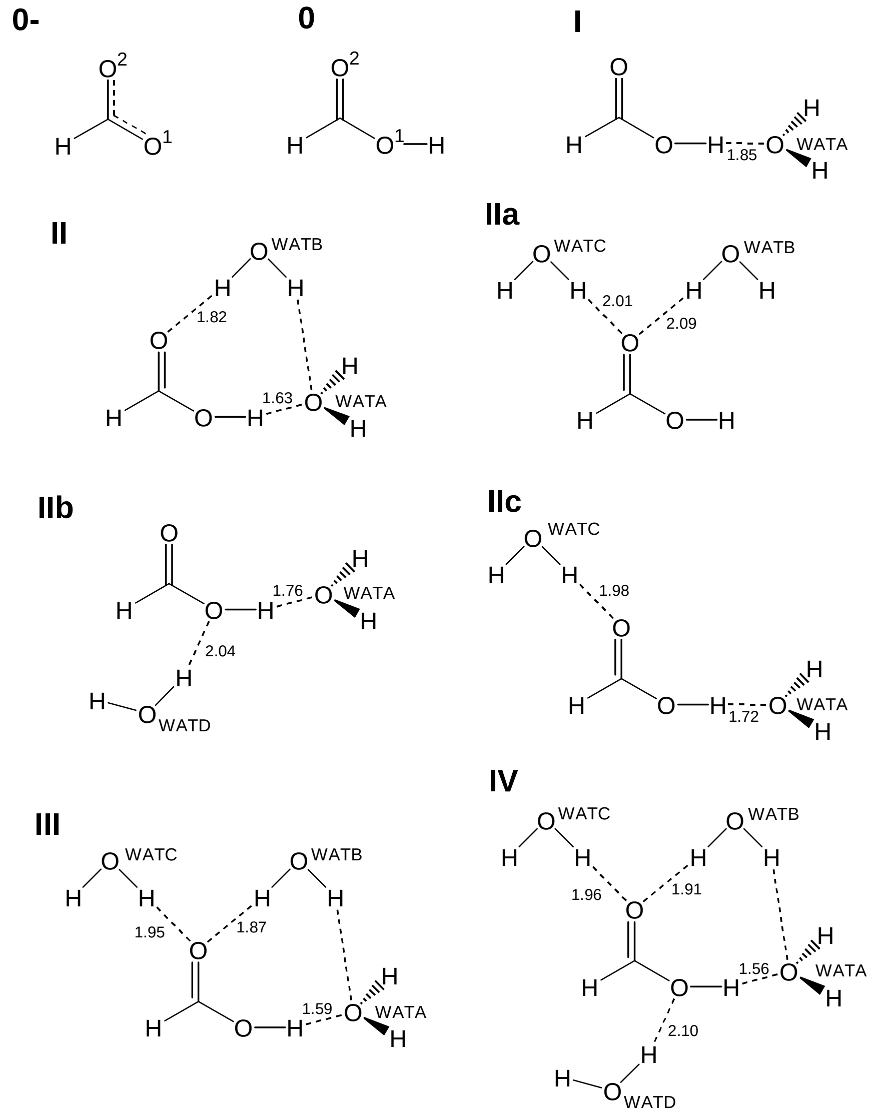
0-
0
I
II
IIa
IIb
IIc
III
IV
O2
O1
WATA
WATB
WATC
WATD
1.85
1.82
1.63
2.01
2.09
1.76
2.04
1.98
1.72
1.95
1.87
1.59
1.96
1.91
1.56
2.10

Figure 15: Hydrated complexes of formic acid considered in the calculations. Carboxyl oxygen atoms and water molecules are labeled by 0- and 0. The hydrogen bonding distances are also indicated.

[95]. This modeling has already proven to be able to reproduce the structural properties of the active site of the free enzyme [98].

11.2.3 Calculated Properties

Sampling for a relatively large number of configurations is necessary to provide reliable estimations of chemical shift, as the latter experience significant fluctuations during the dynamics. Chemical shifts are calculated every 800 steps of MD, corresponding to 80 fs of dynamics. A1 is unstable and evolves to a different pattern (A2) after a few hundreds femtoseconds.Thus, ^{13}C chemical shifts are calculated for 20 configurations of A2, (Fig. 16a). an 55 configurations of B are considered. (Fig. 16b).

To investigate the dependence of the results on the choice of pseudopotentials and basis set, test calculations are carried out also on 10 configurations taken from B with Goedecker pseudopotentials [29] at a cutoff of 100 Ry. It turns out that the relative shifts change by as little as 0.1 ppm.

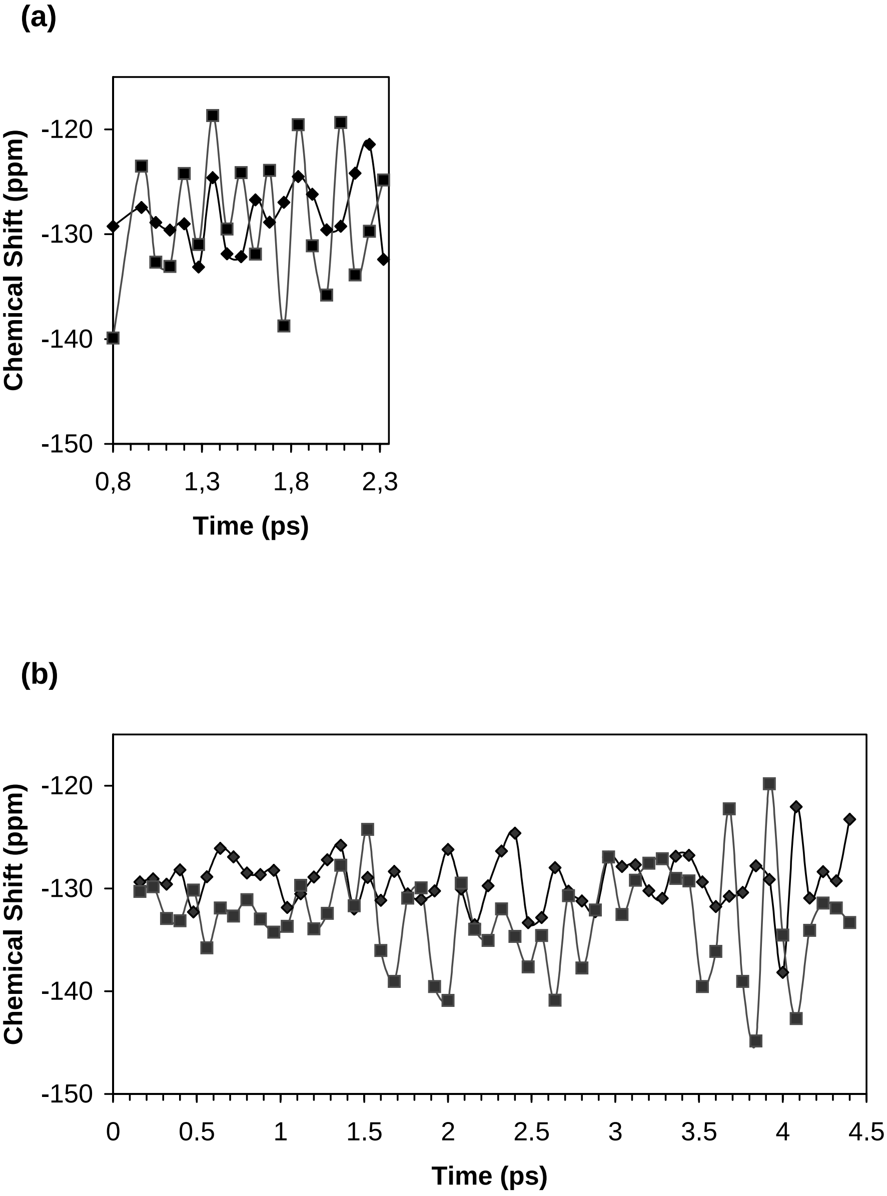

Figure 16: Calculated chemical shifts (ppm) of Cγ Asp25 (diamonds) and Cγ Asp25' (squares) during the ab initio molecular dynamics simulation. The configurations are A2 in (a) and B in (b).

11.3 Results

Monoprotonated form. The H-bond pattern proposed based on ^{13}C NMR data [85] (A1 in Fig. 14) is unstable already on the sub-picosecond time scale. Indeed, after about 0.5 ps, Hδ 2 (Asp25') is transferred to Oh (pepstatin A), and simultaneously, Ho (pepstatin A) is transferred to Oδ 2 (Asp25). In the new structure (A2 in Fig. 14), which is stable up to the end of the simulation, both aspartyl groups interact strongly with the pepstatin hydroxyl group, one as H-bond acceptor (Asp25') and one as H-bond donor (Asp25). The calculated ^{13}C chemical shifts of the carboxyl carbon atoms (Fig. 15a) are almost the same (128.4ppm and 128.7ppm for Cγ (Asp25) and Cγ (Asp25'), respectively, with standard deviations of 1.1ppm and 1.0ppm.). Thus, the pattern of type A2 does not exhibit the experimentally measured, well-separated ^{13}C chemical shifts [85].

The discrepancy from experiment could arise in principle from the relatively small size of the model and short time-scale. However, calculated chemical shifts are well converged in the timescale considered (as shown by their small standard deviation). Furthermore, the complex appears to capture the relevant chemical interactions at the active site, since: i) it includes all the groups interacting with the Asp dyad; ii) the cleavage site is buried inside a hydrophobic region which is unlikely to affect the cleavage site with large electrostatic interactions; iii) the electronic structure in the presence of the protein external electrostatic field exhibits small differences with that in vacuum. It is therefore plausible that the chemical inequivalence of the two Asp groups is due to a state other than the monoprotonated.

There are both theoretical [102] and experimental [103, 104, 105] evidences that the magnitude of the observed isotope effect on the ^{13}C chemical shift is directly related to the strength of the hydrogen bond made by the deuterated proton. The signal that remains unaltered upon changing the solvent from H_2O to D_2O, in the ^{13}C NMR spectra of the enriched pepstatin/protease complex [85], resonates at an extremely low resonance frequency (172.4 ppm compared to 176 ppm for a protonated and 180 ppm for a deprotonated aspartic acid). As stated by the authors themselves, this could be an indication that the group is in a low polar medium making only a few, weak hydrogen bonds with the surrounding residues [85]. On these basis, it appears possible that both aspartic side chains are protonated in the pepstatin/HIV-1 PR complex, but, due to the asymmetric nature of the inhibitor, one of the two aspartates has much weaker H-bonding interactions with the surrounding. This would lead to an uncommon shielding of the ^{13}C signal and a very small isotopic shift upon deuteration.

This hypothesis can be tested against a new calculation, on pattern B, whose protonation state is already known for other HIV-1 PR/transition state analog complexes [78, 80, 91].

Diprotonated form. The system is stable during the entire simulation time (5.2 ps). The asymmetric inhibitor carbon points its hydroxyl group towards the Asp 25 carboxyl group forming a very strong (d_{OH}=1.65(0.2)Å and Θ=158°(11°)) H-bond with Asp25 and weaker interactions with Asp25' (d_{OH} = 2.07(0.2)Å and Θ=146°(15°)). Furthermore, during the simulation, each Asp is stabilized by two additional hydrogen bonds: one coming from the other Asp group ($O\delta$ 1-H$\cdots$ O δ 1) and another coming from the interaction with the Thr26(26')-Gly27(27') peptide bond (N-H$\cdots$ O δ 1).

The calculated chemical shifts of the carboxyl carbons differ by 4 ppm: Cγ (Asp25) Cγ (Asp25') resonate at 129.2(0.4) and 132.9(0.6) ppm, respectively (Fig. 15b). Thus, this pattern exhibits ^{13}C NMR peaks in much better agreement than those of A pointing to the strong inequivalence of the two groups in the doubly protonated form.

11.4 Discussion

Interpretation of ^{13}C NMR data at the cleavage site of HIV-1 PR is highly nontrivial as the effect of local chemical and physical interactions are very difficult to estimate.

Within the limitation of the timescale investigated and the relatively small size of the model complex used, the calculations suggest that the protonation state proposed for HIV-1 PR-pepstatin complex on the basis of ^{13}C NMR data (A1 in Fig. 14) is unstable. Through a double proton transfer process, the complex evolves in the sub-picosecond time scale to a different protonation pattern (A2 in Fig. 14). A2 is stable for the rest of the dynamics and exhibits almost equivalent chemical shifts of the carboxyl carbons, in contradiction to experiment [85]. The chemical equivalence of the Asp groups is explainable in terms of similar H-bond stabilization of the two Asp groups, leading to a similar amount of deshielding.

The calculations indicate the presence of a diprotonated, neutral form of the Asp dyad in the HIV-1 PR-pepstatin complex. Indeed, pattern B (Fig. 14) is stable in the timescale investigated (5.2 ps) and the two ^{13}C resonances are calculated at markedly different frequencies, in qualitative agreement with experiment. The inequivalence is explainable in terms of a deep modification of the chemical environment of the two Asp groups due to the hydroxyl group of the inhibitor. The difference in calculated chemical shifts is slightly smaller than the experimental one (6.4 ppm), possibly because of the relatively small size of the model used (for instance usage of acetic acid for the Asp groups) and of the short time-scale. Further, this difference represents the limit of the overall accuracy of the NMR calculation. However, the model complex captures the difference in the chemical shift of two identical groups in an anisotropic chemical environment.

One remaining question is whether the neutral state can be consistent with isotopic shift measurements. Experimentally, it is found that only one of the carboxylic groups undergoes an isotopic shift [85], apparently suggesting that only one aspartyl is protonated. However, the absolute magnitude of the isotope effect on the ^{13}C chemical shift is very small (about 0.1-0.2ppm) and proportional to the strength of the hydrogen bond formed by the Asp proton with the surrounding residues [102, 103, 104]. In the MD simulation of model B, the carboxylic proton of Asp 25' forms much weaker hydrogen bonds than those of Asp 25. This can lead to an isotopic shift being within the experimental error. Thus, it appears that the absence of an isotopic shift in a carboxylic acid upon solvent substitution from H_2O to D_2O cannot be taken as an absolute indication of deprotonation of the acid.

In conclusion, the calculations show that different ionization states of the aspartyl dyad in pepstatin/HIV-1 PR complex turn out to be almost chemically equivalent, whereas the two doubly protonated Asp groups may be inequivalent because of the strong interactions with non symmetric neighboring groups.

This type of calculations is expected to be used increasingly to interpret NMR signals in this and other proteins.

12 Liquid water

12.1 Water under normal and supercritical conditions

NMR chemical shifts are often used as a measure of the hydrogen bond strength. In liquids, however, the NMR line results from an ensemble average. The atoms and molecules move so quickly that during the irradiation of the NMR pulse into the sample, they visit an large part of the available phase space. Thus, the resonance frequency measures only the ensemble average of the theoretical instantaneous chemical shift. A calculation from first principles can provide a bridge between the single number returned by experiment and the underlying water structure. The microscopic configurations give rise to a very broad distribution of individual shieldings, due to the strong conformational fluctuations, which the experiment can not resolve.

The calculation must be done for a certain number of configurations in order to sample a sufficient part of the phase space of the system. This is done by combining the NMR calculation with a Car-Parrinello ab-initio molecular dynamics simuation [3] that offers a description of the ionic trajectories from first principles. After computing the average of the NMR shieldings over the simulation, this combination thus gives a quantum mechanical description of the NMR experiment.

In molecular dynamics simulations of bulk water, periodic boundary conditions are commonly used in order to minimize finite size errors and to eliminate any surface effects. A certain number of water molecules in a large unit cell is periodically repeated in space. The artificial periodicity induced by this arrangement represents an approximation of the true disordered structure of a liquid. However, by choosing the unit cell large enough, the error due to this periodicity can be minimized. By analyzing the pair correlation functions, it can be verified that the local water structure corresponds well to the situation in reality [106, 107].

Concerning the theoretical NMR resonance lines of such a periodic system, there are no quantum chemical calculations, because the conventional IGLO and CSGT implementations can only be applied to isolated systems in the vacuum. A comparison is only possible with experiment and with the recently developed MPL method. The performance of the method presented in this work shall be demonstrated by this comparison on different water systems. For water under standard ambient conditions, such a calculation has already been performed by Pfrommer et al. [54]. Their calculation will be repeated in order to check the new method. Further, the study

Supercritical water is a system that has recently gained a lot of interest. It is generally defined as water at temperatures above the critical point, T_c=647K, ρ_c=0.32g/cm^3. Under these conditions, it significantly changes its solvation properties [108, 109, 110]. In particular, it can promote chemical reactions such as the oxidation of organic wastes [111, 112] and the geological formation of hydrocarbons like methane [113, 114, 115, 116]. These properties, which are not observed in normal liquid water under ambient conditions, are probably to be associated with the different structure of the hydrogen bond network.

The computational setup is equivalent to that used for the standard liquid water, section 12. To elimitate surface and finite size effects, the liquid is considered as a unit cell containing 32 water molecules taken under periodic boundary conditions. The unit cell dimensions are adapted to the desired environmental conditions.

In particular, the comparison between normal and supercritical water will allow a better understanding of how the NMR signal is affected by the modifications in the H-bond network that are observed in the supercritical state.

The results are in good agreement with recently performed NMR experiments [117, 118, 119], thus providing significant support also for the ab-initio model used to obtain the ionic trajectory. The trajectories used in the calculation were generated by M. Boero et al. [107].

12.1.1 Molecular dynamics

The systems under investigation are trajectories of 32 water molecules obtained under different environmental conditions:

- normal state at standard density and ambient temperature: $T=$300K, $\rho=$1.0g/cm^3 [106]
- supercritical state at high density: $T=$653K, $\rho=$0.73g/cm^3 [107]
- supercritical state at low density: $T=$647K, $\rho=$0.32g/cm^3 [107]

These trajectories have been obtained via a Car-Parrinello molecular dynamics [3] using the CPMD program package [57]. The calculations are performed in the framework of density functional theory using the gradient corrected functionals proposed by Becke [23] and Lee, Yang, Parr [24] (BLYP). Plane waves are used as basis set, together with pseudopotentials of Martins-Troullier type [28], and a plane wave cutoff of 70Ry. Further details can be found in ref. [107]. The shielding calculation is always done at the same level of theory as used for the generation of the trajectory in order to provide a consistent description of the system. For the reference gas phase water molecule, the experimental geometry [120] is used. The shielding is decreased by about 0.3ppm when the BLYP-relaxed geometry at 0K is taken instead. The quantum mechanical zero point motion of the hydrogen atoms are not considered the calculations. Vaara et al. [121] have computed its influence on the shielding to be about half a ppm. However, one can assume that this effect has a similar magnitude in the gas, liquid and supercritical phases, so that it cancels out in the calculation of the relative shift δ .

Experiments measure the trace of the tensor δ ($\mathbf{R}$), averaged over all hydrogen nuclei $\mathbf{R}$ and over a time in the range of about a microsecond. However, it can be expected that within a time span of 9ps, which is the duration of a typical ab initio simulation, all relevant relaxation processes have taken place and the averages are accurate. In order to verify this, the results for the fifth and nineth picosecond of the simulations are compared, considering the first few picoseconds as an equilibration period. In practice, twenty instantaneous atomic configurations are extracted from each of the trajectories at 5ps and at 9ps. It turns out that the chemical shift spectra at 5ps and at 9ps differ by less than 0.15ppm, which indicates a sufficient equilibration of the system.

12.1.2 Magnetic susceptibilities

In order to evaluate the chemical shieldings, Eq. (130), a spherical shape is assumed for the sample. If the experimental conditions are different, for instance in the case of a cylindrical sample geometry (which is the case for a reaction tube), it is customary to convert the measured shieldings to a spherical geometry. For this, one needs the magnetic bulk susceptibility χ or the molar susceptibility χ^m of the system, which is usually assumed to be constant regardless of the thermodynamical conditions. However, for the available experiments concerning liquid water under nonstandard conditions, this assumption, which leads to a linear dependence of the bulk susceptibility on the water density, has never been measured or theoretically confirmed.

Therefore, it is interesting to investigate the magnetic susceptibility per unit volume for these systems with the ab initio method described in this work.

The results are plotted in fig. 17. They are directly expressed in units of the susceptibility correction, i.e. multiplied with the geometrical factor $8\pi/3$ from Eq. (130). It is found that within the theoretical approximations, the magnetic susceptibility depends linearly on the water density and is almost insensitive to the temperature. Thus the assumptions made in experiment [118, 119] can be confirmed.

The molar susceptibility χ^m has been measured for water at room temperature in the liquid phase [122, 123]. Its value, -12.96 ppm cm^3/mol, differs slightly from the one calculated here (-13.4 ppm cm^3/mol) and from that found by Pfrommer et al. (-13.2 ppm cm^3/mol) [54].

For water in the gas phase, there is no experimental susceptibility value. The present implementation yields a χ^m of -13.3 ppm cm^3/mol for the experimental and -13.5 ppm cm^3/mol for the BLYP-relaxed geometry of the water molecule. Pfrommer et al. [54] report a calculated value of -14.6 ppm

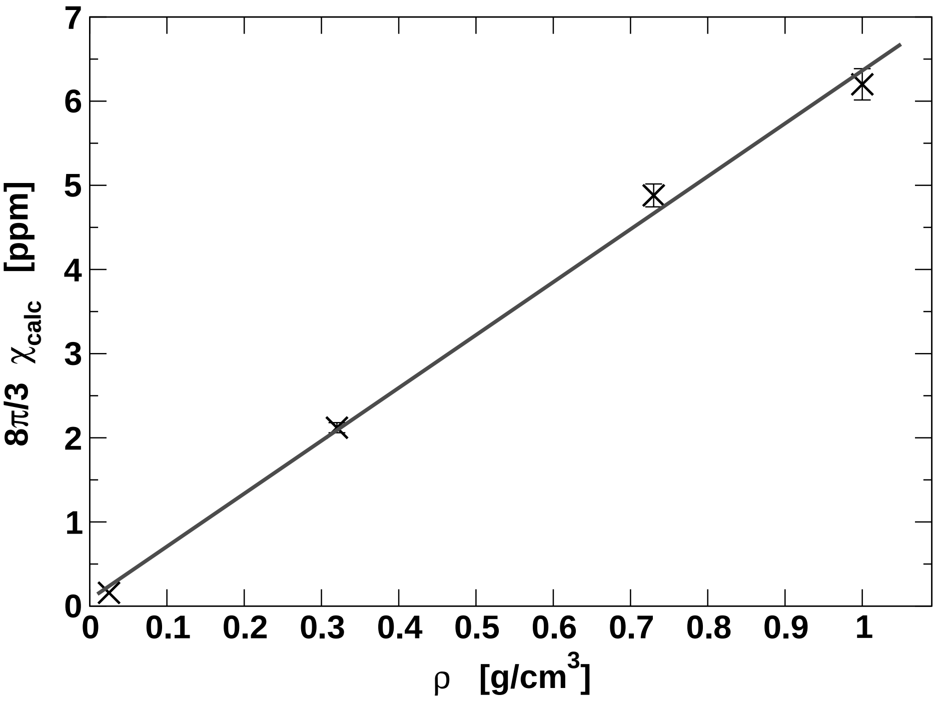

Figure 17: Volumetric susceptibility of water

cm^3/mol in DFT/LDA, whereas a calculation with Gaussian [59] yields -13.8 ppm cm^3/mol in DFT/BLYP, -13.9 ppm cm^3/mol in DFT/LDA and -13.56 ppm cm^3/mol in MP2 (6-311G basis set).

Thus, within the typical numerical accuracy of these calculations, all values are comparable and in agreement with the experimental susceptibility of the liquid. This agreement is reassuring and the errors made are not such as to influence the estimation for the chemical shifts δ .

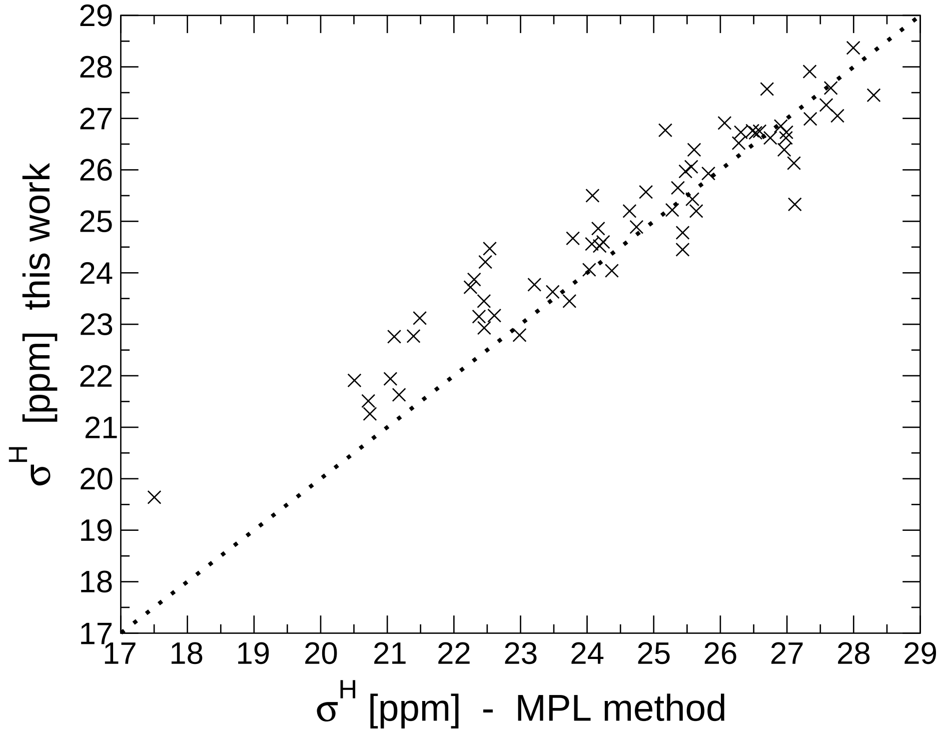

Figure 18: Direct comparison MPL method – this work

12.2 Liquid water under ambient conditions

In fig. 18, a direct comparison is presented for a given system. It is a snapshot taken from an *ab-initio* trajectory of liquid water at room temperature and consists of 32 water molecules within periodic boundary conditions.

The correlation with the shieldings obtained through the MPL approach shows a satisfactory overall agreement. The distribution of the shift values is very similar, although some of the individual shieldings differ significantly. The maximum discrepancy is about 2ppm, which can be explained through the different approximations assumed in the two methods.

The gas-to-liquid shift of water resulting from a statistical analysis of a longer trajectory (9ps) [106] of liquid water is shown in table 1. The experimental values are taken from [121].

	$\delta_{\text{liq}}(^1\text{H})$ [ppm]	$\delta_{\text{liq}}(^{17}\text{O})$ [ppm]
This work	4.1	30
MPL method	5.8	37
Experiment	4.3	36.1

Table 1: ^{1}H and ^{17}O gas to liquid shifts.

As in the recently published calculation by Pfrommer et al. [54], the gas to liquid shifts δ (^{1}H) and δ (^{17}O) of water (table 1) are well reproduced. The hydrogen shift turns out to be closer to experiment than that of oxygen. This is not surprising, because in the frozen core approximation, the pseudopotentials cannot take into account the changes of the electronic structure in the core region. In addition, the error induced by neglecting the terms of Eq. (143) are stronger for heavier nuclei.

12.3 Water under supercritical conditions

In the experiment, the measured shift is an average over all microscopic configurations and over time. One can analyze the individual shift values of the supercritical systems. Their distribution changes significantly when going from the standard to supercritical state. Accumulated histograms are provided in fig. 19 and 20, fitted to Gaussian distributions. The lower the density, the narrower become the distributions. Since the susceptibility correction is not yet added, these graphs measure directly the hydrogen bond

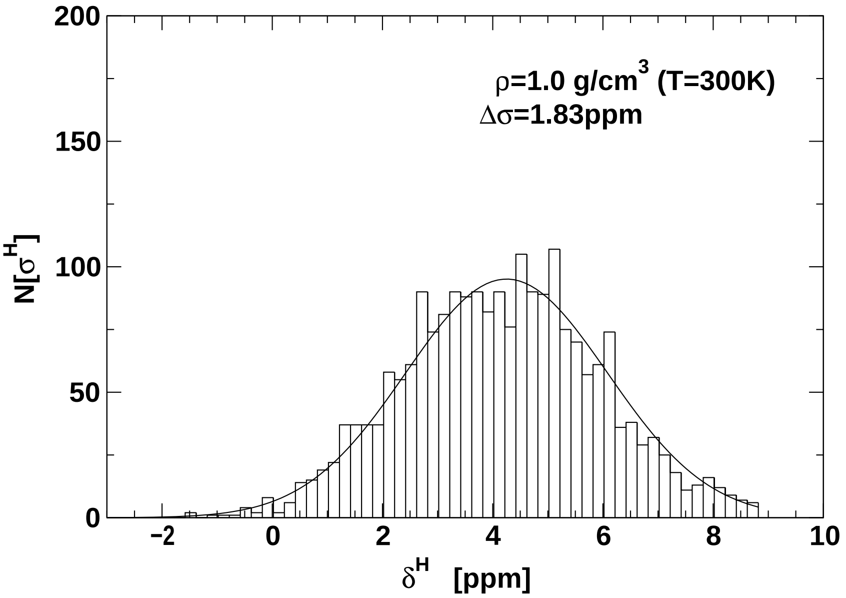

Figure 19: Distribution of the relative shifts for normal conditions. $\Delta\sigma$ is the spread of the fitted Gaussian.

strength.

It is important to note that although broad, these three distributions are clearly separated and the average values can be discriminated. There is an interesting trend in the width of the distributions which decreases as a function of the density.

In fig. 21 these data are put in line with experimentally measured shifts.

Both in theory and in experiment, there is a large jump in the shifts between the supercritical and normal water phases. In terms of hydrogen bonding, this indicates a significantly weaker interaction through the hydrogen bond network in the supercritical state, as expected. Nevertheless, hydrogen bonding is still present, even at very low density.

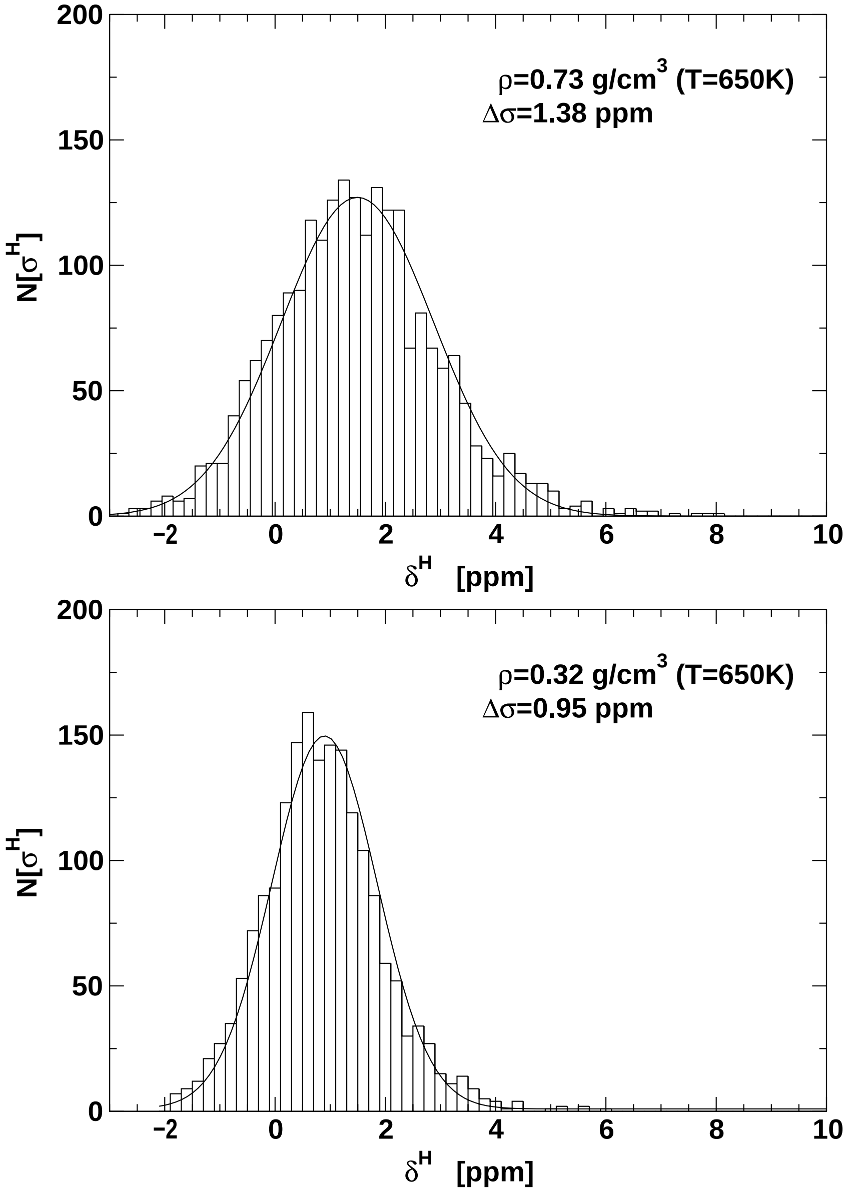

Figure 20: Distribution of the relative shifts for supercritical conditions (top: high density, bottom: low density).

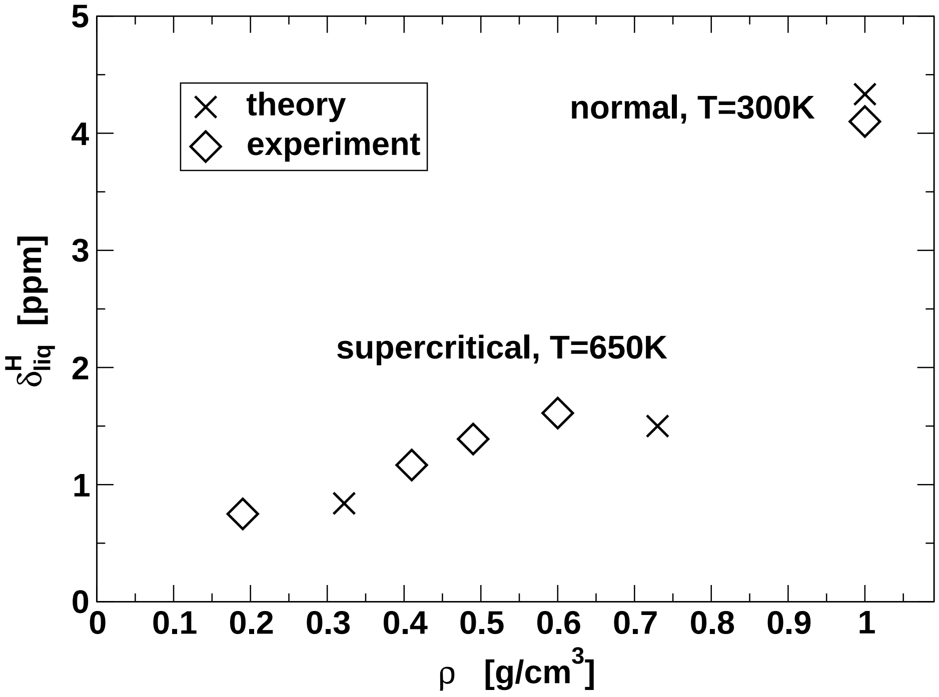

Figure 21: NMR chemical shifts of liquid water relative to the gas phase. Experimental values are taken from [118, 119, 124].

12.3.1 Anomalous hydrogen bond configurations

It has been shown [107] that there are several atypical hydrogen bond (HB) configurations in supercritical water, which are absent in normal liquid water. Their geometries are depicted in fig. 22. Since hydrogen bonds have a very strong effect on the chemical shielding, the question arises to which extent these anomalous arrangements are responsible for the total NMR chemical shift.

In this section, the chemical shifts of these configurations are analyzed. It turns out that their typical shielding is basically the same as for normal H-bonded protons. In addition, the average number of these geometries is very small [107]. On the average, only less than five percent of the water molecules are H-bonded in such an anomalous way. In contrast to that, normal linear HBs are formed by almost every second molecule. The average percentage of H-bonded protons in the simulations is shown in table 2. The definition of a hydrogen bridge is that the next oxygen atom is closer than a certain distance $d_{\mathrm{OH}}^{\mathrm{max}}$, which is varied between 2.0Å and 2.45Å.

In conclusion, the total chemical shift of the supercritical systems is not determined or even significantly influenced by the anomalous H-bond ar-

$d_{\mathrm{OH}}^{\mathrm{max}}$	ρ =0.32g/cm^3	ρ =0.73g/cm^3	ρ =1.0g/cm^3
2.0Å	3.7%	15%	63%
2.3Å	11%	39%	87%
2.45Å	16%	53%	93%

Table 2: Average percentage of protons that form a HB.

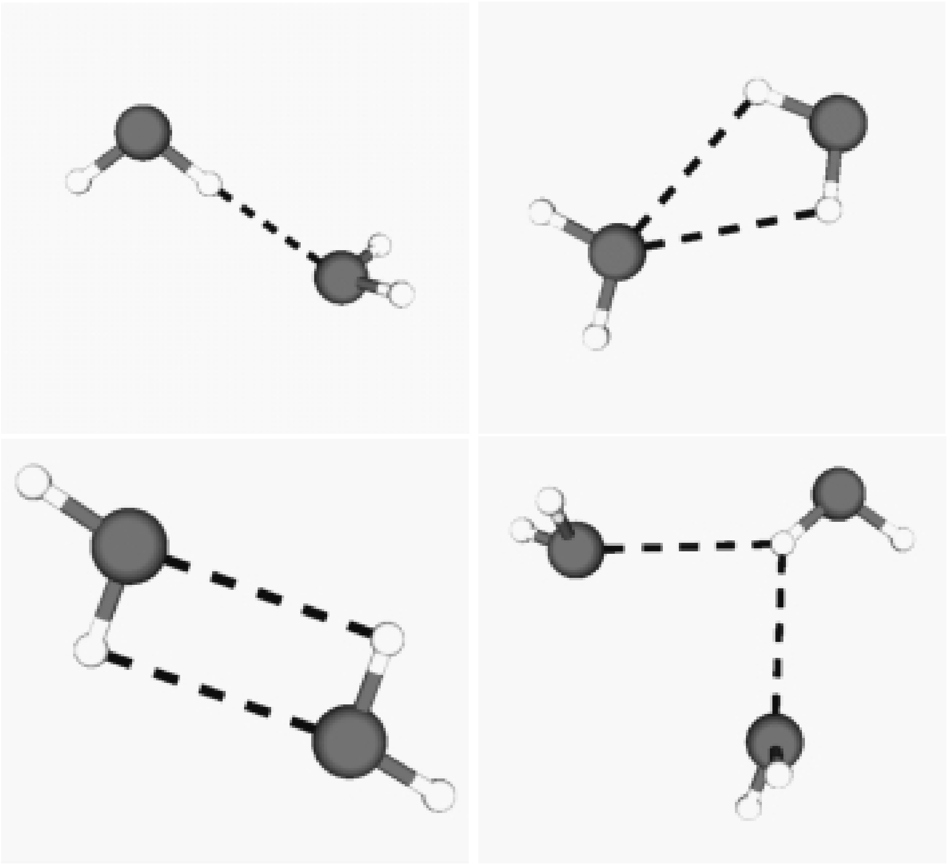

Figure 22: Possible types of hydrogen bond (HB) configurations which exist in supercritical water. From upper left: standard linear HB, bifurcated HB, cyclic HB and twofold HB. Only linear HBs are present in normal liquid water.

rangements. Instead, the very different coordination numbers of the hydrogens due to the H-bond network are responsible for the variation of the shieldings.

12.3.2 Validity of empirical functions for the shift

The ab initio calculation of the NMR chemical shifts of a given configuration has a computational cost comparable to a total energy calculation. Although on modern computers, this is not a tremendous task, it is still expensive to sample a representative statistics of configurations. On the other hand, a large number of empirical formulae and rules of thumb are commonly used in chemistry to predict the NMR line of an atom in a molecule in function of its coordination number and other simple parameters. Since these rules have a surprising accuracy, it is tempting to try to establish such rules for extended systems like liquid water, in order to avoid the fully quantum mechanical calculation. In this chapter, is shall be investigated which range of validity such a formula can have.

Mauri et al. [54] have published an empirical formula that yields the chemical shift of a proton in function of the local geometry of the corresponding water molecule and its neighbors. In particular, this formula takes into account the length d_1 of the closest OH–bridge as well as the distance d_3, d_4 of the two nearest neighboring molecules:

$$\delta\,_i^{\text{empirical}} = A_0 + A_1 d_c + \frac{A_2}{{d_1}^3} + A_3 \left(\frac{1}{{d_3}^3} + \frac{1}{{d_4}^3} \right) + A_4 \alpha. \tag{146}$$

Here, d_c and α are the proton's covalent bond length and the molecular angle, respectively. The parameters A_0 through A_4 are determined by a least square fitting procedure.

Such an empirical formula can be of great use since it significantly reduces the computational cost for the analysis of the trajectory. The only question is whether such a formula can be valid for other environmental conditions than those its parameters have been fitted for. Therefore, the formula will be verified on the normal liquid water system and then applied to the supercritical state. Further, a correlation will be presented between the shift values returned by the empirical function and those obtained from first principles. The results are shown in figures 23 for the $\rho = 1.0\text{g/cm}^3$, $\rho = 0.73\text{g/cm}^3$ and $\rho = 0.32\text{g/cm}^3$ systems, respectively.

The results are reasonably well for the normal conditions (fig. 23, top), although the ab-initio shifts are not always exactly reproduced. The reason for this can be found in the different approximations of the two ab initio methods, as well as the different trajectory the formula has been optimized for.

The shapes of the correlation graphs for the supercritical states (fig. 23, bottom) are still acceptable. Since the overall variations of the shift are smaller, however, the deviations of the empirical formula induce a large relative error. One can compute the standard deviation of the empirical formula for several configurations. Labeling the ab initio shifts by δ_i^{theo}, the standard deviation for a given number N of protons is defined by:

$$\Delta^{(2)} = \frac{1}{N} \sum_i \left[\left(\delta_i^{\text{theo}} - \delta_i^{\text{empirical}} \right)^2 \right]^{1/2} . \qquad (147)$$

The results are shown in table 3. Comparing these standard deviations with those found for the system which the formula parameters have been fitted for, one can get an idea about the transferability of the empirical approach.

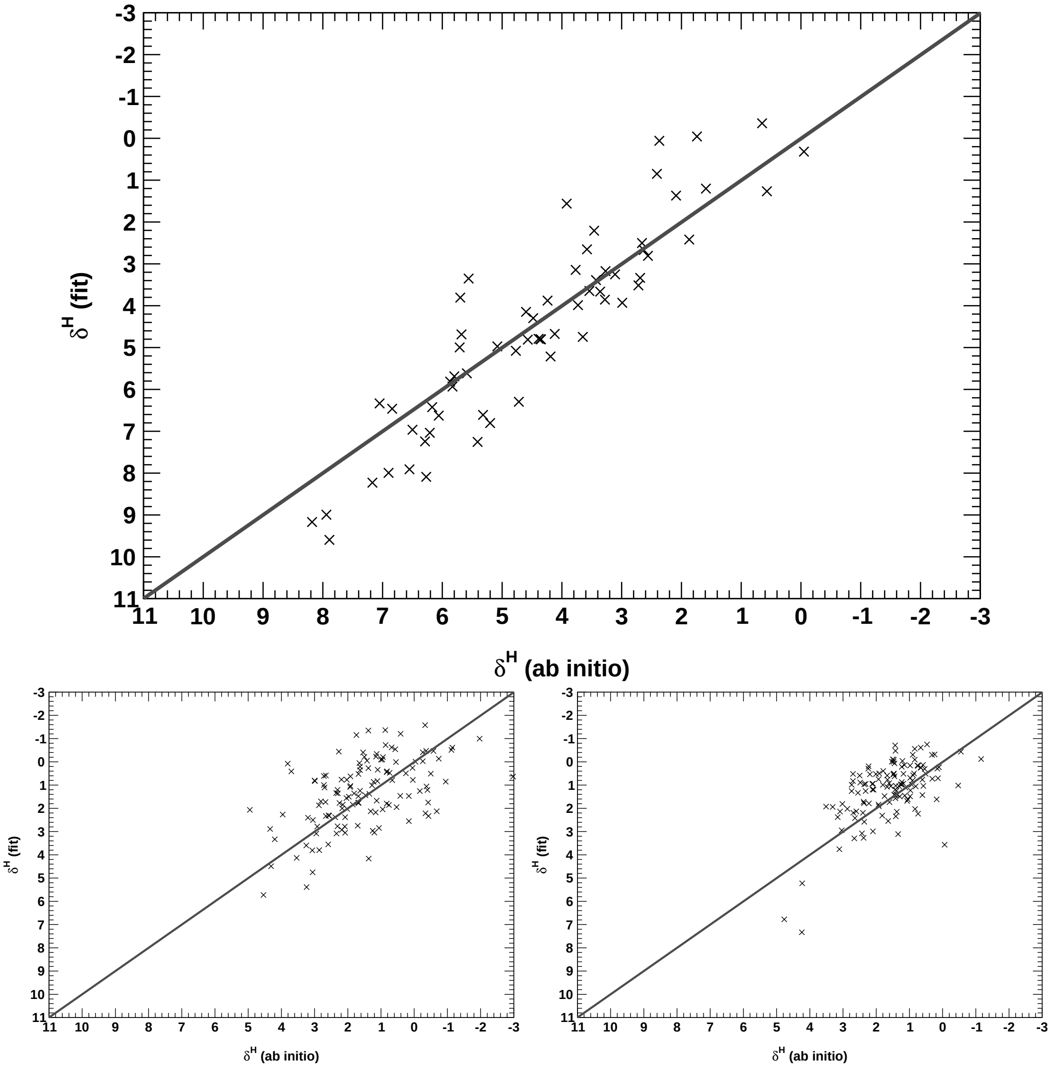

Figure 23: Correlation of the empirical formula with the ab-initio calculation for normal water (top) and supercritical water with $\rho = 0.73\text{g/cm}^3$ (left) and $\rho = 0.32\text{g/cm}^3$ (right)

Since the total chemical shift of the supercritical water is only about around 1 ppm, a standard deviation of the same magnitude seems somwehat too large. However, if the parameters are adapted to the chemical situation, the empirical approach can save computer time, and allows for a considerably better statistics.

The problem of the description through the empirical function is that its parameters implicitly include information about the system as a whole. As an example, one can consider the influence of the hydrogen bridge of the proton. In the formula (146) by Mauri et al., its effect is described through the parameter A_2, which is found to be:

$$\frac{A_2}{{d_1}^3} = \left(\frac{3.17\text{Å}}{d_1}\right)^3 . \tag{148}$$

When considering a single isolated water dimer forming such a hydrogen bridge, the shift of the proton actually decays in $1/{d_1}^3$, as shown in fig. 24. However, the characteristic length of the effect comes out differently. Instead of 3.17Å, the decay length is found to be of 2.36Å.

For this calculation, the optimized dimer geometry is taken and the two molecules are displaced along the OH-bond axis. The $\delta = 0$ limit corresponds to the isolated water molecule. Even if this procedure is only a raw approximation of the situation in the true liquid, it indicates the limit of any

system	ρ =0.32g/cm^3	ρ =0.73g/cm^3	ρ =1.0g/cm^3	MPL method [54]
$\Delta^{(2)}$	1.16 ppm	1.91 ppm	0.99 ppm	0.43 ppm

Table 3: Standard deviation of the empirical formula for the chemical shifts.

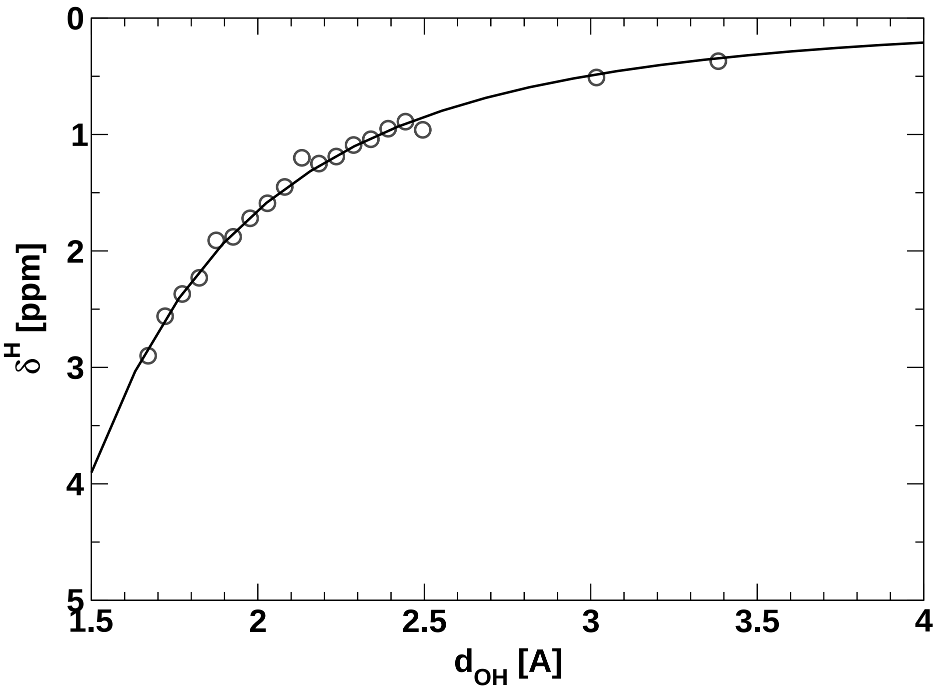

Figure 24: NMR chemical shift of the H-bonded proton of a water dimer in function of the OH-distance. The fitted curve is $\left(2.36\text{Å}/\ d_1\right)^3$.

empirical fit formula.

12.4 Discussion

The results of the ab-initio analysis of the magnetic susceptibilities and the proton NMR chemical shifts of liquid water under normal and supercritical conditions agree well with experiment and confirm the existence of hydrogen bonding in supercritical water even at low density. The calculations also validate the assumption that the magnetic susceptibility is linear in the water density, regardless of the thermodynamical conditions.

The calculations presented in this section give further support to the accuracy of the BLYP functional in water calculations, since one can reproduce quantitatively the drop in the hydrogen bond strength from normal to supercritical water, as measured by the NMR chemical shift.

The ab initio analysis of the magnetic susceptibilities and the proton NMR chemical shifts of water supercritical conditions presented in this section can provide an important contribution to the validation of ab initio generated trajectories. The results agree well with experiment and confirm the existence of hydrogen bonding in supercritical water even at low density.

The calculations also validate the assumption that the magnetic susceptibility is linear in the water density, regardless of the thermodynamical conditions.

The calculations give further support to the accuracy of the BLYP functional in water calculations, since the drop in the hydrogen bond strength from normal to supercritical water, as measured by the NMR chemical shift, can be reproduced quantitatively.

The validity of empirically fitted formula to predict the NMR lines based on a few variables is shown to be valid as far as the average shift position is concerned, whereas the individual shieldings are only reproduced up to a relatively large error.

13 Conclusion

In this thesis, a new *ab initio* method is presented which allows the efficient calculation of magnetic susceptibilities and NMR chemical shielding tensors from first principles. It is formulated in the context of variational density functional perturbation theory and implemented in a pseudopotential plane-wave computer program package.

The approach is based on the localized nature of the electronic wavefunctions in the Wannier orbital representation. When considering periodic systems with extended electronic wavefunctions, this representation can be obtained by a unitary rotation of the occupied subspace of these electrons. There is evidence [50] that in insulators, there is always such a representation of the electronic structure. In particular, the individual electronic orbitals can be shown to have an exponentially decaying amplitude. This formulation allows a relatively straightforward solution of the fundamental problem of magnetic orbital responses in periodic systems, the application of the position operator. It shall be noted here, that there is no simple extension of the Berry phase approach, which can tackle the problem of the *expectation value* of the position operator in a periodic system.

To recapitulate the approach presented in the preceding sections, the perturbation Hamiltonian which represents the action of the external homogeneous magnetic field, Eq. (112), is applied to the localized orbitals. A virtual cell (VC) is placed around each of these orbitals, such that the electron is entirely contained inside this VC. The magnetic perturbation Hamiltonian contains a new orbital-specific position operator (fig. 1), individually defined for each virtual cell. The first order perturbation wavefunctions $\varphi^{(1)}$ are then obtained variationally through the minimization of the second order energy functional, Eq. (116), in the framework of density functional perturbation theory.

The total electronic current density is computed as the periodically repeated sum of all orbital currents obtained from the first order perturbation wavefunctions by Eq. (133). To make this formula computationally efficient, the approximation of neglecting the term of Eq. (143) is adopted. The validity of the approximation in different chemical situations is checked by an exact calculation for isolated molecules. It is shown that the error induced by the approximation is comparable to the overall accuracy of the implementation.

The current leads to the chemical shieldings over the periodic part of the induced magnetic perturbation field through Eq. (126), and to the magnetic susceptibility over the spatially constant part of the induced field through Eq. (130).

The results presented in the previous sections show that the technique presented in this work can be used for amorphous as well as periodic systems with good accuracy.

The calculations can give further support to the accuracy of the trajectories of condensed phases generated by density functional theory. In particular, the systems investigated in this thesis, in particular water in the liquid state, require special care due to the complex hydrogen bond network. Since this network has a large effect on NMR parameters, their calculation can help to estimate the quality of the trajectory. Here, the description of H-bonds through the BLYP exchange correlation functional in water calculations could be validated, since the decrease in the hydrogen bond strength from normal to supercritical water, as measured by the NMR chemical shift, can be reproduced quantitatively.

The practical advantage of the method presented here compared to the existing formulation for periodic systems by Mauri et al. [5] is the computational effort, which can be significantly smaller. For systems that can be described through a very small primitive cell, like defect-free crystals, one would have to use a supercell technique to obtain sufficiently localized Wannier functions in the method presented here. The MPL approach works with the primitive cell only, making it much more efficient in such a case.

However, for systems that require a large unit cell, the computational effort is considerably smaller in the new approach. The computer time needed to calculate a system of 32 water molecules in the liquid state at ρ =1g/cm^3 is about six times smaller compared to the MPL approach [125]. This becomes especially important in the combination with molecular dynamics. In such a case, in order to obtain a good statistical average, the NMR chemical shift has to be calculated for a large number of atomic configurations (snapshots) out of the trajectory.

The method presented in this thesis is currently being applied to a variety of systems, including biologically important molecules, and provides a powerful tool to interpret experimental results.

Appendix

A Discrete Fourier transformations

In general, a Fourier transformation switches the representation of a function φ between two conjugate spaces. In the present case, they are the direct and reciprocal space, being the representations of the function in three-dimensional cartesian position coordinates $\varphi(\mathbf{r})$ and in plane waves $\varphi(\mathbf{G})$, respectively. The textbook Fourier transformation consists of two integrals converting between continuous direct and continuous reciprocal space:

$$\begin{aligned} \varphi(\mathbf{G}) &= \int \mathrm{d}^3 r \; \mathrm{e}^{-i\,\mathbf{G}\cdot\mathbf{r}} \, \varphi(\mathbf{r}) && (149) \\ \varphi(\mathbf{r}) &= \frac{1}{(2\pi)^3} \int d^3G \; \mathrm{e}^{i\,\mathbf{G}\cdot\mathbf{r}} \, \varphi(\mathbf{G}). && (150) \end{aligned}$$

In principle, this formula is only valid for $\mathcal{L}_2$-functions, where the convergence of Eq. (149) is assured. Through these definitions, it is automatically assured that Eq. (150) is actually the inverse transformation of (149):

$$\begin{aligned} \varphi(\mathbf{r}) &= \frac{1}{(2\pi)^3} \int d^3G \; \mathrm{e}^{i\,\mathbf{G}\cdot\mathbf{r}} \int \mathrm{d}^3 r\,' \; \mathrm{e}^{-i\,\mathbf{G}\cdot\mathbf{r}'} \, \varphi(\mathbf{r}') \\ &= \frac{1}{(2\pi)^3} \int \mathrm{d}^3 r\,' \; \varphi(\mathbf{r}') \int d^3G \; \mathrm{e}^{i\,\mathbf{G}\cdot(\mathbf{r}-\mathbf{r}')} \\ &= \frac{1}{(2\pi)^3} \int \mathrm{d}^3 r\,' \; \varphi(\mathbf{r}') \; (2\pi)^3 \, \delta^{\,3}(\mathbf{r}-\mathbf{r}') \\ &= \varphi(\mathbf{r}). && (151) \end{aligned}$$

The simulation program package underlying this work uses periodic boundary conditions, so that every function is supposed to have the periodicity of the calculation cell. This can be achieved by restricting the **G**-vectors to a discrete set, in such a way that the associated plane waves obey that periodicity. Then, every function represented in terms of these plane waves automatically satisfies the periodic boundary conditions.

However, the integral representation, Eq. (149) and (150), cannot hold any more. The **G**-integral becomes a discrete sum over the allowed **G**-vectors. In addition, the representation in real space cannot be done in a continuous way either. In a computer code, the values of the function are stored on a finite grid. Thus, also the integral over the direct space, Eq. (149), becomes a sum over the points of that grid. Of course, the normalization changes as well, since the Riemann sum is only done over one simulation cell. The new definition reads:

$$\begin{aligned} \psi(\mathbf{G}) &= \sum_{\mathbf{r}} \mathrm{e}^{-i\,\mathbf{G}\cdot\mathbf{r}}\, \psi(\mathbf{r}) && (152) \\ \psi(\mathbf{r}) &= \frac{1}{N_G} \sum_{\mathbf{G}} \mathrm{e}^{i\,\mathbf{G}\cdot\mathbf{r}}\, \psi(\mathbf{G}) && (153) \end{aligned}$$

where N_G is the number of G-vectors in the discrete back-transformation (153). One now imposes that the number of grid points be identical on the real space grid and on the reciprocal space grid. It will be shown that this is neccessary to assure that these two transformations are actually the inverse of each other. A forth and back transformed wavefunction can be written:

$$\begin{aligned} \psi(\mathbf{r}) &= \frac{1}{N_G} \sum_{\mathbf{G}} \mathrm{e}^{i\,\mathbf{G}\cdot\mathbf{r}} \sum_{\mathbf{r}'} \mathrm{e}^{-i\,\mathbf{G}\cdot\mathbf{r}'}\, \psi(\mathbf{r}') \\ &= \frac{1}{N_G} \sum_{\mathbf{r}'} \psi(\mathbf{r}') \sum_{\mathbf{G}} \mathrm{e}^{i\,\mathbf{G}\cdot(\mathbf{r}-\mathbf{r}')} && (154) \end{aligned}$$

The last sum in Eq. (154) is nontrivial. One can first investigate the case where $\mathbf{G} \cdot (\mathbf{r} - \mathbf{r}')$ is zero or a multiple of 2π. This happens only when

$\mathbf{r} = \mathbf{r}'$ under periodic boundary conditions. Then, the sum simply yields the total number of G-vectors, N_G, which directly cancels with the normalization prefactor $1/\ N_G$ of Eq. (153).

For all other positions, $\mathbf{r} \neq \mathbf{r}'$, the situation is more involved. It can be shown that for this case, the sum vanishes:

$$\sum_{\mathbf{G}} \mathrm{e}^{i\,\mathbf{G}\cdot\mathbf{r}} \;=\; 0 \qquad \forall \mathbf{r} \neq 0. \tag{155}$$

The G-vectors represented in the sum are taken from the cell's reciprocal lattice,

$$\mathbf{G}_i \;=\; k_i\mathbf{b}_1 + l_i\mathbf{b}_2 + m_i\mathbf{b}_3, \tag{156}$$

and they verify the *energy cutoff* criterion:

$$\langle \mathbf{G}|\mathcal{T}|\mathbf{G}\rangle \;=\; \frac{1}{2}\mathbf{G}^2 \leq E_c \tag{157}$$

with a certain cutoff-energy E_c. The vectors $\mathbf{b}_1, \mathbf{b}_2, \mathbf{b}_3$ are the basis vectors of the reciprocal lattice and (k_i, l_i, m_i) designate the Miller indices of the G-vector $\mathbf{G}_i$. Eq. (157) describes a sphere where all the considered vectors are inside.

Unfortunately, the sum in Eq. (155) is rather tricky to calculate with a spherical cutoff for the G-vectors as defined by Eq. (157). Therefore, a different condition is adopted in practice, which makes the calculus straightforward: we use a cubic cutoff instead of the sphere. The Miller indices (k_i, l_i, m_i) are allowed to vary *independently* in a symmetric interval:

$$-K \;\leq k_i \leq\; +K \tag{158}$$

$$-L \;\leq l_i \leq\; +L \tag{159}$$

$$-M \;\leq m_i \leq\; +M. \tag{160}$$

Now, the sum in Eq. (154) can be done analytically:

$$\sum_{\mathbf{G}} \mathrm{e}^{i\,\mathbf{G}\cdot\mathbf{r}} = \sum_{k=-K}^{K}\sum_{l=-L}^{L}\sum_{m=-M}^{M} \mathrm{e}^{i\,k\,\mathbf{b}_1\cdot\mathbf{r}}\,\mathrm{e}^{i\,l\,\mathbf{b}_2\cdot\mathbf{r}}\,\mathrm{e}^{i\,m\,\mathbf{b}_3\cdot\mathbf{r}} \tag{161}$$

$$= \frac{\sin\left(\left(K+\frac{1}{2}\right)\ \mathbf{b}_1\cdot\mathbf{r}\right)}{\sin\left(\frac{1}{2}\mathbf{b}_1\cdot\mathbf{r}\right)}\ \frac{\sin\left(\left(L+\frac{1}{2}\right)\ \mathbf{b}_2\cdot\mathbf{r}\right)}{\sin\left(\frac{1}{2}\mathbf{b}_2\cdot\mathbf{r}\right)} \tag{162}$$

$$\frac{\sin\left(\left(M+\frac{1}{2}\right)\ \mathbf{b}_3\cdot\mathbf{r}\right)}{\sin\left(\frac{1}{2}\mathbf{b}_3\cdot\mathbf{r}\right)} \tag{163}$$

under the condition that $\mathbf{b}_1\cdot\mathbf{r}$, $\mathbf{b}_2\cdot\mathbf{r}$ and $\mathbf{b}_3\cdot\mathbf{r}$ are not multiples of 2π, such that the denominators in Eq. (163) do not vanish. If one or two of them are, the corresponding fractions must be replaced by $2K+1$, $2L+1$ or $2M+1$, respectively. But at least one of the factors remains.

Any position vector can be written as

$$\mathbf{r} = \frac{j_1}{N_1}\mathbf{a}_1 + \frac{j_2}{N_2}\mathbf{a}_2 + \frac{j_3}{N_3}\mathbf{a}_3 \tag{164}$$

with the basis vectors of the direct lattice, $\mathbf{a}$, integers numbers j and the corresponding number of grid points N. One now uses the fact that the dimension of the real space grid has been chosen to be identical to that of the reciprocal space. This means that $N_1 = 2K+1, N_2 = 2L+1$ and $N_3 = 2M+1$, and thus for any position vector $\mathbf{r}$,

$$\left(K+\frac{1}{2}\right)\ \mathbf{b}_1\cdot\mathbf{r} = \frac{1}{2}N_1\ \mathbf{b}_1\cdot\left(\frac{j_1}{N_1}\mathbf{a}_1 + \frac{j_2}{N_2}\mathbf{a}_2 + \frac{j_3}{N_3}\mathbf{a}_3\right) \tag{165}$$

$$= \frac{1}{2}j_1\ 2\pi \tag{166}$$

$$= j_1\ \pi, \tag{167}$$

since $\mathbf{b}_i\cdot\mathbf{a}_j = \delta_{\ ij}$. The sine of a multiple of π being zero, Eq. (163) vanishes and Eq. (155) is fulfilled.

In other words, the identity of the number of mesh points on the direct and reciprocal space grids assures that the discrete transformations given by Eqs. (152) and (153) are actually the exact inverse of each other.

B A particular Fourier transformation

In this appendix a particular expression shall be evaluated, which will be needed in section 5.5 (Eq. (128)). The starting point is the electronic current density $\mathbf{j}(\mathbf{r})$, given in the unit cell, which is assumed to be periodically repeated throughout space. The goal is to compute the induced magnetic field at a given location $\mathbf{r}$ inside the unit cell. In direct space, this field can be expressed (cf. Eq. (127)) as:

$$\begin{aligned}
\mathbf{B}^{\text{ind}}(\mathbf{r}) &= \frac{\mu_0}{4\pi} \int d^3r' \, \frac{\mathbf{r}' - \mathbf{r}}{|\mathbf{r}' - \mathbf{r}|^3} \times \mathbf{j}(\mathbf{r}') && (168) \\
&= \frac{\mu_0}{4\pi} \int d^3r' \left(\frac{\partial}{\partial\, \mathbf{r}} \frac{1}{|\mathbf{r}' - \mathbf{r}|} \right) \times \mathbf{j}(\mathbf{r}') && (169) \\
&= \frac{\mu_0}{4\pi} \, \varepsilon_{\alpha\beta\gamma} \, \mathbf{e}_\alpha \, \frac{\partial}{\partial\, r_\beta} \int d^3r' \, \frac{1}{|\mathbf{r}' - \mathbf{r}|} \, j_\gamma(\mathbf{r}'), && (170)
\end{aligned}$$

where the integral is understood to go over all space, not only the unit cell. The vector product has been written with the help of the totally antisymmetric tensor $\varepsilon_{\alpha\beta\gamma}$, the Levi-Cività-symbol. The vector $\mathbf{e}_\alpha$ denotes the unit vector in the cartesian direction α, and the indices α, β, γ are subject to Einstein summation. The current is periodically repeated, whereas the function $\frac{\mathbf{r}'-\mathbf{r}}{|\mathbf{r}'-\mathbf{r}|^3}$ resp. $\frac{1}{|\mathbf{r}'-\mathbf{r}|}$ is not.

Mathematically, the integral in Eq. (170) is somewhat dangerous, since the integration of a function decaying like $1/\,r$ normally does not converge. But the current, although it is periodically repeated and therefore not vanishing at $r' \mapsto \infty$, is an alternating function. This is clear because the net current of every cell must be zero:

$$\int \mathrm{d}^3 r \; \mathbf{j}(\mathbf{r}) \;=\; 0. \qquad (171)$$

Thus, the integral is constituted of an algebraically decaying term times an alternating expression, which makes it convergent.

For simplicity, only the expression

$$I_\gamma(\mathbf{r}) \;=\; \int \mathrm{d}^3r' \, \frac{1}{|\mathbf{r}' - \mathbf{r}|} \, j_\gamma(\mathbf{r}') \tag{172}$$

shall be treated, taking only one cartesian component of the current density $\mathbf{j}(\mathbf{r})$ as a scalar function. The property Eq. (171) applies to each of these components, and when expressed in reciprocal space, it is therefore equivalent to

$$j_\gamma(\mathbf{G} = 0) \;=\; 0. \tag{173}$$

This will make Eq. (172) somewhat easier to handle. Using the representation in G-space according to Eq. (153):

$$\begin{aligned}
I_\gamma(\mathbf{r}) &= \int \mathrm{d}^3r' \, \frac{1}{|\mathbf{r}' - \mathbf{r}|} \, \frac{1}{N_G} \sum_{\mathbf{G}\neq 0} \mathrm{e}^{i\mathbf{G}\cdot\mathbf{r}'} j_\gamma(\mathbf{G}) && (174)\\
&= \frac{1}{N_G} \sum_{\mathbf{G}\neq 0} j_\gamma(\mathbf{G}) \mathrm{e}^{i\mathbf{G}\cdot\mathbf{r}} \int \mathrm{d}^3r' \, \frac{1}{|\mathbf{r}' - \mathbf{r}|} \, \mathrm{e}^{i\mathbf{G}\cdot(\mathbf{r}'-\mathbf{r})} && (175)\\
&= \frac{1}{N_G} \sum_{\mathbf{G}\neq 0} j_\gamma(\mathbf{G}) \, \mathrm{e}^{i\mathbf{G}\cdot\mathbf{r}} \int \mathrm{d}^3\tau \, \frac{1}{\tau} \, \mathrm{e}^{i\mathbf{G}\cdot\boldsymbol{\tau}}, && (176)
\end{aligned}$$

where $\boldsymbol{\tau} = \mathbf{r}' - \mathbf{r}$ has been substituted. Clearly, the integral in Eq. (176) would diverge for $\mathbf{G} = 0$. The usual trick to calculate it for $\mathbf{G} \neq 0$ is to replace it by the expression

$$\lim_{a\mapsto 0} \int \mathrm{d}^3\tau \, \frac{1}{\tau} \mathrm{e}^{-a\tau} \, \mathrm{e}^{i\mathbf{G}\cdot\boldsymbol{\tau}}, \tag{177}$$

which is easily evaluated to be

$$\begin{aligned}
\int \mathrm{d}^3\tau \, \frac{1}{\tau} \mathrm{e}^{-a\tau} \, \mathrm{e}^{i\mathbf{G}\cdot\boldsymbol{\tau}} &= \int d\varphi \, d(\cos\theta_\tau) \, d\tau \; \tau^2 \frac{1}{\tau} \mathrm{e}^{-a\tau} \, \mathrm{e}^{iG\tau\cos\theta_\tau} && (178)\\
&= \frac{4\pi}{a^2 + G^2}. && (179)
\end{aligned}$$

The limit $a \mapsto 0$ yields for Eq. (176)

$$I_\gamma(\mathbf{r}) \;=\; \frac{1}{N_G} \sum_{\mathbf{G}\neq 0} j_\gamma(\mathbf{G})\, \mathrm{e}^{i\mathbf{G}\cdot\mathbf{r}}\, \frac{4\pi}{G^2}, \tag{180}$$

which is nothing else but the discrete Fourier back-transform (cf. Eq. (153)) of the periodic function

$$\frac{4\pi}{G^2}\, j_\gamma(\mathbf{G}) \;=\; I_\gamma(\mathbf{G}). \tag{181}$$

Finally, the induced magnetic field can be written, using this result in Eq. (170), as:

$$\begin{aligned}
\mathbf{B}^{\mathrm{ind}}(\mathbf{r}) &= \frac{\mu_0}{4\pi}\, \varepsilon_{\alpha\beta\gamma}\, \mathbf{e}_\alpha\, \frac{\partial}{\partial\, r_\beta} I_\gamma(\mathbf{r}) && (182)\\
&= \frac{\mu_0}{4\pi}\, \varepsilon_{\alpha\beta\gamma}\, \mathbf{e}_\alpha\, \frac{\partial}{\partial\, r_\beta} \frac{1}{N_G} \sum_{\mathbf{G}\neq 0} \mathrm{e}^{i\mathbf{G}\cdot\mathbf{r}}\, I_\gamma(\mathbf{G}) && (183)\\
&= \frac{1}{N_G} \sum_{\mathbf{G}\neq 0} \mathrm{e}^{i\mathbf{G}\cdot\mathbf{r}}\, iG_\beta\, I_\gamma(\mathbf{G}) \left[\frac{\mu_0}{4\pi}\, \varepsilon_{\alpha\beta\gamma}\, \mathbf{e}_\alpha\right] && (184)\\
&= \frac{1}{N_G} \sum_{\mathbf{G}\neq 0} \mathrm{e}^{i\mathbf{G}\cdot\mathbf{r}} \left[i\mu_0\, \varepsilon_{\alpha\beta\gamma}\, \mathbf{e}_\alpha\, \frac{G_\beta}{G^2}\, j_\gamma(\mathbf{G}) \right]. && (185)
\end{aligned}$$

Thus, there is a very simple representation of the magnetic field in reciprocal space:

$$\begin{aligned}
\mathbf{B}^{\mathrm{ind}}(\mathbf{G}) &= i\mu_0\, \varepsilon_{\alpha\beta\gamma}\, \mathbf{e}_\alpha\, \frac{G_\beta}{G^2}\, j_\gamma(\mathbf{G}) && (186)\\
&= \frac{i\mu_0}{G^2}\, \mathbf{G} \times \mathbf{j}(\mathbf{G}). && (187)
\end{aligned}$$

One finds the expression as presented in Eq. (128). As already mentioned there, the $\mathbf{G} = 0$ component needs a special treatment, because it determines the homogeneous field, spread over the whole system. It depends on the macroscopic shape of the sample and cannot be calculated under periodic boundary conditions. A calculation for a typical experimental geometry (a spherical sample) is presented in section C.

C Macroscopic susceptibility

C.1 General

In this section, the $\mathbf{G} = 0$ component of the induced magnetic field is computed and it is shown how it affects the shieldings of a system.

The formula to calculate the induced field from the current density, Eq. (127), remains unchanged. Only when transforming it into reciprocal space, the integration for $\mathbf{G} = 0$ needs special care. The Integral representation is used instead of the discrete sum, because the latter is only an auxiliary mean to actually perform the calculations on a computer. The physical definition instead is always based on the integral representation, Eq. (149). It reads:

$$\mathbf{B}^{\text{ind}}(\mathbf{G} = 0) = \int_{\mathcal{S}} \mathrm{d}^3r \; \mathbf{B}^{\text{ind}}(\mathbf{r}), \tag{188}$$

where the integral includes the whole space, i.e. the complete macroscopic sample, designated by S. Like in the case $\mathbf{G} \neq 0$, the induced field can be calculated from the induced orbital current (cf. Eq. (127)) by:

$$\mathbf{B}^{\text{ind}}(\mathbf{r}) = \frac{\mu_0}{4\pi} \int_{\mathcal{S}} \mathrm{d}^3r' \; \frac{\mathbf{r}' - \mathbf{r}}{|\mathbf{r}' - \mathbf{r}|^3} \times \mathbf{j}(\mathbf{r}'). \tag{189}$$

Together with Eq. (188), this becomes:

$$\begin{aligned}
\mathbf{B}^{\text{ind}}(\mathbf{G} = 0) &= \frac{\mu_0}{4\pi} \int_{\mathcal{S}} \mathrm{d}^3r \, \mathrm{d}^3r' \; \frac{\mathbf{r}' - \mathbf{r}}{|\mathbf{r}' - \mathbf{r}|^3} \times \mathbf{j}(\mathbf{r}') &(190)\\
&= \frac{\mu_0}{4\pi} \int_{\mathcal{S}} \mathrm{d}^3r \, \mathrm{d}^3r' \; \mathbf{j}(\mathbf{r}') \times \frac{\partial}{\partial \, \mathbf{r}'} \frac{1}{|\mathbf{r}' - \mathbf{r}|} &(191)\\
&= \frac{\mu_0}{4\pi} \int_{\mathcal{S}} \mathrm{d}^3r' \; \mathbf{j}(\mathbf{r}') \times \frac{\partial}{\partial \, \mathbf{r}'} \int_{\mathcal{S}} \mathrm{d}^3r \; \frac{1}{|\mathbf{r}' - \mathbf{r}|}. &(192)
\end{aligned}$$

Both integrals can only be done if the macroscopic geometry of the system, $\mathcal{S}$, is known. However, a general statement about the form of the resulting expression can already be made using dimensional arguments. The last integral, over $\mathbf{r}$, will have the dimension of a surface. After taking the gradient, a position vector will remain. Since the integral only depends on the position $\mathbf{r}'$ within the sample $\mathcal{S}$, one would expect to find an expression of the type

$$\frac{\partial}{\partial\,\mathbf{r}'} \int_{\mathcal{S}} \mathrm{d}^3 r \; \frac{1}{|\mathbf{r}' - \mathbf{r}|} \quad = \quad -(\mathbf{r}' - \mathbf{R}_c)\; f(\mathbf{r}') \tag{193}$$

with the center of mass of the sample, $\mathbf{R}_c$, and $f(\mathbf{r}')$ a dimensionless function, varying slowly with $\mathbf{r}'$. Lateron in this section, this function will be calculated for a particular geometry. Thus, the field becomes:

$$\mathbf{B}^{\mathrm{ind}}(\mathbf{G} = 0) \quad = \quad -\frac{\mu_0}{4\pi} \sum_{s \in \mathcal{S}} \int_{\Omega_s} \mathrm{d}^3 r' \;\; \mathbf{j}(\mathbf{r}') \times \Big[(\mathbf{r}' - \mathbf{R}_c)\; f(\mathbf{r}') \Big], \tag{194}$$

where the integral over the total system has been split up into the sum over its constituting unit cells. The cells are indicated by s, their volume being Ω_s.

Considering the very large number of unit cells that form a macroscopic sample, it is certainly a reasonable approximation to assume that $f(\mathbf{r}')$ actually only depends on the location of the unit cell, i.e. on the index s resp. on the vector $\mathbf{R}_s$ pointing to that cell, and not on the position inside it. Then, Eq. (194) simplifies considerably and finally metamorphoses to Eq. (129):

$$\begin{aligned}
\mathbf{B}^{\mathrm{ind}}(\mathbf{G}=0) &\approx -\frac{\mu_0}{4\pi}\sum_{s\in\mathcal{S}}\int_{\Omega_s}\mathrm{d}^3r'\ \mathbf{j}(\mathbf{r}')\times\Big[(\mathbf{r}'-\mathbf{R}_c)\ f(\mathbf{R}_s)\Big] && (195)\\
&= -\frac{\mu_0}{4\pi}\sum_{s\in\mathcal{S}} f(\mathbf{R}_s)\int_{\Omega_s}\mathrm{d}^3r'\ \mathbf{j}(\mathbf{r}')\times\mathbf{r}' && (196)\\
&= \Omega_{\mathcal{S}}\ \ \frac{\Omega_1}{2\pi\,\Omega_{\mathcal{S}}}\sum_{s\in\mathcal{S}} f(\mathbf{R}_s)\ \ \frac{\mu_0}{2\Omega_1}\int_{\Omega_1}\mathrm{d}^3r'\ \mathbf{r}'\times\mathbf{j}(\mathbf{r}') && (197)\\
&= \Omega_{\mathcal{S}}\,\kappa\,\chi\ \mathbf{B}^{\mathrm{ext}} && (198)
\end{aligned}$$

with the definitions

$$\begin{aligned}
\Omega_{\mathcal{S}} &= \text{system volume}, && (199)\\
\Omega_1 &= \text{one particular (but arbitrary) unit cell}, && (200)\\
\kappa &= \frac{\Omega_1}{2\pi\,\Omega_{\mathcal{S}}}\sum_{s\in\mathcal{S}} f(\mathbf{R}_s), && (201)\\
\chi &= \frac{\mu_0}{2\Omega_1}\,\frac{\partial}{\partial\,\mathbf{B}^{\mathrm{ext}}}\int_{\Omega_1}\mathrm{d}^3r'\ \mathbf{r}'\times\mathbf{j}(\mathbf{r}'). && (202)
\end{aligned}$$

Several details of this last calculation are worthwhile being explained in more detail. First, Eq. (171) is used to eliminate the center of gravity $\mathbf{R}_c$ of the system from Eq. (195). For the same reason (assuming in addition that the current density is fully periodic), the integrals are equal for all unit cells:

$$\begin{aligned}
\int_{\Omega_s}\mathrm{d}^3r'\ \mathbf{j}(\mathbf{r}')\times(\mathbf{r}'-\mathbf{R}_c) &= \int_{\Omega_s}\mathrm{d}^3r'\ \mathbf{j}(\mathbf{r}')\times\mathbf{r}' && (203)\\
= \int_{\Omega_1}\mathrm{d}^3r'\ \mathbf{j}(\mathbf{r}')\times(\mathbf{r}'+\mathbf{R}_s) &= \int_{\Omega_1}\mathrm{d}^3r'\ \mathbf{j}(\mathbf{r}')\times\mathbf{r}', && (204)
\end{aligned}$$

so that a particular, but arbitrary one can be chosen to obtain the magnetic bulk susceptibility χ. The derivative with respect to the external field shall only clarify the tensor nature of the susceptibility as well as the assumption that the current density is purely linear in the external field:

$$\chi \cdot \mathbf{B}^{\text{ext}} = \left[\frac{\partial}{\partial\,\mathbf{B}^{\text{ext}}} \int_{\Omega_1} \mathrm{d}^3r' \;\; \mathbf{r}' \times \mathbf{j}(\mathbf{r}')\right] \cdot \mathbf{B}^{\text{ext}} \tag{205}$$

$$= \int_{\Omega_1} \mathrm{d}^3r' \;\; \mathbf{r}' \times \mathbf{j}(\mathbf{r}'). \tag{206}$$

Finally, one more operation is neccessary to obtain the actual contribution of $\mathbf{B}^{\text{ind}}(\mathbf{G} = 0)$ to the total magnetic field in the cell, the back transformation to direct space. The forth transformation of a constant field $\mathbf{B}(\mathbf{r}) = \mathbf{B}_0$ to reciprocal space through Eq. (149) gives a $\mathbf{G} = 0$ value of $\Omega_{\mathcal{S}}\mathbf{B}_0$, so that the inverse transformation consists just of dividing by the total system volume. That means for the total induced magnetic field in direct space:

$$\mathbf{B}_0^{\text{ind}} = \kappa\,\chi\;\mathbf{B}^{\text{ext}} \tag{207}$$

with the defining relations Eq. (201) and (202) for χ and κ.

C.2 Special case: spherical geometry

In this part, the value of κ shall be determined for the most commonly used system, a spherical sample. In this case, one starts from the exact expression Eq. (192), which can be calculated analytically. When evaluating it, it is found that the function f (cf. Eq. (193)) is actually constant number. The integration is done in polar coordinates, and it is assumed that the sphere has a radius $R_{\mathcal{S}}$:

$$\int_{\mathcal{S}} \mathrm{d}^3 r \, \frac{1}{|\mathbf{r}' - \mathbf{r}|} = \int\limits_0^{R_{\mathcal{S}}} dr\, r^2 \int\limits_{-1}^{+1} du \int\limits_0^{2\pi} d\varphi \frac{1}{(r^2 + r'^2 - 2rr'u)^{1/2}} \tag{208}$$

$$= 2\pi \int_0^{R_{\mathcal{S}}} dr\, r^2 \, \frac{1}{rr'} \left[|r + r'| - |r - r'| \right] \tag{209}$$

$$= 2\pi \left(R_{\mathcal{S}}^2 - \frac{1}{3} r'^2 \right), \tag{210}$$

where $r' < R_{\mathcal{S}}$ has been used. The gradient with respect to r' is then simply

$$\frac{\partial}{\partial \, \mathbf{r}'} \int_{\mathcal{S}} \mathrm{d}^3 r \, \frac{1}{|\mathbf{r}' - \mathbf{r}|} = -\frac{4\pi}{3} \, \mathbf{r}' \tag{211}$$

so that the function f is identically equal to $4\pi/3$. That makes the calculation of κ through Eq. (201) trivial. The sum over a constant term just corresponds to the number of elements in the sum, which is right the number of unit cells in the sample, $\Omega_{\mathcal{S}}/\Omega_1$:

$$\kappa = \frac{\Omega_1}{2\pi \, \Omega_{\mathcal{S}}} \sum_{s \in \mathcal{S}} f(\mathbf{R}_s) \tag{212}$$

$$= \frac{2}{3}. \tag{213}$$

References

[1] P. Hohenberg and W. Kohn, *Phys. Rev.* **136**, B864 (1964).

[2] W. Kohn and L. Sham, *Phys. Rev.* **140**, A1133 (1965).

[3] R. Car and M. Parrinello, *Phys. Rev. Lett.* **55**, 2471 (1985).

[4] M. Parrinello, *Solid State Comm.* **102**, 107 (1997).

[5] F. Mauri, B. Pfrommer and S. Louie, *Phys. Rev. Lett.* **77**, 5300 (1996).

[6] R. Resta, *J. Phys.: Condens. Matter* **12**, R107 (2000).

[7] R. Jones and O. Gunnarsson, *Rev. Mod. Phys.* **61**, 689 (1989).

[8] R. G. Parr and W. Yang, *Density functional theory of atoms and molecules*, Oxford Science Publications,1989.

[9] Ashcroft, *Solid state physics*, Saunders, Philadelphia,1976.

[10] I. Shavitt, in *Modern Theoretical Chemistry*, edited by H. F. Schaefer,Plenum Press, New York,1977.

[11] A. C. Wahl and G. Das, in *Modern Theoretical Chemistry*, edited by H. F. Schaefer,Plenum Press, New York,1977.

[12] H. J. Werner, in *Ab Initio Methods in Quantum Chemistry*, edited by K. Lawley,John Wiley, Chichester,1987.

[13] J. Cízek, *J. Chem. Phys.* **45** (1966).

[14] J. Cízek, *Adv. Chem. Phys.* **14** (1969).

[15] J. Cízek, *Int. J. Quantum Chem.* **5** (1971).

[16] E. E. Pickett, *Comput. Phys. Reports* **9** (1989).

[17] S. Lundqvist and N. H. March, editors, *Theory of the inhomogeneous electron gas*, Plenum Press, New York,1983.

[18] D. M. Ceperley and B. J. Alder, *Phys. Rev. Lett.* **45**, 566 (1980).

[19] J. Perdew and A. Zunger, *Phys. Rev. B* **23**, 5048 (1981).

[20] P. Giannozzi, S. de Gironcoli, P. Pavone and S. Baroni, *Phys. Rev. B* **43**, 7231 (1991).

[21] X. Gonze, D. C. Allan and M. P. Teter, *Phys. Rev. Lett.* **68**, 3603 (1992).

[22] C. S. Wang, B. M. Klein and H. Krakauer, *Phys. Rev. Lett.* **54**, 1852 (1985).

[23] A. Becke, *Phys. Rev. A* **38**, 3098 (1988).

[24] C. Lee, W. Yang and R. Parr, *Phys. Rev. B* **37**, 785 (1988).

[25] M. Sprik, J. Hutter and M. Parrinello, *J. Chem. Phys.* **105**, 1142 (1996).

[26] D. Hamann, M. Schluter and C. Chiang, *Phys. Rev. Lett.* **43**, 1494 (1979).

[27] D. H. G.B. Bachelet and M. Schluter, *Phys. Rev. B* **26**, 4199 (1982).

[28] N. Troullier and J. L. Martins, *Phys. Rev. B* **43**, 1993 (1991).

[29] S. Goedecker, M. Teter and J. Hutter, *Phys. Rev. B* **54**, 1703 (1996).

[30] L. Kleinman and D. Bylander, *Phys. Rev. Lett.* **48**, 1425 (1982).

[31] P. Pulay, *Mol. Phys.* **17** (1969).

[32] W. Press, S. Teukoldky, W. Vetterling and B. Flannery, *Numerical recipes*, Cambridge University Press,second edition edition,1992.

[33] A. Putrino, D. Sebastiani and M. Parrinello, *J. Chem. Phys.* **113**, 7102 (2000).

[34] G. Wannier, *Phys. Rev.* **52**, 191 (1937).

[35] G. Berghold, C. Mundy, A. Romero, J. Hutter and M. Parrinello, *Phys. Rev. B* **61**, 10040 (2000).

[36] N. Marzari and D. Vanderbilt, *Phys. Rev. B* **56**, 12847 (1997).

[37] P. L. Silvestrelli, N. Marzari, D. Vanderbilt and M. Parrinello, *Solid State Comm.* **107**, 7 (1998).

[38] R. Resta, *Phys. Rev. Lett.* **80**, 1800 (1998).

[39] R. Resta, *Phys. Rev. Lett.* **82**, 370 (1999).

[40] S. F. Boys, *Rev. Mod. Phys.* **32**, 296 (1960).

[41] P. L. Silvestrelli, *Phys. Rev. B* , 9703 (1999).

[42] M. Parrinello and A. Rahman, *Phys. Rev. Lett.* **45**, 1196 (1980).

[43] J. M. Lighthill, *Introduction to Fourier Analysis and Generalized Functions*, Cambridge University Press, Cambridge,1958.

[44] C. Edmiston and K. Ruedenberg, *Rev. Mod. Phys.* **35**, 457 (1963).

[45] H. Goldstein, *Classical mechanics*, Addison-Wesley,1980.

[46] R. Ditchfield, *J. Chem. Phys.* **56**, 5688 (1972).

[47] W. Kutzelnigg, *Isr. J. Chem.* **19**, 193 (1980).

[48] T. Keith and R. Bader, *Chem. Phys. Lett.* **210**, 223 (1993).

[49] F. Mauri and S. Louie, *Phys. Rev. Lett.* **76**, 4246 (1996).

[50] W. Kohn, *Phys. Rev.* **115**, 809 (1959).

[51] F. Mauri, B. Pfrommer and S. Louie, *Phys. Rev. Lett.* **79**, 2340 (1997).

[52] Y. Yoon, B. Pfrommer, F. Mauri and S. Louie, *Phys. Rev. Lett.* **80**, 3388 (1998).

[53] F. Mauri, B. Pfrommer and S. Louie, *Phys. Rev. B* **60**, 2941 (1999).

[54] B. Pfrommer, F. Mauri and S. Louie, *J. Am. Chem. Soc.* **122**, 123 (2000).

[55] W. Kutzelnigg, U. Fleischer and M. Schindler, *NMR basic principles and progress* **23** (1990).

[56] T. Gregor, F. Mauri and R. Car, *J. Chem. Phys.* **111**, 1815 (1999).

[57] J. Hutter et al., computer code CPMD, version 3.3,1990-1999.

[58] The geometries used for the isolated molecules are: $\mathbf{H_2O}$: r_{OH}=0.9578Å; $\mathbf{CH_4}$: r_{CH}=1.094Å; $\mathbf{C_2H_2}$: r_{CC}=1.206Å, r_{CH}=1.061Å; $\mathbf{C_2H_4}$: r_{CC}=1.337Å, r_{CH}=1.103Å; $\mathbf{C_2H_6}$: r_{CC}=1.532Å, r_{CH}=1.096Å; $\mathbf{C_6H_6}$: r_{CC}=1.399Å, r_{CH}=1.101Å.

[59] M. J. Frisch et al., computer code gaussian 94, revision b.2,1995.

[60] A. Jameson and C. Jameson, *Chem. Phys. Lett.* **134**, 461 (1987).

[61] R. Gupta, *Landolt-Börnstein*, volume 16: diamagnetic susceptibility, Springer Verlag,1967.

[62] C. Debouck et al., *Biochemistry* **84**, 8903 (1999).

[63] L. Hong, J. A. Hartsuck, S. Foundling, J. Ermolieff and Tang, *J. Protein Sci* **7**, 300 (1998).

[64] S. Seelmeier, H. Schmidt, V. Turk and K. von der Helm, *Proc Natl Acad Sci USA* **85**, 6612 (1988).

[65] P. M. D. Fitzgerald and J. P. Springer, *Annu. Rev. Biophys. Biophys. Chem.* **20**, 299 (1991).

[66] M. Baca and B. H. S. Kent, *Proc Natl Acad Sci USA* **90**, 11638 (1993).

[67] N. E. Kohl et al., *Proc Natl Acad Sci USA* **85**, 4686 (1988).

[68] T. J. McQuade et al., *Science* **247**, 454 (1990).

[69] A. H. Kaplan et al., *J Virol* **67**, 4050 (1993).

[70] A. Wlodawer and J. Vondrasek, *Annu. Rev. Biophys. Biomol. Struct.* **27**, 249 (1998).

[71] S. Gulnik, J. W. Erickson and D. Xie, *Vitamins and Hormones* **58**, 213 (2000).

[72] A. Wlodawer and J. W. Erickson, *Annu. Rev. Biochem.* **62**, 543 (1993).

[73] J. P. Vacca, Design of tight-binding human immunodeficiency virus type 1 protease inhibitors, in *Methods in enzymology,*pages 311–334,Academic Press: San Diego,1994.

[74] J. P. Vacca and J. H. Condra, *Drug Des.Discovery* **2**, 261 (1997).

[75] C. N. Flexner, *Engl.J.Med.* **338**, 1281 (1998).

[76] J. W. Erickson and M. E. Eissenstat, HIV protease as a target for the design of antiviral agents for AIDS, in *Proteases of infectious agents*, edited by B. Dunn,pages 1–60,Academic Press: San Diego, CA,1999.

[77] G. J. Tawa, I. A. Topol, S. K. Burt and J. W. Erickson, *J Am Chem Soc* **120**, 8856 (1998).

[78] W. E. Harte and D. L. Beveridge, *J Am Chem Soc* **115**, 3883 (1993).

[79] X. Chen and A. Tropsha, *J Med Chem* **38**, 42 (1995).

[80] J. Trylska et al., *Protein Sci* **8**, 180 (1999).

[81] A. Tropsha and J. Hermans, *Protein Eng* **5**, 29 (1992).

[82] R. W. Harrison and I. T. Weber, *Protein Eng* **7**, 1353 (1994).

[83] L. J. Hyland et al., *Biochemistry* **30**, 8441 (1991).

[84] L. J. Hyland, T. A. Tomaszek and T. D. Meek, *Biochemistry* **30**, 8454 (1991).

[85] R. Smith, I. M. Brereton, R. Y. Chai and S. B. H. Kent, *Nature Struct Biol* **3**, 946 (1996).

[86] R. Ishima, P. T. Wingfield, S. J. Stahl, J. D. Kaufman and D. A. Torchia, *J Am Chem Soc* **120**, 10534 (1998).

[87] D. I. Freedberg et al., *J Am Chem Soc* **120**, 7916 (1998).

[88] E. Katoh et al., *J Am Chem Soc* **121**, 2607 (1999).

[89] Y. X. Wang et al., *Biochemistry* **35**, 9945 (1996).

[90] Y. X. Wang et al., *Biochemistry* **35**, 12694 (1996).

[91] T. Yamazaki et al., *J Am Chem Soc* **116**, 10791 (1994).

[92] T. Yamazaki et al., *Eur J Biochem* **219**, 707 (1994).

[93] S. Grzesiek et al., *J Am Chem Soc* **116** (1994).

[94] R. Hagen and J. D. Roberts, *J.Am.Chem.Soc.* **91**, 4504 (1969).

[95] P. M. D. Fitzgerald et al., *J Biol Chem* **265**, 14209 (1990).

[96] S. Piana, D. Sebastiani, P. Carloni and M. Parrinello, *J. Am. Chem. Soc.* **submitted** (2001).

[97] H. M. Berman et al., *Nucleic Acids Research* **28**, 235 (2000).

[98] S. Piana and P. Carloni, *PROTEINS: Str.Funct.Gen.* **39**, 26 (2000).

[99] R. N. Barnett and U. Landman, *Phys.Rev.B* **48**, 2081 (1993).

[100] J. Hutter, H. P. Luthi and M. Parrinello, *Comput.Mater.Sci.* **2**, 244 (1994).

[101] L. De Santis and P. Carloni, *PROTEINS: Str.Funct.Gen.* **37**, 611 (1999).

[102] J. Abildgaard, S. Bolvig and P. E. Hansen, *J Am Chem Soc* **120**, 9063 (1998).

[103] J. Reuben, *J Am Chem Soc* **109**, 316 (1986).

[104] J. Reuben, *J Am Chem Soc* **108**, 1735 (1985).

[105] J. Bordner, P. D. Hammen and E. B. Whipple, *J Am Chem Soc* **111**, 6572 (1989).

[106] P. Silvestrelli, M. Bernasconi and M. Parrinello, *Chem. Phys. Lett.* **277**, 478 (1997).

[107] M. Boero, K. Terakura, T. Ikeshoji, C. C. Liew and M. Parrinello, *Phys. Rev. Lett.* **85**, 3245 (2000).

[108] J. W. Tester et al., in *Emerging Technologies in Hazardous Waste Management III*, edited by D. W. Tedder and F. G. Pohland, volume 518,page 35,American Chemical Society, Washington DC, USA,1991.

[109] L. W. Flanagin, P. B. Balbuena, K. P. Johnston and P. J. Rossky, *J. Phys. Chem.* **99**, 5196 (1995).

[110] D. M. Pfund, J. G. Darab, J. L. Fulton and Y. Ma, *J. Phys. Chem.* **98**, 13102 (1994).

[111] D. M. Harradine et al., *Haz. Waste Haz. Mater.* **10**, 233 (1993).

[112] W. R. Kililea, K. C. Swallow and G. T. Hong, *J. Supercrit. Fluids* **5**, 72 (1992).

[113] F. D. Mango, J. W. Hightower and A. T. James, *Nature* **368**, 536 (1994).

[114] E. L. Shock, *Nature* **368**, 499 (1994).

[115] J. S. Seewald, *Nature* **370**, 285 (1994).

[116] L. C. Price, *Nature* **370**, 253 (1994).

[117] M. M. Hoffmann and M. S. Conradi, *J. Am. Chem. Soc.* **119**, 3811 (1997).

[118] N. Matubayashi, C. Wakai and M. Nakahara, *Phys. Rev. Lett.* **78**, 2573 (1997).

[119] N. Matubayashi, C. Wakai and M. Nakahara, *J. Chem. Phys.* **107**, 9133 (1997).

[120] The experimental geometry of an isolated water molecule has an equilibrium radius of r_{OH}=0.9578Å and an angle of θ=104.54° [126]. The BLYP-relaxed geometry is slightly different, its radius is r_{OH}=0.973Å and the angle becomes θ=104.4°.

[121] J. Vaara, J. Lounila, K. Ruud and T. Helgaker, *J. Chem. Phys.* **109**, 8388 (1998).

[122] B. Cabrera and H. Fahlenbach, *Z. Physik* **82**, 759 (1933).

[123] B. Cabrera and H. Fahlenbach, *Naturwiss.* **22**, 417 (1934).

[124] I. M. Svishchev and P. G. Kusalik, *J. Am. Chem. Soc.* **115**, 8270 (1993).

[125] F. Mauri, private communication.

[126] A. Katrusiak, *Phys. Rev. Lett.* **77**, 4366 (1996).

Curriculum Vitae

Daniel Sebastiani, geboren am 26.4.1973 in Wiesbaden

1979–1983: Grundschule Koblenz-Moselweiß

1983–1992: Görres-Gymnasium Koblenz; Abitur mit den Leistungskursen Mathematik, Physik, Englisch

1992–1994: Studium der Physik an der Universität Fridericiana, Karlsruhe

1994–1997: Studium der Physik an der Ecole Normale Supérieure de Lyon (ENSL). Abschluß: Diplôme d'Etudes Approfondies de Physique Théorique Rhône-Alpin an der ENSL
Forschungspraktika: Naval Research Laboratory, Washington D.C., USA; Laboratoire de Physique der ENSL, Lyon, Frankreich; Institut de Physique et Chimie des Matériaux de Strasbourg, Frankreich

7/1997-1/2001 Promotion bei Michele Parrinello am Max-Planck-Institut für Festkörperforschung, Stuttgart

Stuttgart, Januar 2001

Acknowledgements

First of all, I am particularly grateful to my advisor Prof. Dr. Michele Parrinello, who cordially accomodated me in his department during the last three years. Not only did he provide essential advice in all questions concerning physics, but also constant interest in my personal progress.

This thesis would not have been possible without the detailed knowledge of the CPMD implementation which Prof. Dr. Jürg Hutter helped me with whenever I was not sure of a detail. From him I learned that theoretical physics does not only consist in inventing formulae, but also in their realization.

Special thanks also go to my various collaborators inside and outside the Stuttgart group, who supported this work either with illucidating questions or with pertinent answers. In particular, I want to thank Dr. David Benoit, Dr. Gerd Berghold, Dr. Mauro Boero, Dr. Francesco Filippone, Prof. Dr. Martin Kaupp, Dr. Stefano Piana, and Dr. Anna Putrino.

I was happy to share many interesting times with the other group members, especially during the roughly 2000 coffee breaks and the numerous nights in the few good pubs of Stuttgart.